THE SIGNAL OF MODERN TO HOLOCENE DRIVERS OF COMPLEX CHANNEL

RESPONSE OF A SMALL ALLUVIAL STREAM

by

Scott D. Ducar

A thesis

submitted in partial fulfillment

of the requirements for the degree of

Master of Science in Hydrologic Sciences

Boise State University

December 2020

BOISE STATE UNIVERSITY GRADUATE COLLEGE

DEFENSE COMMITTEE AND FINAL READING APPROVALS

of the thesis submitted by

Scott D. Ducar

Thesis Title: The Signal of Modern to Holocene Drivers of Complex Channel Response of a Small Alluvial Stream

Date of Final Oral Examination: 23 October 2020

The following individuals read and discussed the thesis submitted by student Scott D. Ducar, and they evaluated their presentation and response to questions during the final oral examination. They found that the student passed the final oral examination.

Jen Pierce, Ph.D.	Chair, Supervisory Committee
James McNamara, Ph.D.	Member, Supervisory Committee
Caroline Nash, Ph.D.	Member, Supervisory Committee
Spencer Wood, Ph.D.	Member, Supervisory Committee
Elowyn Yager, Ph.D.	Member, Supervisory Committee

The final reading approval of the thesis was granted by Jen Pierce, Ph.D., Chair of the Supervisory Committee. The thesis was approved by the Graduate College.

DEDICATION

This thesis is dedicated to my grandparents, Doug and Eileen Cresswell, for encouraging me to pursue higher education.

ABSTRACT

Small alluvial streams (~100km^2 drainage area) are important for water resources
and aquatic habitat. Small streams throughout the Western United States are impacted by
anthropogenic land-use including urban development, mining, logging, beaver trapping,
grazing, and farming. Land-use change can trigger a complex series of channel response
(such as stream channel incision or channel migration) that vary spatially and temporally
in the watershed. However, streams also respond to other external forcings, such as
tectonically or climatically-driven changes in discharge or base-level, which make
disentangling the drivers of channel response complicated. Therefore, it is important to
place modern channel changes into a longer geomorphic context to fully understand the
complex response initiated by land-use. In order to understand how changes in land-use
may drive spatially variable channel response, we examine a representative small alluvial
stream, Lower Dry Creek (LDC), a tributary to the Boise River in Idaho.

LDC marks the transition from the rugged and largely undeveloped upland Dry
Creek Experimental Watershed to the lower gradient, agricultural, and residential section
of the watershed. LDC has a complex history of placer mining, beaver trapping, grazing,
and farming since the 1850's. Recent (post-1997) growth in the region converted LDC's
expansive floodplain from agricultural land to housing developments. Most of the recent
development and historic and current farmland are on the broad, low gradient Hidden
Springs Terrace. We use remote sensing, hydraulic modeling, grain size analysis, and
field observations to quantify how the distinct reaches of LDC are changing over human

time scales; we use Quaternary dating methods and geomorphic mapping to examine how LDC has changed over centennial to millennial time scales.

Optically Stimulated Luminescence (OSL) dates of fluvial sediments in an upper reach indicate incision in LDC after 4.79 ± 1.05 ka. Around 0.79 to 0.67 ka, LDC deposited a large packet of sheetfloods and cross-bedded sands, which correlate to a period of more fire activity and alluvial fan deposition in the region. After approximately 0.67 ka the reach incised 2.4 m. In the late 1800's, placer mining in the upper reach of LDC shifted the channel behavior from incision to lateral adjustment. We measured an average of 0.6 m/yr of meander migration from 1938 to 2019. Migration rate increased threefold after 1992 (which corresponds temporally with a large rain-on-snow flood event in 1997), but slowed after 2011.

Comparison of the modern longitudinal profile of LDC with the longitudinal profile of the Hidden Springs Terrace, combined with grain size analysis and historic dating reveals the impact of prior land use change on the present channel. LDC's current profile is convex in middle reaches, and grain size analysis shows a fining in the middle reaches and then coarsening downstream. The convexity and grain size change is consistent with increased aggradation from a slug of sediment from upstream placer mining progressing downstream. Downstream where the valley is unconfined, LDC aggraded 0.75 cm/yr from 1642 to 1950 AD to form the broad Hidden Springs Terrace.

Notably, a lower reach of LDC has recently and profoundly incised, affecting local landowners and cutting off access of the stream to its floodplain. This downstream reach is incised 4.7 m below the Hidden Springs Terrace; a modern radiocarbon date provides evidence the incision happened post-1950 AD, potentially from channelization

of Currant Creek (a tributary of LDC) as farmland is converted to housing. Hydraulic modeling shows LDC's median grain size is mobile at estimated bankfull flows for all reaches, which allows the stream to rapidly adjust both vertically and laterally.

LDC channel response in the upper and lower reaches indicates anthropogenic land-use resulted in vertical and lateral channel change: upstream aggradation and meander migration following placer mining, and downstream incision following farmland conversion. This represents a shift from the observed channel adjustments and large-scale formation of the Hidden Springs Terrace observed over Holocene timescales. LDC illustrates textbook 'complex response' as the stream both incises and aggrades in different locations due to differing drivers.

This study shows small alluvial streams can be very sensitive to changes in land-use. Stream incision, aggradation, and channel shifts impact aquatic and riparian species and developments adjacent to the channel. This study illustrates the importance of examining the drivers of modern channel change within a longer more complete context. Results of this study can support stakeholders as they strive to understand the characteristics and response of small alluvial streams to anthropogenic land-use, and best options for restoration of degraded systems.

TABLE OF CONTENTS

LIST OF TABLES

LIST OF FIGURES

LIST OF ABBREVIATIONS

AD	Anno Domini
cal yr BP	Calibrated radiocarbon age in years before present
CAM	Central Age Model
cfs	Cubic feet per second
D_{50}	Median grain size
DCEW	Dry Creek Experimental Watershed
DEM	Digital Elevation Model
DOQs	Digital Orthophoto Quadrangles
ESRI	Environmental Systems Research Institute
GPS	Global Positioning System
HEC-RAS	Hydrologic Engineering Center River Analysis System
IDW	Inversed Distance Weighting
ka	Kiloannum (one thousand years)
LDC	Lower Dry Creek
LG	Lower Gage
LiDAR	Light Detection and Ranging
LLNL	Lawrence Livermore National Laboratory
Ma	Megaannum (one million years)
MAM	Minimum Age Model
NAIP	National Agriculture Imagery Program

NRCS	National Resources Conservation Service
OSL	Optically Stimulated Luminescence
QSI	Quantum Spatial Incorporated
R^2	Coefficient of determination
SAR	Single-Aliquot Regenerative
SVC	Spring Valley Creek
USGS	United States Geological Survey
USULL	Utah State University Luminescence Laboratory

CHAPTER 1: INTRODUCTION

Small streams (~ 100 km^2 drainage area) are important for water resources and

aquatic habitat (Wohl, 2017). During early settlement of the Western USA, large river

corridors provided fertile soil and access to water for irrigation. As the population of

these areas grew, settlement expanded to the terraces and floodplains of smaller stream

systems, which provide fertile soils and water for agriculture. Today, flat terraces of

small streams are sites of housing development as metropolitan areas in the Western

United States grow. Land-use impacts the hydrology and sediment supply of small

streams (Leopold et al., 1964; Richards, 1982); however, the channel response caused by

land-use is complex as it varies between watersheds and within the same stream.

Fluvial geomorphology involves understanding thresholds, equilibrium, and

disequilibrium of stream systems. A system in equilibrium can be defined by real

parameters that have a limited range of values; if these conditions are exceeded the

system is no longer in equilibrium and change ensues (Schumm, 1973). The critical

conditions, or thresholds, vary for each stream system and within the same system. Lane

(1955) explained the thresholds of stream systems as a balance of sediment load,

sediment size, slope, and discharge. Changes to these parameters beyond a threshold

results in incision or aggradation of the channel. The incision or aggradation of stream

systems doesn't happen in straight forward ways and there can be multiple perturbations

occurring at different times and locations in the watershed. The series of reactions after

crossing a threshold is known as a complex response (Schumm and Parker, 1973).

External variables, such as tectonics, base level, climate, and land-use impact stream channels. The complex response of stream systems caused by land-use is important to place into the longer geomorphic context because of the long period of time required for a stream to reach dynamic equilibrium. It is also complicated by several land-uses impacting the stream simultaneously. Small alluvial streams that provide water and aquatic resources throughout the west are being degraded by land-use. Degraded streams have accelerated streambank erosion, lower water table, reduced land productivity, degraded riparian ecosystems, and altered downstream sedimentation impacting aquatic species (Booth, 1990; Schilling et al., 2004, Hardison et al. 2009; Pollock et al., 2014)

In the Treasure Valley surrounding Boise, Idaho, urban areas are expanding into agricultural land (Dahlal et al., 2017). The terraces and floodplains of small streams that drain the foothills of the Boise Range are the sites of extensive residential development. Dry Creek, a tributary to the Boise River, is representative of a small (100 km^2) watershed with a complex geomorphic and land-use history undergoing rapid development. The watershed has or is experiencing land-use known to impact streams, such as logging, grazing, beaver trapping, mining, farming, and development.

Lower Dry Creek (LDC) is an alluvial channel that is vertically and laterally responsive. Aerial photos and testimony from local landowners indicate the channel response has occurred over the last approximately 100 years. An upper reach of LDC is laterally migrating at a rapid rate, while other reaches appear laterally stable. A lower reach of LDC is incising through loose unconsolidated sands and gravels. However, the

incision is spatially constrained. LDC provides an opportunity to study a single stream channel that is responding in opposite directions to multiple land-uses in various reaches.

This study investigates the history of channel change in LDC in order to decipher the drivers and responses of recent and long term channel change. We use a combination of Quaternary dating, remote sensing, sediment characteristics, and surveys to map and quantify evidence of lateral and vertical channel change in LDC. This study examines stream and sediment characteristics in order to 1) characterize the geomorphic history of the reaches of LDC, 2) compare the long-term geomorphic history with recent channel changes and 3) determine possible driving forces resulting in high reach-scale variability in lateral and vertical adjustment of LDC.

We find evidence of complex channel response that varies spatially along the stream profile. Within a 15 km section of LDC, the upper section of the channel displays modern lateral meander migration and Holocene cut and fill. The mid-section shows limited change and is connected to the broad Holocene terrace and able to adjust, but is likely experiencing increased aggradation from upstream land-use. The lower section is undergoing rapid incision, but late Holocene dates in bank stratigraphy show major aggradational events in this same reach within the past ~400 years. LDC illustrates textbook complex response of lateral migration, Holocene cut and fill, and recent incision and sedimentation likely as a result of anthropogenic land-use. This study shows that determining the drivers of modern channel change needs to be placed within a longer more complete context.

CHAPTER 2: BACKGROUND

Streams adjust laterally and vertically depending upon sediment input and

transport capacity (Darby and Simon, 1999). If sediment supply is greater than sediment

capacity the stream aggrades and laterally migrates; while if sediment supply is less than

sediment capacity the stream incises. Lane's balance (Figure 1), which describes the

relationship between sediment transport and stream power, is

$$Q_s D_{50} \propto QS$$

where Q_s is sediment discharge, D_{50} is the median grain size, Q is stream discharge, and S

is the streambed slope (Lane, 1955). Conceptually, when stream power is proportional to

sediment discharge the stream is in what is called dynamic equilibrium. Stream power

determines the capacity of a given flow to transport sediment and is defined by the

equation

$$\Omega = \rho g Q S$$

where Ω is stream power, ρ is the density of water, g is the acceleration due to gravity, Q

is discharge, and S is the channel slope. Dynamic equilibrium of a stream is when the

channel elevation oscillates around a central tendency, but is following a longer term

trend, such as gradually lowering the landscape. When the stream power is proportional

to the sediment discharge the stream is in dynamic equilibrium. Changes to these

parameters beyond a threshold results in degradation or aggradation of the channel.

However, the degradation or aggradation of stream systems doesn't happen in straight

forward ways and there can be multiple perturbations occurring at different locations in the watershed resulting in a complex response.
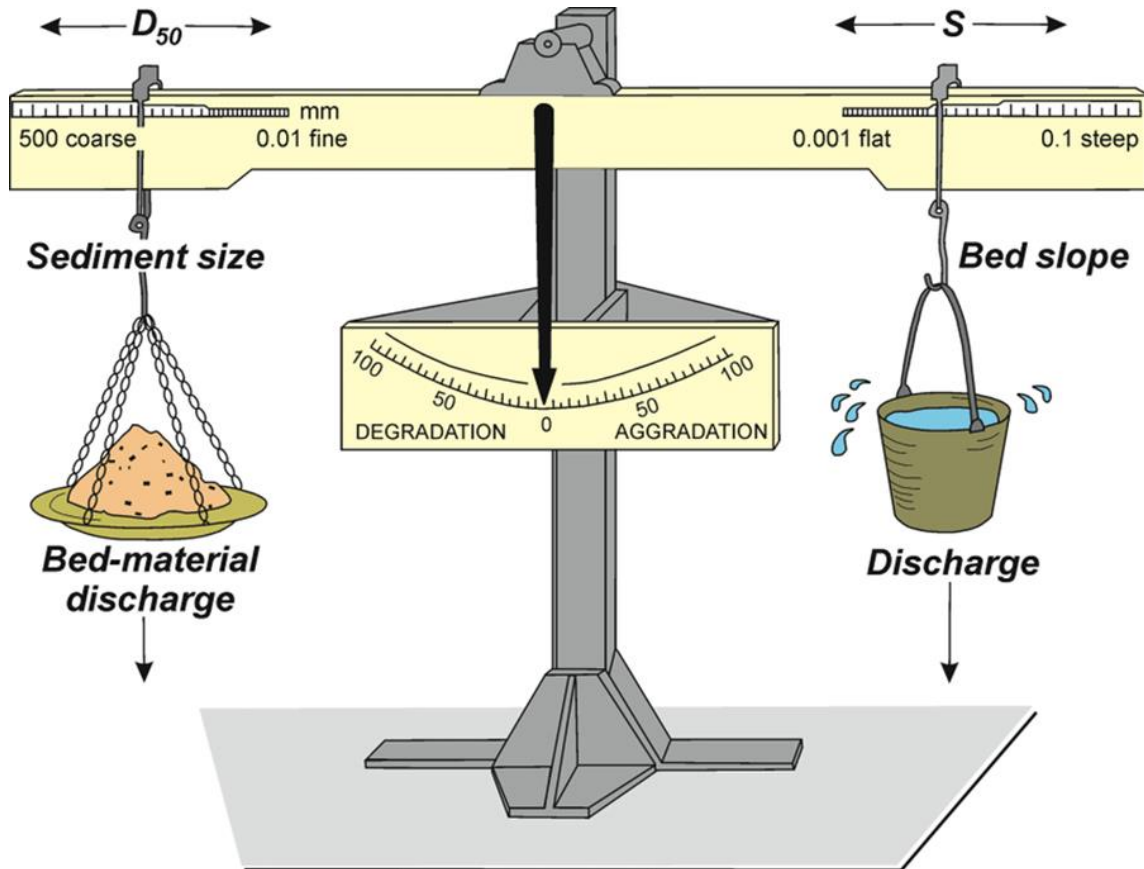
Figure 1 **Conceptual schematic showing equilibrium conditions of stream channels as a balance of stream power and sediment discharge from Rinaldi et al. (2015, p. 90). The figure shows the qualitative expression $Q_wS\alpha Q_sD_s$ which relates water discharge (Q_w), channel slope (S), sediment discharge or load (Q_s) and bed sediment size (D_s). A change in the relationship tilts the scale out of equilibrium towards either degradation or aggradation.**

A complex response of the degradation and aggradation of streams was described by Schumm and Parker (1973) using an artificial basin. The study induced a base-level decline at the mouth of the basin, which caused downcutting of the stream and the formation of terraces. However, tributaries remained in their equilibrium state and didn't experience downcutting. As time progressed, the incision of the main channel migrated upstream, lowering the base level of tributaries and entrenchment of the tributaries began.

The incision of the tributaries provided an increased amount of sediment to the main channel. The increased sediment load caused aggradation at the mouth because the stream was incapable of transporting the increased load from the entrenched tributaries. The complex response from a base-level decline was expanded on by Summerfield (1991) who found several cycles of aggradation and incision. Figure 2 is a schematic diagram from the study that describes seven sequential time scales a stream can follow after base-level decline. Summerfield (1991) describes what is happening upstream, downstream, as well as changes to the sediment supply from upstream. In stage 1, a fall in base level causes a local steeping of the channel gradient. Erosion in the steepened section lowers the channel elevation and steepens the gradient upstream. The downstream reach incises, but upstream there is no change. Over time, in stage 2, incision propagates upstream and the amount of sediment from upstream increases. The increase in sediment supply results in a buildup of sediment downstream in stage 3. The aggradation results in a decrease in channel gradient downstream. Additionally in stage 3, incision continues upstream. In stage 4, aggradation propagates upstream as the channel gradient continues to decrease further upstream. The sediment supply from upstream decreases, due to the decrease in downcutting. The reduction in sediment supply means there is additional energy for erosion and incision starts downstream. In stage 6, incision propagates upstream causing an increase in sediment supply downstream. Finally in stage 7, the increased sediment supply leads to aggradation at the downstream end of the channel. Therefore, a downstream perturbation, base-level decline, caused changes which propagated upstream. Then the changes upstream caused changes downstream resulting

in a series of aggradation and downcutting events that vary spatially and temporally in the basin.
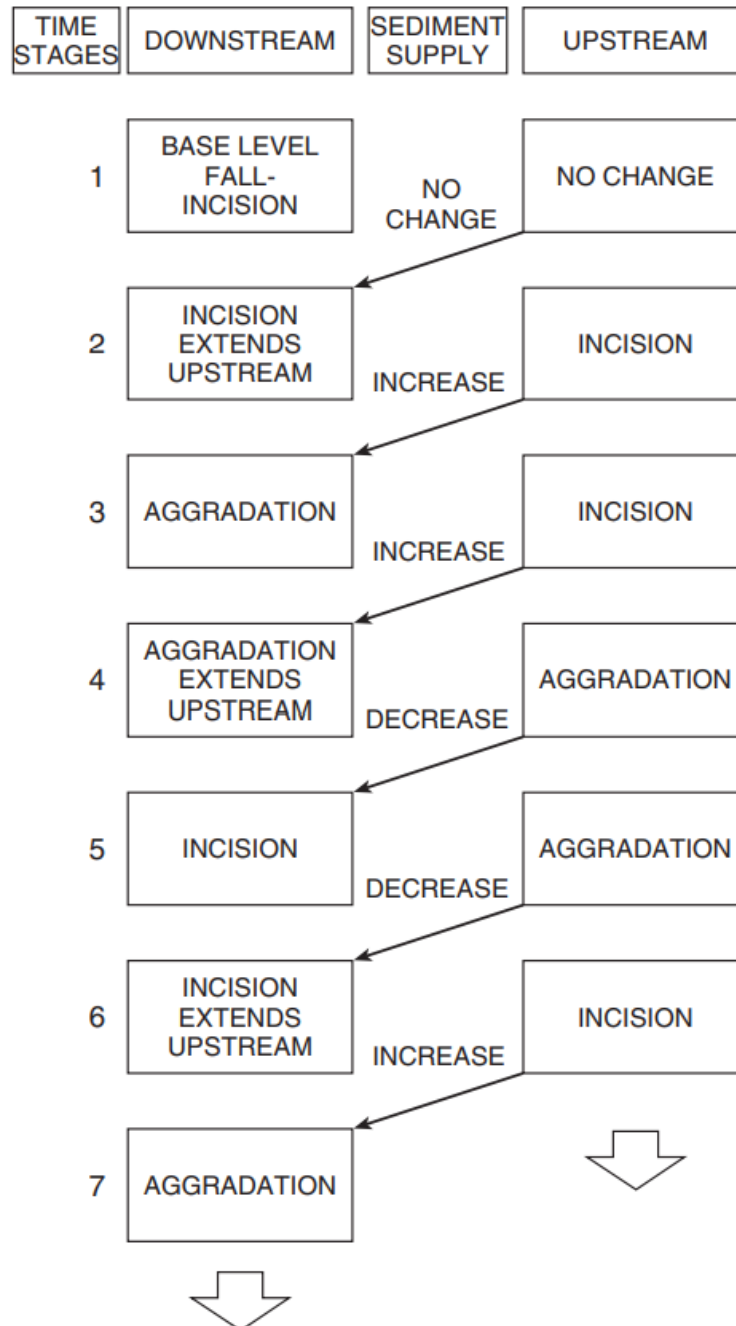
Figure 2 Schematic representation of a complex response as a result of a decline in base-level from Summerfield (1991, p. 227). The time stages are on the left from 1 to 7. The boxes describe the channel response during the time stage. The arrows show the change in sediment supply from upstream to downstream.

Outside of these artificial drainage basins, it becomes difficult to document the complex response of natural stream systems. The sequence of events usually takes a long time to reach equilibrium after its final adjustment. The complex response described by Schumm (1977) relates the nonlinear erosion and aggradation of alluvial systems to external variables of climatic, tectonic, base level, or human activity (Figure 3). Any change to one of these variables results in a complex series of adjustments in the stream system. The adjustments can result in positive or negative feedback in the system as shown in the simplified schematic (Figure 3).
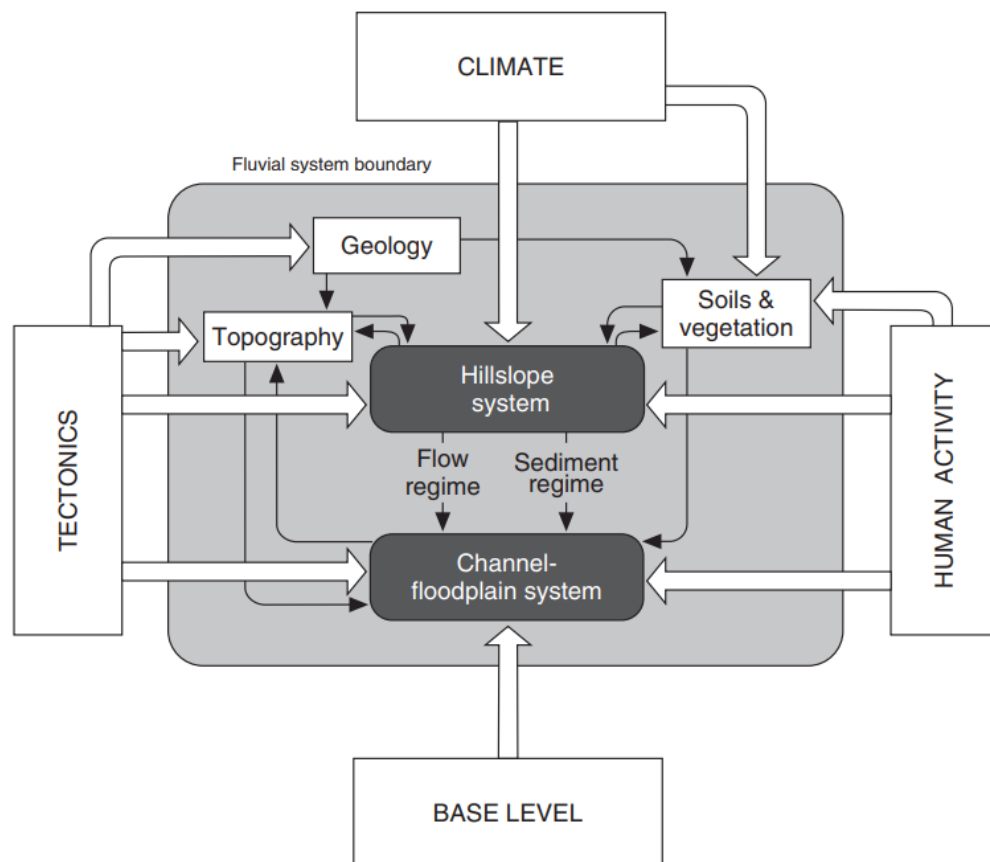
Figure 3   **Simplified representation of the stream system from Charlton (2008, p. 14).**

In the arid southwestern USA, arroyo cut and fill stratigraphy records the complex response and is useful to understand the feedback between the external variables. Studies on arroyos have contributed the cut and fill to climate change and land-use. Early studies hypothesized arroyo incision was caused by human disturbance of plant cover from the introduction of livestock, farming, and roadways (Bryan, 1925; Antevs, 1952). Further investigations studied the cut and fill episodes preserved in the terraces to infer a response to a climatic change (Love and Rhodes, 1979). It was found that a change in the frequency and magnitude of rainfall can initiate arroyo cutting (Leopold et al., 1954; Schumm and Hadley, 1957; Riley et al., 2019). Since land-use change and climatic variations occur simultaneously, it is complicated to disentangle. In the Southwest, large numbers of livestock were introduced around the 1880s which can be correlated to incision of arroyos, yet arroyos are observed in areas that have never been grazed (Peterson, 1950). Womack and Schumm (1977) described a complex cycle of a stream system when high sediment loads produced by channel incision caused aggradation, followed again by incision as sediment production decreases.

While the examples above demonstrate the influence of external drivers such as climate and tectonics changes on stream systems, human modifications of vegetation and land-use also drastically impact streams (Gregory et al., 1995). During the Gold Rush of the late 1800's, many watersheds in western North America were profoundly impacted by placer and hydraulic mining. Gilbert (1917) showed hydraulic mining in river basins of the Sierra Nevada produced abnormally high sediment loads, since the mining caused the release of a large amount of sand and gravel mine tailings in river channels. The rivers were unable to transport the increased load resulting in high amounts of

aggradation in sections of the basin, covering downstream farm fields with packets of sediment from upstream mining (Figure 4). As segments of the river filled, the gradient increased at the downstream extent of aggradation allowing for the river to transport sediment further downstream. Gilbert (1917) found that channel segments stopped aggrading depending on the distance from the source of the sediment and the amount of sediment load. However, Gilbert also discovered that even when mining activity stopped, the downstream reaches continued to aggrade in some reaches. The rivers continue to aggrade because the upstream reaches were no longer receiving the large input of sediment from hydraulic mining and had excess energy to transport sediment that the river had established during mining activity. The upstream reaches incised and transported sediment to downstream reaches which aggraded as the gradient decreased. The remedial action exaggerated the initial aggradation when ceasing mining eliminated the source of the sediment load which resulted in another aggradational event, instead of a remedy to the problem. This second aggradational event is the result of environmental managers not understanding fluvial response and the time it takes for a stream system to reach equilibrium. This study illustrates a channel response caused by a land-use disturbance in which the stream system is aggrading in part and incising in others.

Figure 4   Photo of Sierra Canyon clogged by placer mining debris in 1908 from Gilbert (1917, p. 26).

Alluvial channels respond to natural and human influenced disturbances in a variety of ways. One common model showing a stream channel's evolution after channelization and the series of channel form through time is shown in figure 5 (Schumm and Hadley, 1957; Simon and Hupp, 1986). The model has six stages and the time associated with each stage of the evolution varies between different stream systems and may vary within the same stream system (Schumm et al., 1984, Kondolf and Piegay, 2003). In stage 1, the channel is eroding on the outside of meanders and depositing on the inside. Overall the channel is in equilibrium with sediment being transported into and out of the reach. Then a disturbance is placed on the channel and the system enters stage 2. The disturbance causes degradation in stage 3, resulting in incision and steepened banks. The stream reaches a threshold when the bank height becomes greater than the

critical bank height and material slumps off widening the channel. The channel widening

allows for a decrease in stream power, increase in accumulation space of sediment, and

the channel to enter the aggradation stage. After time the channel is able to reestablish an

equilibrium. The new equilibrium is the goal of stream restoration even though it may not

be the "natural" channel form, but is not degraded and provides beneficial use and

aquatic habitat.

Figure 5 **Schematic of a six-stage channel evolution model from Wohl et al. (2016, p. 106). The six stages are shown in cross section views. The lower box is a longitudinal profile showing the stages of channel adjustment simultaneously along a channel. Light brown shading is valley sediment or bedrock and gray is recent alluvium.**

CHAPTER 3: STUDY AREA

Dry Creek is a perennial tributary of the Boise River in southwest Idaho approximately 16 km northeast of the city Boise. Dry Creek drains from the Boise Foothills to its mouth in Eagle, Idaho located in the Treasure Valley. The study site is 7.5 km upstream of the mouth, above the confluence with Spring Valley Creek (SVC) near the intersection with Highway 55. The drainage area is 97.8 km^2 with elevations from 820 to 2100 meters above sea level.

The upper portion of the watershed is Dry Creek Experimental Watershed (DCEW), an area of long term monitoring of hydrologic and climate data. The study site for this project is downstream of DCEW Lower Gage (LG), which is the outlet of the experimental watershed, and is defined as Lower Dry Creek (LDC). The study area includes 15 km of stream length from 820 to 1000 meters above sea level. Daniels Creek and Currant Creek are the major perennial tributaries to LDC in the study area, however numerous unnamed intermittent tributaries also flow into Dry Creek (Figure 6).

LDC is in a semi-arid climate consisting of hot and dry summers and cold and mildly wet winters. Average annual precipitation in the upper portions of the study area is ~37 cm consisting of a mix of snow in the winter and rain in the spring, summer, and fall. The lower portion of the study area receives ~30 cm of annual precipitation as a mix of rain and snow.

LDC flows through a confined canyon, then becomes less confined with active and historical grazing, and finally into a broad valley with agricultural land and residential development. LDC flows through the planned community of Hidden Springs.

Hidden Springs was established in 1997 and has a population of 2,280 in 2010. In 2020, there is ongoing development of the Cartwright Ranch planned community upstream of Hidden Springs and Dry Creek Ranch downstream.

3.1 Geologic Background

The geology of the Dry Creek watershed consists of two major units; Idaho batholith and ancient Lake Idaho sand and mudstone deposits. The Idaho batholith is a fractured Cretaceous biotite granodiorite (Lewis et al., 1987). The batholith is only exposed in the upper portion of the study area. The Idaho batholith contacts Lake Idaho sediment at approximately 1,100 meters, which was the high stand of the lake determined by oolite deposits (Wood and Clemens, 2002). In the study area, LDC down-cuts through Lake Idaho deposits.

The Treasure Valley, Idaho is an intercontinental rift basin located in the Western Snake River Plain. The valley is a normal-fault bounded, down warped graben with approximately 2-3 km of Neogene sedimentary fill (Wood and Clemens, 2002). The mountains are Cretaceous Idaho batholith, which is separated from the valley by foothills known as the Boise Front. The Western Snake River Plain experienced rapid subsidence early in its formation, which resulted in a large lacustrine system known as Lake Idaho (Othberg, 1994). Lake Idaho dominated the landscape from approximately 9.5 to 1.7 Ma (Wood and Clemens, 2002). During this time, the lake experienced episodes of draining and filling. Major Lake Idaho units have been mapped as the Chalk Hills, Glenns Ferry, and Pierce Gulch formations (Wood and Burnham, 1983; Othberg, 1994; Wood and Clemens, 2002). The oldest unit is the Chalk Hills formation which was deposited before a major draining event at 6.5 Ma. The Chalk Hills formation is a thick noncalcareous mudstone. Above the Chalk Hills formation is the Glenns Ferry formation with the

transgressive Terteling Spring formation. The Glenns Ferry formation is a mudstone with interbedded sands and silts. The Pierce Gulch Sand is a Gilbert-type delta formation with cross-bedded and foreset-bedded sequences overlain by pebble to cobble sized gravels deposited during the draining of Lake Idaho (Othberg and Stanford, 1992).

The timing of the drainage of Lake Idaho is poorly constrained. It is hypothesized that headwater erosion by a tributary of the Columbia River system captured and drained Lake Idaho (Wheeler and Cook, 1954; Wood, 1994, Wood and Clemens, 2002). Dating has constrained the rise, spillover, and fall of Lake Idaho between 6.4 Ma and 1.67 Ma (Wood and Clemens, 2002). The draining of Lake Idaho resulted in a major base-level fall of the Boise and Snake rivers. At least eight terraces are cut into Lake Idaho sediments by the Boise River. Gravels and soils of the Boise River terraces are described by Othberg (1994) and dated using relationships to basalt flows. Pleistocene basalt flows of the Western Snake River Plain are usually thin (~4 meters). The lavas are medium to dark gray olivine basalts with varying sizes and amounts of phenocrysts. Typically, there is a thin deposit of loess covering the surface of the basalt flows that shows an increase in soil development with an increase in age of the flow (Othberg, 1994).

Dry Creek experienced a major base level decline due to the draining of Lake Idaho. Dry Creek has down cut through Lake Idaho sediments to form its current valley; terrace surfaces above the channel record intervals of stability and incision of historic Dry Creek. Terraces along Boise Front streams are not well studied. Birt (2002) measured a suite of terraces in two tributaries (Hulls Gulch and Freestone Creek) and correlated them to terraces of the Boise River. The broad valley of LDC is characterized

by a ~1 km wide by 6.5 km long terrace, named here the Hidden Springs Terrace,
indicating substantial aggradation during the Holocene.

An extensive study by Poulos (2016) describes the soil, asymmetric hillslopes,
and alluvial fans of upper Dry Creek. He found that Boise River incision is more than
double the uplift rate in the basin and concluded base level fall is the main driver of
erosion over the last million years. South facing catchments in DCEW are bigger, less
steep, and more well developed drainages (Poulos and Pierce, 2018). The differences are
related to localized changes in the surface energy balance and temperature due to
insolation. Alluvial fans in DCEW have episodic deposition with a reoccurrence interval
of 200-600 years. Fire is a primary driver of erosion in the mountains of Central Idaho
over the Holocene. Fire return interval in DCEW is 300-400 years in north facing
catchments. Poulos and Pierce (2018) saw an increase in fire activity and fan building
from 900-700 cal yr BP in Dry Creek during the Medieval Climate Anomaly. The
Medieval Climate Anomaly was a time of severe and persistent drought in both North
and South America, as well as variable climate conditions (e.g. Stine, 1994) and
corresponds with major fire-related sedimentation events in central Idaho and
Yellowstone (Pierce et al., 2004).
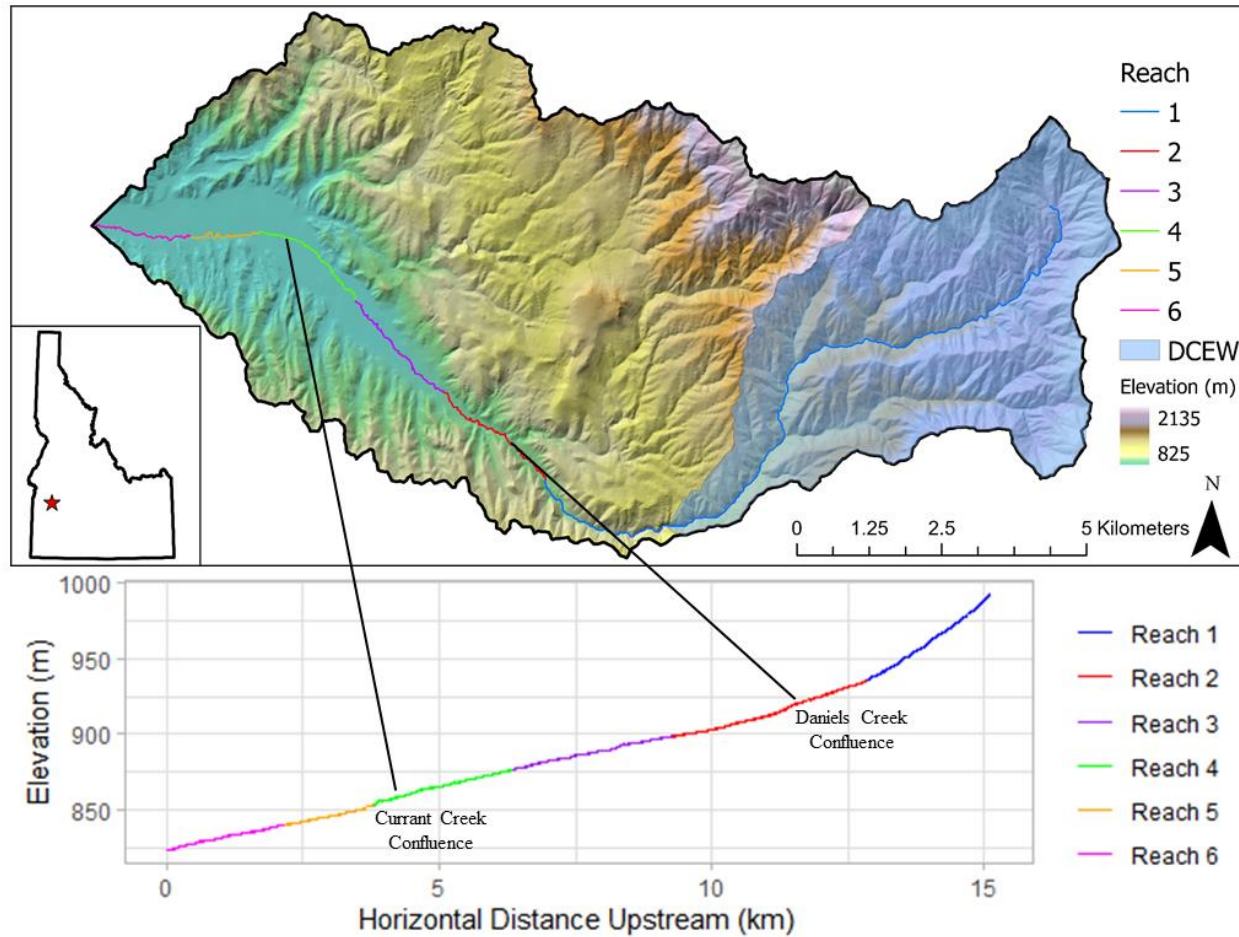
Figure 6 Map showing the Dry Creek watershed north of Boise Idaho and the six distinct reaches of the Lower Dry Creek study area downstream of Dry Creek Experimental Watershed (DCEW). The major tributaries in the study area are Daniels and Currant Creek. The longitudinal profile (bottom) of Lower Dry Creek is measured upstream of the confluence with Spring Valley Creek.

CHAPTER 4: METHODS

We used remote sensing, hydraulic modeling, grain size analysis, and field

observations to quantify how the distinct reaches of LDC are changing over human time

scales; we used Quaternary dating methods and geomorphic mapping to examine how

LDC has changed over centennial to millennial time scales. We compared the

longitudinal profiles of LDC's current channel and terraces to investigate differences

between the long-term geomorphic history of LDC and the current channel. We studied

past land-use in the LDC valley and how it has changed through time. We attempted to

link human disturbances with the modern channel responses we observed. We divided the

LDC study area into six distinct reaches based on gradient, valley confinement, land-use,

and channel characteristics. Reach 1 is farthest upstream and reaches are numbered

sequentially downstream (Figure 6).

4.1 Prior Data

4.1.1 Dry Creek Experimental Watershed

DCEW was established in 1999 to investigate hydrologic processes in a semi-arid

watershed. The watershed is instrumented with meteorological and stream gaging

stations. We used hourly streamflow data from the outlet of the DCEW at LG from 1999

to 2019. LG is located in a step-pool, cascade type reach (Montgomery and Buffington,

1997) with an approximate slope of 0.03 m/m. A Druck water level pressure transducer in

a stilling well measures water stage. A Campbell Scientific logger records data and is

retrieved by site visit or telemetry. Regular site visits are conducted to measure an on-site

staff gage and discharge using velocity-area or dilution methods. A stage-discharge rating

curve is established for the site and is updated annually or sub annually. Additional information regarding DCEW data is found at https://www.boisestate.edu/drycreek/.

4.1.2 Light Detection and Ranging (LiDAR) Data

In the fall of 2015, Quantum Spatial Incorporated (QSI) collected Light Detecting and Ranging (LiDAR) data of the Boise Foothills for the Ada County Enhanced Wildfire Risk Map. The LiDAR survey used a Leica ALS80 system mounted in a Cessna Caravan 208B aircraft. QSI processed the LiDAR data and produced a 1-meter resolution bare earth terrain model. QSI assessed the accuracy of the data using ground survey points and momumentation. The fundamental vertical accuracy of the data is 0.070 meters and the relative vertical accuracy is 0.033 meters.

The LiDAR dataset covers LDC and its tributaries as well as the surrounding topography from Bogus Basin Road to Highway 55 (Figure 7). We used the bare earth digital elevation model (DEM) for terrain analysis and creating a stream longitudinal profile in ESRI's ArcGIS Pro software. Additional technical details of the LiDAR data are found in the Ada Country Enhanced Wildfire Risk Map: LiDAR Technical Data Report (Quantum Spatial Inc., 2015).

4.1.3 Geologic Data

Previous large scale geological studies document the structural geology (Wood and Clemens, 2002), lithology (Wood and Burnham, 1983), and geomorphology (Othberg, 1994) of the Boise Foothills and Dry Creek Watershed. We used the studies as an overview of the geology, but no study has documented the finer scale geology and geomorphology of LDC.
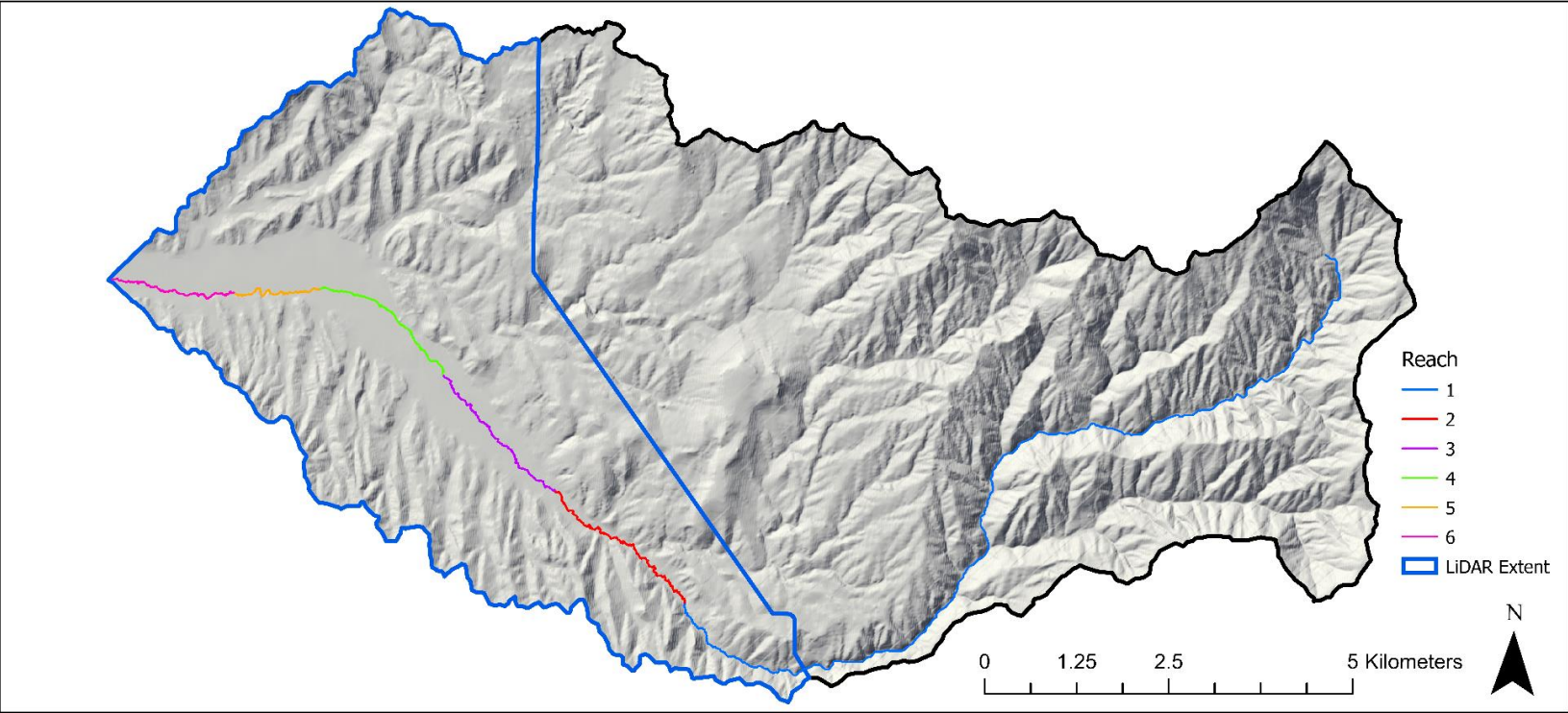
Figure 7   **Map of Dry Creek watershed showing the extent of the 2015 LiDAR dataset.**

4.2 Longitudinal Profile of Lower Dry Creek

4.2.1 Watershed Delineation and Stream Routing

We delineated the LDC watershed from the 2015 1-meter DEM in ArcGIS Pro. The DEM is processed using the fill tool to fill in sinks for routing of water across the terrain. Flow direction of the filled DEM is calculated using the D8 (deterministic eight nodes) method (Martz and Garbrecht, 1992). The flow direction data is used as the input for the flow accumulation tool. A flow line feature is created using flow accumulation cells over 10,000. We used this value because we are concerned with LDC and the main tributaries and not the headwaters of streams. We removed smaller streams from the feature class. The stream is manually checked for deviations from the lowest elevation cell. Around complex terrain, such as bridges and culverts, we manually corrected the stream's flow path.

4.2.2 Longitudinal Profile Extraction

Points were generated every 0.5 meters along the LDC streamline. Horizontal distance starts upstream of the confluence with SVC near Highway 55. The elevation is extracted for each point along the streamline using the pixel elevation value from the DEM. Elevation is plotted against horizontal distance in meters. Slope of the stream is measured using a linear regression best fit line.

4.2.3 Relative Elevation Map

We created a relative elevation map of the LDC Valley. The map displays the height the floodplains, terraces, and hillslopes are above current LDC stream channel. Points were generated along LDC streamline every 2 meters. Elevation data are added to the point features from the DEM. The Inverse Distance Weighting (IDW) tool interpolated the elevation of the points along LDC and created a raster dataset of the

stream elevation for terrain near LDC. The IDW tool used a variable search radius and power of 2. The elevation of the stream is subtracted from the terrain elevation. Relative elevation maps of each reach are available in Appendix D.

4.3 Lower Dry Creek Geomorphic Features Mapping

4.3.1 Preliminary Terrace Mapping

Before field work, we identified potential terrace treads using the 1-meter DEM to aid in efficient mapping. We followed a similar method as Hutchins et al. (2012) used to identify stream terraces in the Appalachian Region. Terrace treads are nearly flat surfaces with adjacent steep terrace risers that represent a period of down-cutting. However, terrace treads represent the paleoslope of the stream and therefore have a gradient. Using ArcGIS Pro we created a slope map from the DEM. The slope surface is reclassified to extract slopes less than 10%. A 10% rise captures all potential terrace surfaces. From reclassification and visual interpretation, we manually delineated terrace surfaces.

Using Natural Resources Conservation Service (NRCS) Web of Soil database, we checked the lithology of the terrace surfaces to determine if the surface's deposit has a fluvial parent material. We removed any surface with a different parent material from investigation. The surfaces with non-fluvial parent material are higher surfaces (greater than 20 meters above current LDC). The purpose of the study is to investigate the Holocene history of LDC, so older, higher surfaces were not mapped or investigated.

We calculated the height of each terrace above current LDC from the 1-meter DEM. Using ArcGIS Pro, we generated a point at the centroid of each terrace. Due to the complex shape of the terraces, the centroid point is forced within the polygon. Elevation of the centroid points is extracted from the DEM. The centroid of each terrace is joined with the nearest point along LDC using the spatial join tool. The elevation of the centroid

is subtracted from the nearest elevation of the stream to calculate the height of the terrace above current LDC.

4.3.2 Hidden Springs Terrace and Profile

The Hidden Springs Terrace is a broad aggradational surface located on either side of LDC where the valley becomes unconfined. It is named here for the residential community on the surface by the same name. The surface is LDC's active floodplain in areas, but is abandoned in other reaches due to stream incision. The surface is extensive and is mapped separate from other terraces of LDC.

We manually delineated the Hidden Springs Terrace in ArcGIS Pro. Contour lines and elevation profiles were used to confirm the surface is continuous. A profile line was created along the Hidden Springs Terrace nearest to current LDC. Points were created along the profile every 0.5 meters and elevation data were extracted from the DEM. The points of the Hidden Springs Terrace profile were joined with the nearest point along LDC using the spatial join tool. The elevation of LDC for each Hidden Springs Terrace profile point were matched with the longitudinal profile of LDC elevation. The horizontal stream distance were added to the Hidden Springs Terrace profile data frame. Due to sinuosity differences between LDC and Hidden Springs Terrace profile, some horizontal distance locations had multiple matching Hidden Springs Terrace points. Using R's group-by function we calculated the mean elevation of points with the same horizontal distance. The Hidden Springs Terrace profile was then plotted against the longitudinal profile of LDC. Finally, we calculated the amount of incision between the Hidden Springs Terrace and LDC.

4.3.3 Field Mapping, Soil Pits, and Terrace Height Surveying

Field mapping of recent geomorphic processes was conducted during the summer of 2019. Using the preliminary terrace map, 15 terrace locations were selected for further investigation. The terraces ranged from 0.6 to 7.5 meters above bankfull of LDC. We dug a soil pit at each terrace location. The purpose of the pits were to investigate the parent material of the terrace and soil development to use in conjunction with height above LDC to correlate terrace surfaces.

At each pit location a GPS location is recorded. The pit is dug until an obvious C-horizon is reached, usually less than 1 meter. Soil horizons and original bedding were flagged where visible. We collected samples for each layer. Where horizonation and bedding isn't visible, we collected samples every 10 cm. We recorded the moist color, consistency, hand texture, and soil structure for each sample. We measured the height above bankfull using a stadia rod and eye level. We visually correlated the terrace to surrounding surfaces that were not measured to check the accuracy of the DEM measured terrace heights.

Additional geomorphic information is mapped while in the field. We mapped major alluvial fans and separated fan terraces from the fill terraces. In addition we mapped the location of large cobble piles of placer mining tailing deposits.

4.3.4 Limitations of Mapping

The geomorphic mapping of this project purpose is to provide evidence of past aggradation and incision of LDC to compare with the streams behavior since humans changed the landscape. The mapping is a reconnaissance study and the geomorphology mapped is not comprehensive. Further work including surveying terrace heights, soil

characterization, and additional dating is needed to more accurately correlate the terraces of LDC. Geomorphic maps of each reach, photos of soil pits, and descriptions of soil characteristics are available in Appendix B.

4.4 Quaternary Dating

4.4.1 Radiocarbon Dating

Radiocarbon dating is a method to estimate the age since living organisms died. When an organism dies, the carbon-14 of the organism radiometrically decays into nitrogen through beta decay. Charcoal is a common substance used for radiocarbon dating and provides both an age for a deposit and evidence of fire. Assuming the charcoal is deposited in the sediment shortly after the burn, the age of the deposit is estimated from radiocarbon dating.

We selected a well-exposed streambank in incised Reach 5 of LDC for radiocarbon dating. Dating the exposure provided an aggradation rate of the Hidden Springs Terrace and a maximum age of incision. We measured and described the exposure's bedding. We collected sediment samples from each layer. Where charcoal is found, we measured the depth from the bank's surface. The charcoal samples were collected wearing nitrile gloves and placed in a plastic bag for transport.

We cleaned the charcoal samples with deionized water to remove sediment. The samples were dried for 24 hours. Roots and other modern carbon sources were removed using a microscope and forceps. The cleaned charcoal samples were mailed to Lawrence Livermore National Laboratory (LLNL).

LLNL prepared and processed the charcoal samples. Accelerator mass spectrometry measured the concentration of carbon-14 and stable carbon isotopes. Results are quoted in radiocarbon years using the Libby half-life of 5568 years.

Additional laboratory data from LLNL is provided in Appendix C. Calib Rev 7.0.4

radiocarbon calibration program (Stuiver and Reimer, 1993) converted the radiocarbon

years to a calibrated years Before Present (cal yr BP) or Anno Domini (AD) age. We

used the IntCal13 calibration dataset (Reimer et al. 2013).

4.4.2 Optically Stimulated Luminescence Dating

Optically stimulated luminescence (OSL) is a Quaternary dating technique which

measures the last time quartz sediments are exposed to light. During deposition, the

luminescence signal is reset. After deposition, the sediments are removed from light

sources and exposed to low levels of natural radiation from surrounding sediment. Quartz

minerals accumulate a luminescence signal as electrons from radiation become trapped in

defects in the crystal lattice (Aitken, 1998). In the laboratory, sediments are stimulated

and electrons in the crystal lattice are released. The luminescence is measured and

converted to an age using the dose equivalent. The dose equivalent is calculated using the

single-aliquot regenerative (SAR) method (Murray and Wintle, 2000). The age of the

sample is calculated by dividing the equivalent dose by the environmental dose rate of the

sediments surrounding the sample.

We collected OSL samples from two streambank deposits at the Peggy's Trail

site. Dating these deposits we hoped to constrain the timing of incision and aggradation

upstream of the Hidden Springs Terrace. We collected samples in aluminum tubes.

Depth, elevation, and latitude/longitude were noted for calculations of cosmic

contributions. We collected a representative sample for determining water content and

dose rate from within 30 cm of the sample tube. Samples were processed by Utah State

University Luminescence Laboratory (USULL).

All samples were opened and processed under dim amber light conditions at USULL. Samples were sieved to a grain size of 90-150 or 150-250 microns. Samples were treated with HCl and bleach to remove carbonate and organic material. Quartz sediments were separated using heavy mineral separation at 2.72 g/cm^3. USULL followed the SAR procedure to calculate the dose equivalent at three to five different doses. The data were fit with a linear or saturating exponential curve used in the Central Age Model (CAM) or the Minimum Age Model (MAM) (Galbraith and Roberts, 2012). Environmental dose calculations were determined by chemical analysis of U, Th, K, and Rb content using ICP-MS and ICP-AES techniques and conversion factors from Guerin et al. (2011). The OSL ages were calculated by dividing the dose equivalent by the environmental dose rate and a 2σ standard error is reported. Laboratory report from USULL is available in Appendix C.

4.5 Streambed Grain Size Analysis

Streambed grain size distributions were measured at three locations from each of the six reaches of LDC. All samples were collected from riffles. It is good practice to sample from riffles to collect a representative grain size the stream moved in higher energy environments during recent flood events. Reach 1 and 2 were accessible only by foot or bike and the sediment size is too large to collect a representative sample for the laboratory. Reach 3, 4, 5, and 6 have easy access and some reaches have fine-grained sediments, which makes a laboratory sieve analysis more representative. Samples were measured from each location then combined for a reach average. A map showing the sample locations and photos of each sample location is available in Appendix E.

For Reach 1 and 2, a Wolman pebble count (Wolman, 1954) was used to measure the grain size distribution of the bed substrate. At each sample location, we collected GPS

coordinates to add the data to the longitudinal profile. Working from bank to bank, a fist sized spacing is used to randomly select a sediment. Each sediment's intermediate or b-axis is measured to the nearest millimeter. If a sand sized particle ($< 2mm$) is selected it is recorded as 2mm. This process is repeated until 100 sediments including sand were measured and the sampler completed the transect to the other streambank. If 100 sediment were not measured on a single transect, the sampler moved upstream and selected a new spacing interval and repeated until 100 sediments are counted. Sediments were divided into bins and percent finer is plotted against grain size on a semi-log plot. The median grain size (D_{50}) is calculated using a linear relationship between the two adjacent points on the grain size distribution plot.

Samples from Reach 3 to 6 were collected in the field and measured in the lab. We collected sediment from a single transect using a shovel. The samples were split and placed into a 1-gallon plastic bag. In the lab, we split the sample until the sample is approximately 1000 grams. The sample is shaken through a series of sieves for 15 minutes. We measured the material retained on each sieve. Percent finer is plotted against grain size on a semi-log plot and the D_{50} is calculated using a linear relationship between the two adjacent points on the grain size distribution plot.

4.6 Aerial Imagery Analysis

4.6.1 Georeferencing Aerial Imagery

The Boise State University Library Special Collections Department scanned high-resolution historic aerial imagery of the LDC study area from September 1938, September 1951, and July 1971. Two images from 1938 cover the study area except Reach 6. One image from 1951 covers Reach 3 to 6. Two images from 1971 cover the entire study area.

We georeferenced the 5 images using ArcGIS Pro. The images were referenced to 2019 National Agriculture Imagery Program (NAIP) aerial imagery. Identical features were selected on the historic and current imagery. Features included trees, bushes, rocks, buildings, roads, etc. We selected forty controls points on each image for georeferencing. The steep topography of the watershed caused difficulty for a first or second order polynomial transformation. Instead, we used a spline transformation. A spline transformation is a piecewise polynomial that optimizes for local accuracy around the control points. Spline transformation matches the control points exactly; however, the pixels away from the control points are not guaranteed to be accurate. We used forty controls points around LDC to increase the accuracy. We assessed the accuracy of the georeferencing by measuring the distance between two features in the referenced and 2019 NAIP imagery.

4.6.2 Other Aerial Imagery Sources

In addition to the 1938, 1951, and 1971 imagery, we used other publically available aerial imagery. We used the United States Geological Survey (USGS) Digital Orthophoto Quadrangles (DOQs), which removes image displacement caused by terrain relief and camera tilt. DOQs of the study site are from June of 1992 and July of 1998 and has a 1-meter resolution. We used USGS high resolution natural color orthorectified imagery of the Boise Valley from April 2003. The imagery has a 0.3 meter resolution and was collected for urban and county planning. In addition, we used NAIP imagery from June 2011 and July 2019. The 2011 imagery has a 1-meter resolution and the 2019 imagery has a 0.6 meter resolution.

4.6.3 Measuring Meander Migration Rates

We measured the distance the stream is laterally migrating using aerial imagery. Each reach except Reach 2 appeared laterally stable and we were unable to measure lateral migration. We were not able to delineate the banks of LDC because of its small size and abundant riparian vegetation. In Reach 2 we selected 10 meanders that are visible and have a distinct meander shape. We selected the meanders using the 2019 imagery. A point is created in the center of the stream at the crest of the meander wave. We created a point for each imagery year. We measured the distance the stream moved using a straight line distance between the two points. We calculated a rate of lateral meander migration using

$$Lateral\ meander\ rate = \frac{Distance\ between\ meander\ crest}{(Year - Year\ Prior)}$$

Rates are presented in meters per year. Figure 8 shows the stream centerline delineation and points used to measure the meander rate.

4.6.4 Land-use and Riparian Width Index

Recent growth (post-1997) in the Treasure Valley, Idaho converted LDC's expansive floodplain from farmland to housing development. Most of the recent development and historic and current farmlands, are on the broad, low gradient Hidden Springs Terrace. We documented the land-use from 1938 to 2019. We classified land-use into six categories (Table 1).

Table 1 **Description of land-use categories.**

Land-use	Description
Farmland	Land that is irrigated, plowed, planted, or grazed in a confined area.
Grassland	Land that is sagebrush steppe, and is unaltered except trails, roads, and open space grazing.
Rural Development	Land with 5 homes or less in 1,000 m^2 and fields not used for agriculture that are adjacent to the homes.
Residential Development	Land with more than 5 homes in 1,000 m^2, bare ground prepared for building, parks, streets, and other community areas built for residents.
Riparian Vegetation	Land with riparian vegetation adjacent to the stream.
Other	Land with all other land-use including wetlands.

We delineated land-use for the valley adjacent to LDC in Reach 3 to 6 and included portions of the hillslopes in Reach 1 and 2. Reach areas are separated by a perpendicular line across the valley at the end of the reach. Examples of land-use designations are shown in figure 9. Six researchers delineated land-use. We conducted a formal training for the researchers to show the distinctions between the land-use categories. After the training, each researcher delineated land-use for three designated areas of complex land-use. Results were compared to determine if the analysis of each individual is similar.

We analyzed land-use for imagery from 1971, 1992, 2003, 2011, and 2019. We analyzed riparian vegetation area for imagery from 1938, 1951, 1971, 1992, 1998, 2003, 2011, and 2019. Delineation is completed at a 1:750 scale. Area of each land-use is measured and presented as a percentage of the total reach area. Riparian vegetation is

presented as a riparian vegetation index in meters, which is the area of riparian vegetation

for the reach divided by the stream length in the reach.
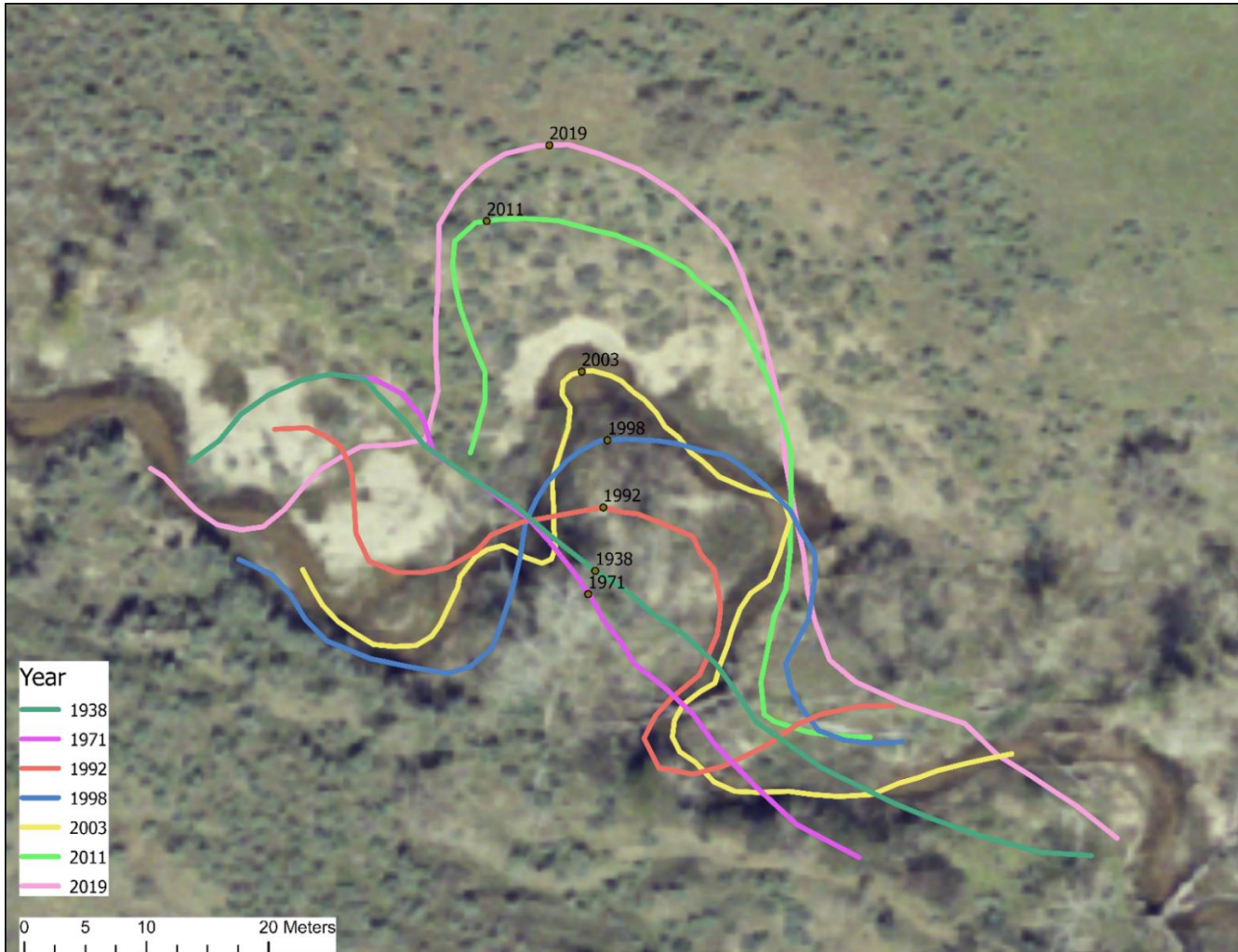
Figure 8 Aerial photo from 2003 showing meander number 2 channel delineation for each imagery year and the point at the crest of meander used to measure the meander movement.

Figure 9　　Examples of the six land-use classification from the 2003 imagery. The other land-use in the image is a drainage ditch. Land that is being prepared for development in the lower right corner is classified as residential development.

4.7 HEC-RAS Hydrologic Modeling of Lower Dry Creek

The U.S. Army Corps of Engineers' Hydrologic Engineering Center River Analysis System (HEC-RAS) is a computer software program that performs one-dimensional steady flow hydraulics. HEC-RAS steady flow analysis is capable of modeling subcritical, supercritical, and mixed flow regime water surface profiles (Brunner, 2010). HEC-RAS is based on the solution to the one-dimension energy equation with energy losses by friction (Manning's equation) and contraction/expansion (coefficient multiplied by the change in velocity head). HEC-RAS utilizes the momentum equation where the water surface profile rapidly changes and the energy equation is not considered applicable. HEC-RAS estimates the average boundary shear stress with a relationship to the drag coefficient determined from the Chezy equation (Brunner, 2010). HEC-RAS one dimensional steady flow has the following assumptions:

1. Flow is steady

2. Flow is gradually varied (except at hydraulic jumps, where the momentum equation is used)

3. Flow is one-dimensional

4. River channels have less than 1:10 slopes

We used HEC-RAS to estimate water surface elevation, depth averaged water velocity, and shear stress on a per cross-sections basis for each reach of LDC. We looked for changes in the flow characteristics which we related to the land-use and channel changes we observe. We are using the outputs of the model as an estimate. Additional field data is need for calibration and validation of the model. To model LDC hydraulics we needed the following inputs:

1. Cross section and terrain data

2. Boundary conditions

3. Bankfull flow

4. Stream bed roughness (Manning's n)

4.7.1 Cross Section and Terrain Data

In the summer of 2019, we surveyed five cross sections using an automatic level and stadia rod. We chose cross section locations based on line of site for surveying and access. Three cross sections are in Reach 3; one cross section in Reach 4, and one cross section in Reach 5. We recorded GPS locations in the center of the stream at each cross section location. The GPS accuracy is less than 5 meters. We strung a measuring tape across LDC perpendicular to flow. The tape extended from each bank's highest terrace surface. We measured the height of the stadia rod to the nearest hundredth of a foot using the automatic level. Spacing between measurements varied from 0.5 ft (0.153 m) in the stream and 1-2 ft (0.305-0.610 m) on the stream banks.

We created a cross section in ArcGIS Pro using the 2015 LiDAR DEM at the survey GPS location. We extracted elevation from the DEM every 0.5 m along the cross section profile. Horizontal distance is plotted against elevation to show the channel shape.

The field survey data has no elevation because there were no survey benchmarks near the survey locations. We calculated the elevation for the field survey cross section by making the lowest survey point the same elevation as the LiDAR cross section. The field survey and LiDAR DEM cross sections were compared for viability of using the DEM for the stream channel geometry in the HEC-RAS. We calculated the coefficient of determination (R^2) as the variance the LiDAR DEM cross section is to the field measured

cross section. The plots comparing the field survey and the LiDAR derived cross sections are available in Appendix F.

4.7.2 Dry Creek Experimental Watershed Lower Gage Flood Frequency Analysis

DCEW LG measures hourly streamflow leaving the experimental watershed and entering the LDC study area since 1999. We calculated a mean daily flow for LG from 1999 to 2019 for each day data is available. We used peak flow for each year of data for flood frequency analysis of the watershed. We estimated bankfull flow for this project as the 2-year return period flow or the flow that has a 50% chance of occurring.

We calculated the 2-year flow from LG using a Log-Pearson Type III distribution. The Log-Pearson Type III distribution is the recommended statistical technique for fitting frequency distribution data for flood frequency analysis (Interagency Advisory Committee on Water Data, 1982). The Log-Pearson Type III distribution is calculated using:

$$\log x = \overline{\log x} + K\sigma_{logx}$$

where x is the annual peak discharge, $\overline{\log x}$ is the average of the $\log x$ discharge values, K is the frequency factor, and σ is the standard deviation of the $\log x$ values. The frequency factor K is a function of the skewness coefficient and the return period and is found using the frequency factor table.

4.7.3 Lower Dry Creek Stream Gages

We installed a stream gage in LDC's Reach 5 on March 18, 2019. We installed the gage in an area where there is limited turbulence from streamflow and will not dry during baseflow. An Odyssey capacitance logger is installed in a two inch stilling well. The two inch stilling well is set within a 4 inch PVC pipe with holes drilled to add

hydraulic connection to the gage. The entire stream gage is anchored to the streambed and a staff gage is attached to the outside for field water level measurements.

We measured stream discharge at the LDC gage location for various water levels. We measured discharge using the velocity-area method following USGS guidelines (Turnipseed and Sauer, 2010). A Marsh McBirney 2000 flow meter is used for stream velocity measurements. We made six discharge and stage measurements before the streambank near the gage failed on May 3, 2019. An additional four discharge and stage measurements were collected after the bank failure. After July 17, 2019, beaver activity caused ponding at the gage and no additional measurements were recorded. We created two rating curves using a power regression. One rating curve is for high flows before the bank failure and the other is for low flow conditions after the bank failure. We calculated hourly discharge of LDC using stage measurement from the capacitance logger and the associated rating curve.

USGS stream gages were located on SVC and on LDC below the confluence with SVC (Figure 10). Stream discharge was measured at both USGS gages from March 2010 to October 2012 at 15-minute intervals. SVC is the only tributary between the USGS gage on LDC and this project's gage installed in Reach 5. Discharge for the USGS SVC gage is subtracted from the USGS gage on LDC for a discharge of LDC above the confluence with SVC. We computed a daily average flow.

Discharge is plotted for each day there is data from DCEW LG against discharge from USGS gage and LDC gage. We fit a linear regression to the data. Using the regression equation we inputted the 2-year discharge for DCEW LG and estimated a 2-year discharge for LDC below Daniels Creek, the major tributary.

4.7.4 Setup of Model Reaches and Cross Sections

We used ArcGIS Pro to create streamline, flow paths, and cross sections for

terrain input in the HEC-RAS model. All terrain data used the 2015 DEM described

earlier. The streamline of LDC is the same as used in the longitudinal profile and is

divided into the six reaches. We manually delineated flow paths along the stream on each

bank. Flow paths allows HEC-RAS to compute different flow lengths for each side of the

stream. We manually delineated cross sections perpendicular to the stream and flow paths

every 20-30 meters. Cross sections vary in length to cover the full extent of inundation.

We setup the stream geometry using RAS-Mapper, HEC-RAS's GIS software.

We imported the 2015 DEM with all stream shapefiles. Additional cross sections were

interpolated, so the maximum spacing between cross sections is 5 meters. We added

terrain data to the cross sections using the interpolate cross section tool in RAS-Mapper.

We modeled each reach separately with boundary conditions upstream and downstream.

We used a normal depth boundary condition. The slope of the upstream and downstream

is measured from the DEM using a 50 meter section of stream. We used the stream slope

as the input for the normal depth boundary condition.

HEC-RAS requires a Manning's n roughness for each cross section. Roughness

varies along LDC and changes with depth. The floodplain has a higher Manning's n than

the stream channel. However, we are concerned with bankfull flow, or the flow that fills

the channel to the top of the banks (Williams, 1978) and therefore we only need a

channel roughness. LDC has a variety of channel condition throughout the reaches

including straight, meandering, deep pools, and instream vegetation. We set the

Manning's n at 0.065 for all cross sections as an average of the conditions we observed

(Chow, 1959). We ran the model again with a low Manning's n of 0.03, which is representative of a straighter channel with limited instream vegetation and pools. Then we ran the model with a high Manning's n of 0.1, which is representative of a sluggish stream with pools and instream vegetation.

4.7.5 Outputs and Assumptions

We ran the HEC-RAS model for each reach using 1.13 m³/s discharge above Daniels Creek and 1.42 m³/s downstream. We ran each reach's model three times with a Manning's n of 0.03, 0.065, and 0.1. The three model runs provided a range of model outputs for the different channel condition present in LDC. We manually processed each cross section's result and removed any that appeared not perpendicular to the flow or inaccurate. Outputs used for this study are channel velocity, flow area, wetted perimeter, hydraulic radius, max depth, stream power, and shear stress. Results were averaged for the reach for each model run.

The purpose of using the HEC-RAS model is to analyze changes to the hydraulics in each reach. We have not calibrated or validated this model and in its current form is not appropriate for flood hazard modeling or instream structure analysis. Our model has the following assumptions:

1. Cross section and slope from the DEM is representative of the channel complexity of LDC.

2. 2-year discharge estimate is representative of LDC bankfull flow.

3. Discharge doesn't change in LDC except at Daniels Creek.

4. Manning's n estimates are representative of LDC and do not change between reaches.

By keeping Manning's n and discharge constant throughout LDC, we were able to analyze how width and depth change in each reach. It also allows for comparison of stream power and shear stress under the same conditions. Additional field data are needed to calibrate and validate the model; however, we believe the 1-meter resolution DEM is appropriate for HEC-RAS modeling of a stream of LDC size. Maps of water depth and velocity from the model are available for each reach in Appendix G.
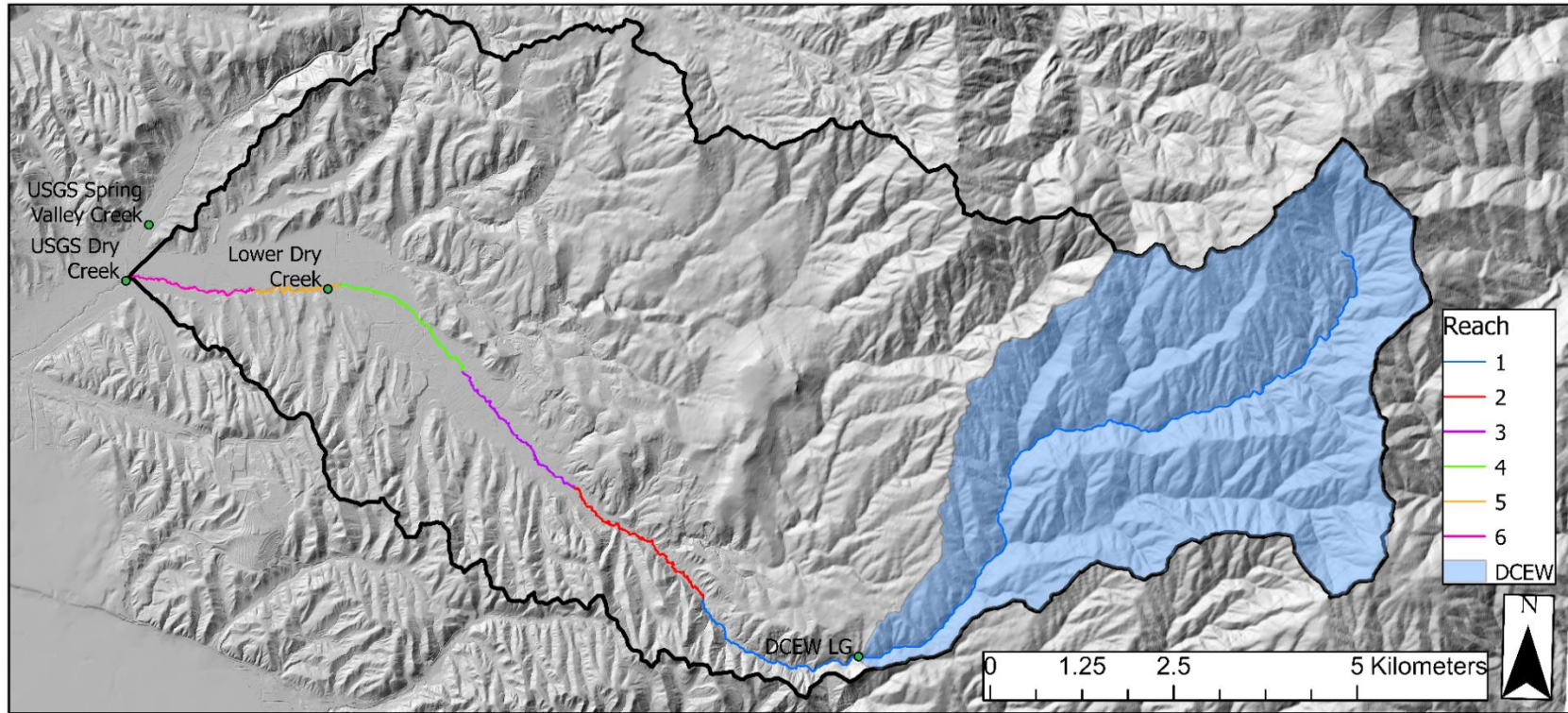
Figure 10 **Map of Dry Creek watershed showing locations of stream gaging stations. Dry Creek Experimental Watershed Lower Gage (DCEW LG) is a long term monitoring site with record of discharge since 1999. For this project we installed the Lower Dry Creek gage and used stream discharge from spring of 2019. The USGS gage sites at Dry Creek and Spring Valley Creek both have records of discharge from 2010 to 2012, which allowed us to subtract the discharges to have comparable flows to this project's Lower Dry Creek gage.**

CHAPTER 5: RESULTS

5.1 Rationale of Lower Dry Creek Reach Division

The quantitative characteristics of the six reaches of LDC are located in Table 2; key defining features of each reach are described below. Reach 1 is steep, dominated by step pools and is gravel bedded. Reach 1's valley is v-shaped and confined. Land-use is limited to cattle grazing and hiking trails. Reach 2 is divided where the valley widens. Reach 2 has high sinuosity and a suite of terraces. A distinct feature of Reach 2 is four placer mining deposits located on the floodplain and terraces of LDC. Placer mining ceased prior to 1938 and since then the land-use in Reach 2 is grazing and hiking trails. Reach 3 begins where the valley becomes unconfined allowing for accumulation space of the broad Hidden Springs Terrace surface. Reach 3 has lower sinuosity than Reach 2. Land-use in Reach 3 was dominated by agriculture until 1997, when farmland was converted to residential development. Today, Reach 3 consists of 22.5 percent farmland and 59.4 percent residential development. Reach 4 channel characteristics are similar to Reach 3, but is distinguished by its convex longitudinal profile. Also, Reach 4 is less entrenched relative to the Hidden Springs Terrace surface than Reach 3. Land-use in Reach 4 follows the same trend as Reach 3, but with more rural housing. We divided Reach 5 where LDC is incised and not connected to the Hidden Springs Terrace surface. Land-use in Reach 5 is currently farming and rural housing. We divided Reach 6 where the stream widens and becomes less incised below the Hidden Springs Terrace surface. Land-use in Reach 6 has historically been farming, but there is ongoing residential development. Representative photos of each reach are in Appendix A.

Table 2   **Summary of the characteristics of the six reaches of Lower Dry Creek.**

	Reach 1	Reach 2	Reach 3	Reach 4	Reach5	Reach 6
Length (km)	2.26	3.60	2.91	2.57	1.62	2.16
Sinuosity	1.18	1.47	1.30	1.18	1.36	1.37
Slope (%)	2.46	1.08	0.76	0.86	0.76	0.76
Hidden Springs Terrace slope (%)	NA	0.07	0.83	0.82	0.72	0.83
Average depth below Hidden Springs Terrace (m)	NA	5.10	2.61	1.36	4.74	2.42
Upstream drainage area (km^2)	29.1	48.4	51.0	86.7	88.3	97.8
Average width bankfull flows (m)	4.6	6.8	9.5	11.6	5.5	11.5
Average max depth bankfull flows (m)	0.46	0.56	0.61	0.59	0.68	0.54
Median grain size (mm)	22	29	2	2	18	7
Average boundary shear stress (N/m^2)	62.9	31.1	21.4	24.9	28.7	20.9
Critical shear stress for median grain size (N/m^2)	15.3	20.3	1.7	1.1	12.7	4.6
Riparian width index in 2019 (m)	18.0	20.2	28.2	26.8	20.7	28.5

NA = Not Available

Reach 1 and 2 grain size measured using Wolman pebble count. Reach 3 to 6 measured using sieve analysis.

Average width, max depth, and boundary shear stress calculated from HEC-RAS model using estimated bankfull flow and Manning's n of 0.065.

Critical shear stress calculated using shields criterion of 0.045 and sediment density of 2.6 g/cm^3.

5.2 Geomorphic Features of Lower Dry Creek

We mapped 184 terrace surfaces in the LDC study area. Terrace heights varied from 0.34 meters to 8.7 meters above current LDC. We correlate the terrace based on height above LDC into four terrace levels (Figure 11). The T1 terrace is the lowest and contains all terraces less than 2 meters above the current channel. The T2 terrace is terraces greater than 2 meters and less than 4 meters above current LDC. The T3 terrace is terraces greater than 4 meters and less than 6 meters above current LDC. The T4 terrace is terraces greater than 6 meters above current LDC.

We sampled 15 soil pits on terraces of various heights (Figure 11). All soil pits have a fluvial parent material C-horizon at various depths. Soil pits on terraces higher above current LDC have a thicker, more developed A-horizon. The T1 soil is poorly developed with an A-horizon thickness of 4-15cm. The T1 terraces have fine-grained over bank deposits and channel sands and gravels with no B-horizon. The T1 terrace is exposed throughout all reaches in LDC. The T2 is mostly exposed in a 3.5 km section of Reach 2. The T2 terraces have a thicker (20-50cm) A-horizon than T1. Vegetation on T2 varies from riparian to upland sagebrush and native grasses. The T3 terrace is also exposed along Reach 2, but is less continuous than T2. Soil is more developed with 30-50 cm thick A-horizon and in a few pits a weakly developed color B-horizon. Vegetation on T3 is upland sagebrush and grasses. The T4 terrace is exposed along a 0.5 km section below a large creep landslide. The T4 terrace A-horizon is the most developed with a thickness of 60cm. A color B-horizon is observed on the T4 terrace. The T4 terrace receives input from alluvial fans and has a sandy-loam texture. The T4 vegetation is grasses and receives heavy grazing traffic. We didn't observe evidence of cut and fill in

the terrace soil pit stratigraphy. Photos and descriptions of the terrace soil pits are in Appendix B.

We mapped seven alluvial fans in Reach 2 (Figure 11). We found four of the alluvial fans have fan terraces at the toe. We mapped four placer mining deposits in Reach 2 (Figure 11). The deposits are large granitic and basalt cobbles placed in piles. We observed channels for diverting water and cuts into the hillside where material was removed. Fine-grained material was removed from the piles during mining (Figure 12).

The purpose of the geomorphic mapping is to provide evidence of past aggradation and incision of LDC to compare with the streams behavior since humans changed the landscape. The mapping is a reconnaissance study and the geomorphology mapped is not compressive. Terraces in Reach 1 and 2 are mapped and correlated based on height above the current channel. Due to rapid changes observed in LDC, correlation based on height above the current channel is problematic. Therefore, further work is needed to more accurately correlate the terraces of LDC.
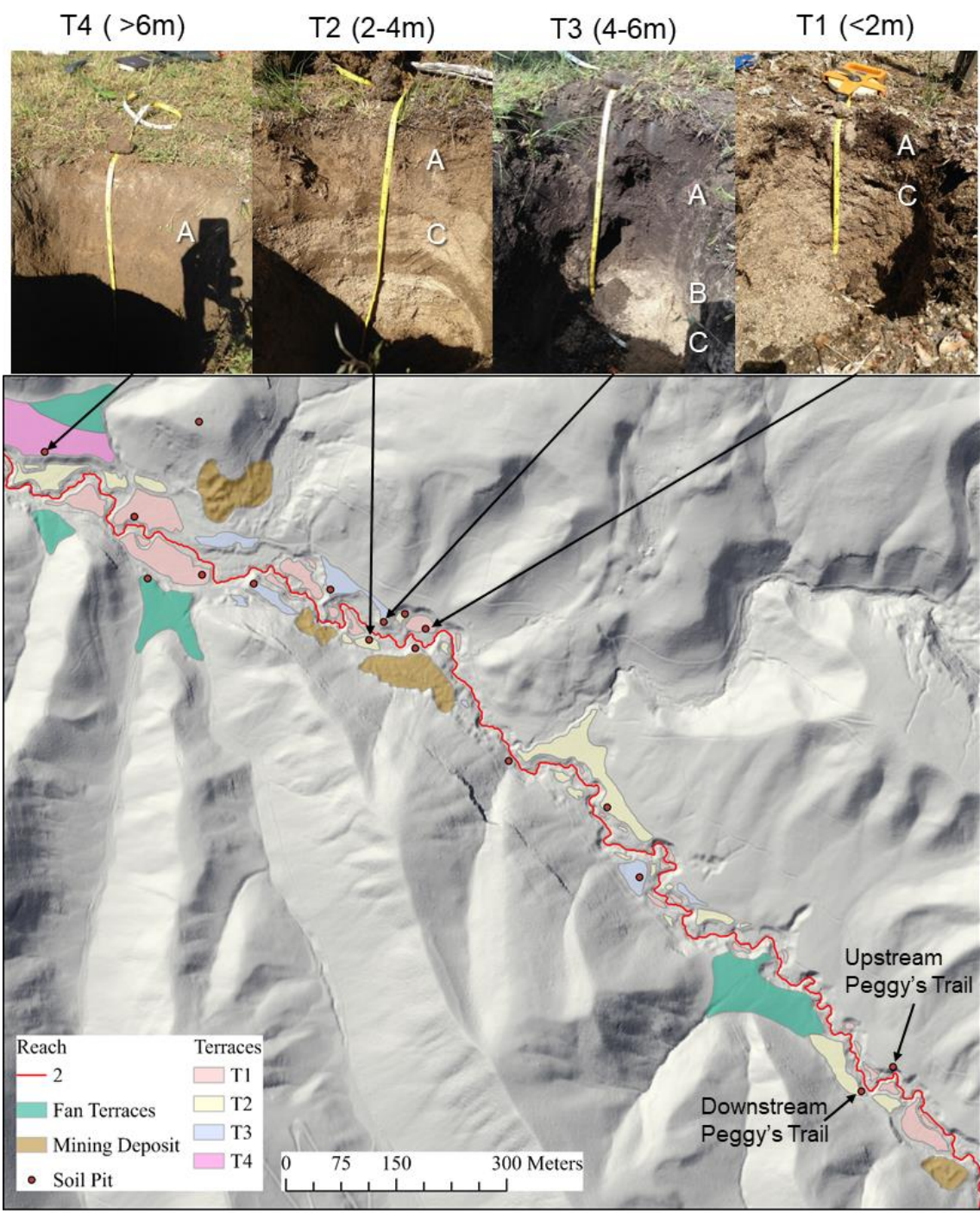
Figure 11 **Geomorphic map of Reach 2 of Lower Dry Creek. Terraces are mapped and correlated based on height about the current stream. T1 is the lowest terrace and T4 is the highest terrace surface mapped. Representative photos of soil pits from terrace height show younger soils on the lower terraces. A, B, and C soil horizons are labeled where visible. The map shows the location of the upstream and downstream sample locations of the Peggy's Trail site (Figure 15).**
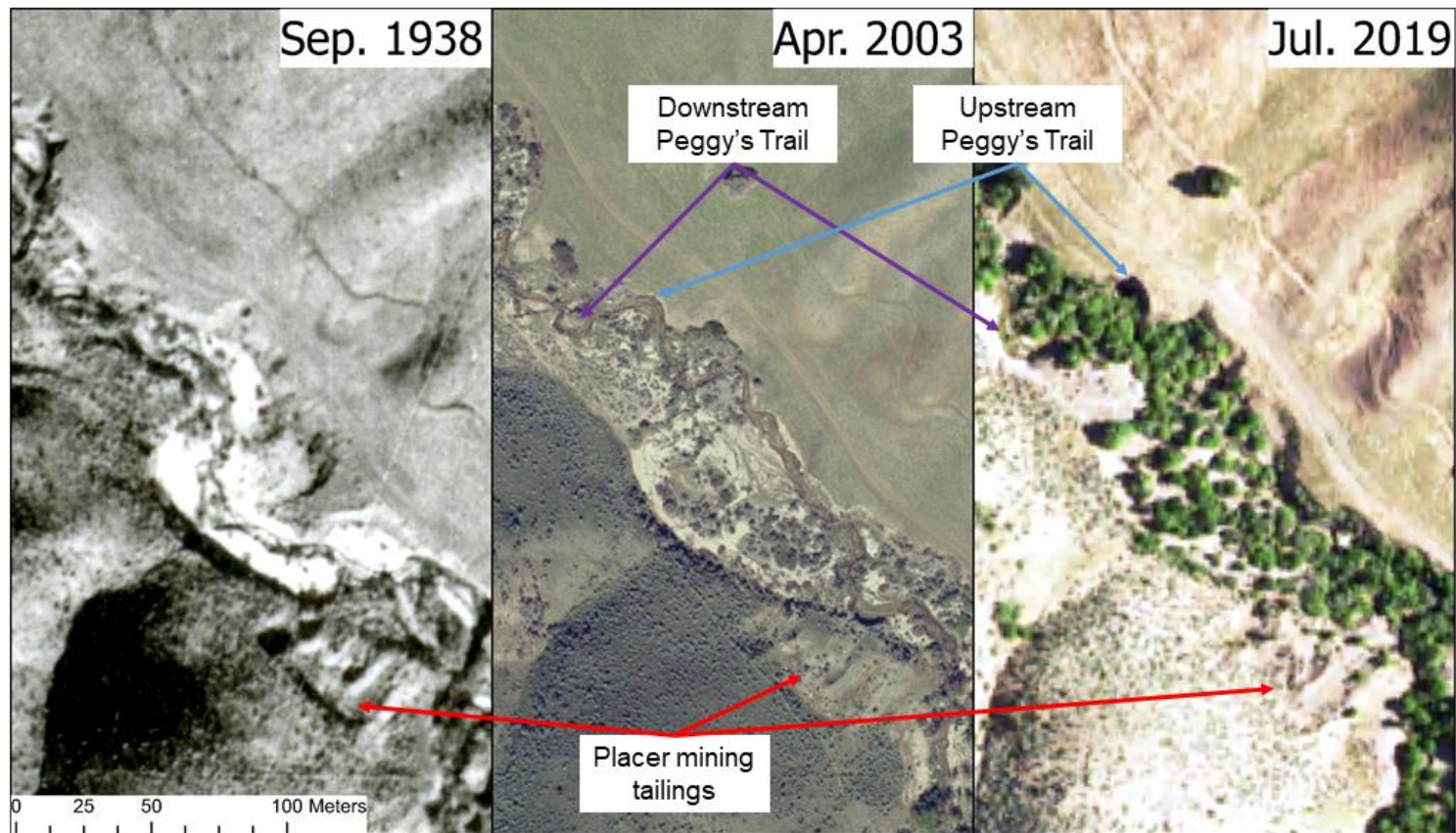
Figure 12   Aerial photos from September 1938, April 2003, and July of 2019 showing a placer mining tailings deposit and the location of the Peggy's Trail stratigraphy site. The red arrows show the location of one of the four placer mining deposits mapped. Observe the channels used for diverting water and cuts into the hillside where material was removed. Fine-grained material was removed from the piles during mining and left large granitic and basalt cobbles. The blue arrows show the location of the upstream bank of the Peggy's Trail site described and dated (Figure 15). The purple arrows show the location of the downstream bank. Observed the amount of meander movement which cut into the T2 terrace between 1938 and 2019, exposing the stratigraphy.

5.3 Quaternary Dating Results

We dated charcoal and sediments exposed in streambank stratigraphy in order to assess longer-term records of channel incision and aggradation in Lower Dry Creek. A well-exposed streambank in Reach 5 of LDC provides an aggradation rate of the Hidden Springs Terrace and a maximum age of incision.

In Reach 5, a well exposed streambank shows the stratigraphy of the Hidden Springs Terrace (Figures 13 and 14). The upper 30 cm is a moderately developed A-horizon. Below the A-horizon is a complex sequence of fine-grained overbank flood deposits, channel gravels, and debris flows. From 30 cm to 125 cm is a sequence of alternating overbank flood deposits and sand and channel gravels. Below, from 125 cm to 139 cm is a dense debris flow deposit with floating sub-angular gravels. Below 139 cm is unconsolidated sand and gravel, with a few thin lenses of fine-grain sediment. Charcoal is abundant throughout the upper 3 meters. We sampled six pieces of charcoal. We radiocarbon dated the highest (DC-1-1 at 65cm depth) and the lowest (DC-1-18 at 295 cm depth) samples. The sample nearest the Hidden Springs Terrace surface (65cm depth) yields a modern ^{14}C age, which is equivalent to 1950 AD or younger. The radiocarbon date for the lower sample (295 cm depth) is 285 ± 25 ^{14}C years which is equivalent to 426-392 cal yr BP (1524-1558 AD) or 319-298 cal yr BP (1631-1652 AD). The two dates are because of overlap or ambiguity of the calendar calibration. Using the youngest median age of 308 cal yr BP (1642 AD), the aggradation rate is 0.75 cm/year. The minimum average incision rate is 5.7 cm/year, using a date of 1950 AD when incision began and a bankfull depth of 3.9 meters below the Hidden Springs Terrace. LLNL report is found in Appendix C.
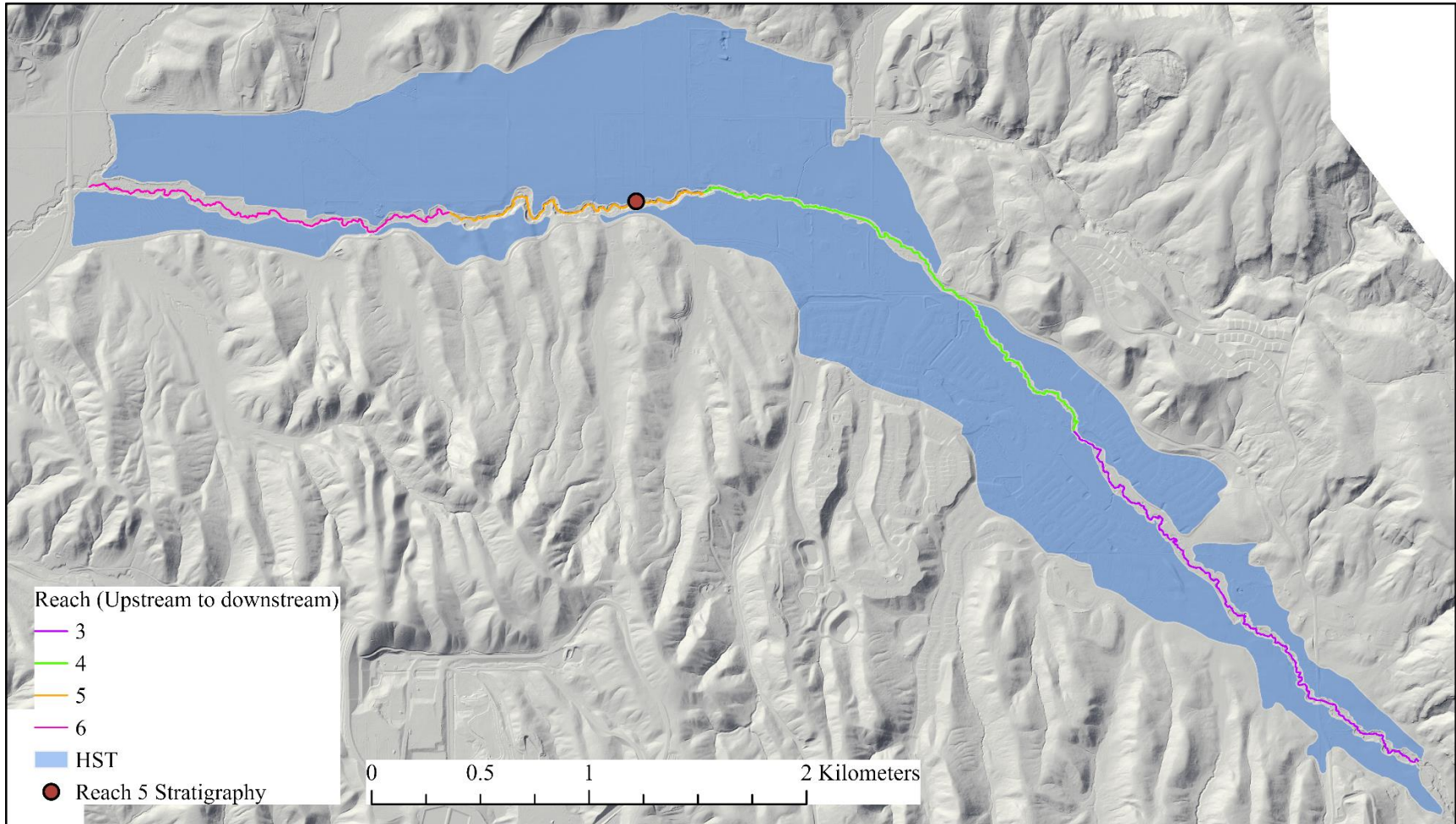
Figure 13   **Geomorphic map of Reach 3 to 6 of Lower Dry Creek. The map shows the extent of the Hidden Springs Terrace surface and the location of the Reach 5 stratigraphy site which shows the aggradational sequence of the Hidden Springs Terrace (Figure 14).**
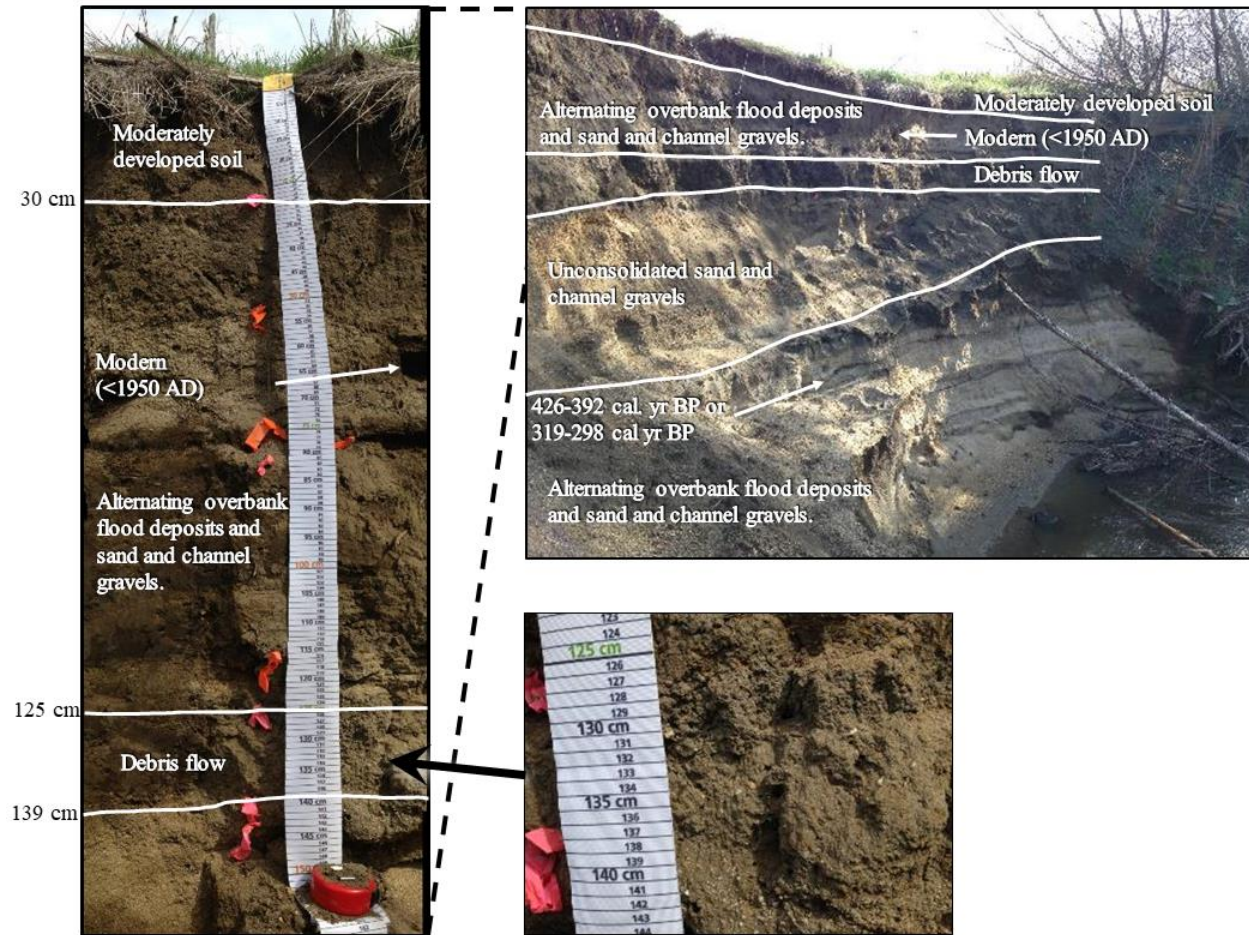
Figure 14 Annotated photos of the stratigraphy of the Hidden Springs Terrace at Reach 5. The photos show the complex sequence of fine-grained overbank flood deposits, channel gravels, and debris flow. Two charcoal samples are dated and calibrated from the site. The minimum aggradation rate between these samples is 0.75 cm/year. Minimum incision rate since deposition of the upper charcoal sample is 5.7 cm/year.

In Reach 2, we sampled stratified sand lenses from two well-exposed stream banks at the Peggy's Trail site (Figures 11, 12, and 15) and dated these samples using OSL. Dating these deposits we hope to constrain the timing of incision and aggradation upstream of the Hidden Springs Terrace. The exposures are downstream from the largest mining deposit. The upstream bank has a well-developed, 170 cm thick, mollic A-horizon. The B-horizon extends from 170 cm to 426 cm. The material is finer-grained than a fluvial deposit (limited gravels and coarse sand), has no original stratigraphy, and stage II carbonate development throughout. Below is a 43 cm thick coarse sand layer. A fine-grained overbank deposit separates another coarse sand layer. There is additional sand, gravel and cobble fluvial deposits down to the current bankfull level. An OSL sample from a depth of 492-495 cm dated as 4.79 ± 1.03 ka.

The downstream exposure shows rapid aggradation. The 18 cm thick soil is poorly developed with no carbonate accumulation. Below the soil is a thick packet of sheet-flood deposits to a depth of 104 cm. Below is a 15 cm thick sand deposit with cross-bedding from rapid deposition. From 119-146 cm is additional sheet-flood deposits of fine and coarse unconsolidated sands and gravels. An organic rich, fine-grained sand layer is from 146-178cm. A medium grain sand deposit is from 178 cm to the current bankfull level at 240 cm. We dated two OSL samples from the exposure. The sample from 55-57 cm dated as 0.79 ± 0.31 ka and the sample from 155-158 cm dated as 0.67 ± 0.29 ka. The uppermost sample is older, but within the error of the lower sample. A likely cause of this is partial bleaching of both samples. These ages are interpreted as a maximum age of the deposit.
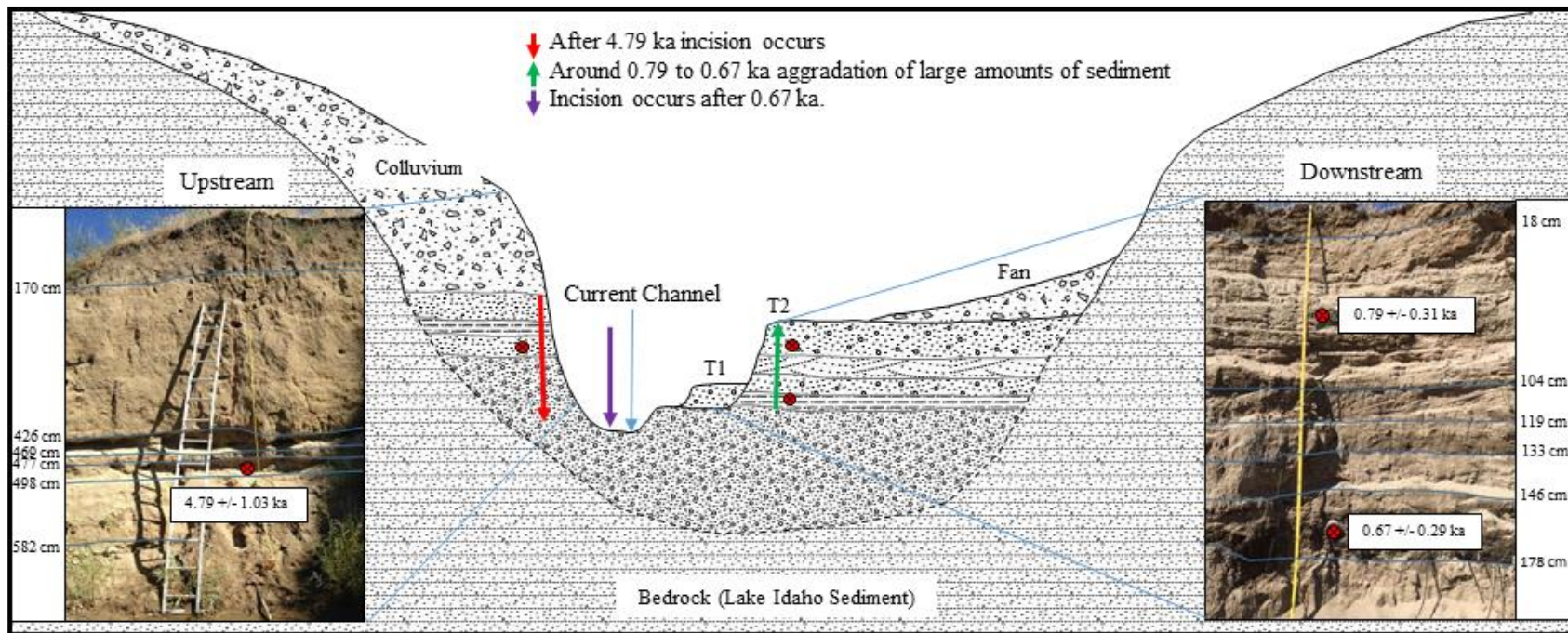
Figure 15 Conceptual drawing of the stratigraphy of Lower Dry Creek Reach 2 at the Peggy's Trail site. The upstream bank shows colluvial material deposits over a fluvial terrace. The terrace dated at 4.79 ±1.03 ka. After the aggradation of the terrace, Lower Dry Creek incised. Around 0.79 to 0.67 ka the T2 terrace of the downstream bank aggraded. The stratigraphy shows sheet flood and crossed bedded sands. Timing of this aggradation correlates to a period of large amount of alluvial fan deposition in Dry Creek Experimental Watershed related to increased fire activity (Poulos and Pierce, 2018). After aggradation of the T2 terrace, Lower Dry Creek incised. Lower terraces (T1) are present between the T2 and current floodplain indicating episodic incision. Today, the stream is laterally migrating which exposed the upstream and downstream bank.

5.4 Longitudinal Profile of Lower Dry Creek

The longitudinal profile of LDC is steep in Reach 1 with a slope of 0.025 m/m. LDC becomes less steep through Reach 2 with a slope 0.011 m/m. There is a knickpoint in Reach 2 where Daniels Creek converges with LDC. Reach 3, 5, and 6 have a slope of 0.008 m/m and Reach 4 is slightly steeper with a slope of 0.009 m/m. There is a knickpoint in Reach 3 below Cartwright Road and a knickpoint between Reach 4 and 5 at Broken Horn Road. The profile has a concave shape, except through Reach 4 where the profile is convex (Figure 16).

The Hidden Springs Terrace profile slope is 0.008 m/m in Reach 3, 4, and 6. The Hidden Springs Terrace profile is gentler through Reach 5 with a slope 0.007 m/m. The average height difference between Hidden Springs Terrace and LDC in Reach 2 is 5.1 m, Reach 3 is 2.6 m, Reach 4 is 1.4 m, Reach 5 is 4.7 m, and Reach 6 is 2.4 m (Figure 16). The relative elevation map shows low lying areas of connection between LDC and Hidden Springs Terrace in Reach 3, 4, and 6 (Figure 17). In the middle of Reach 4 is an area of land which is observed to flood frequently. Reach 5 contains no area of connection between LDC and Hidden Springs Terrace. The 5-meter contours show a consistent gradient of Hidden Springs Terrace despite the changes in height above current LDC and slope of LDC.
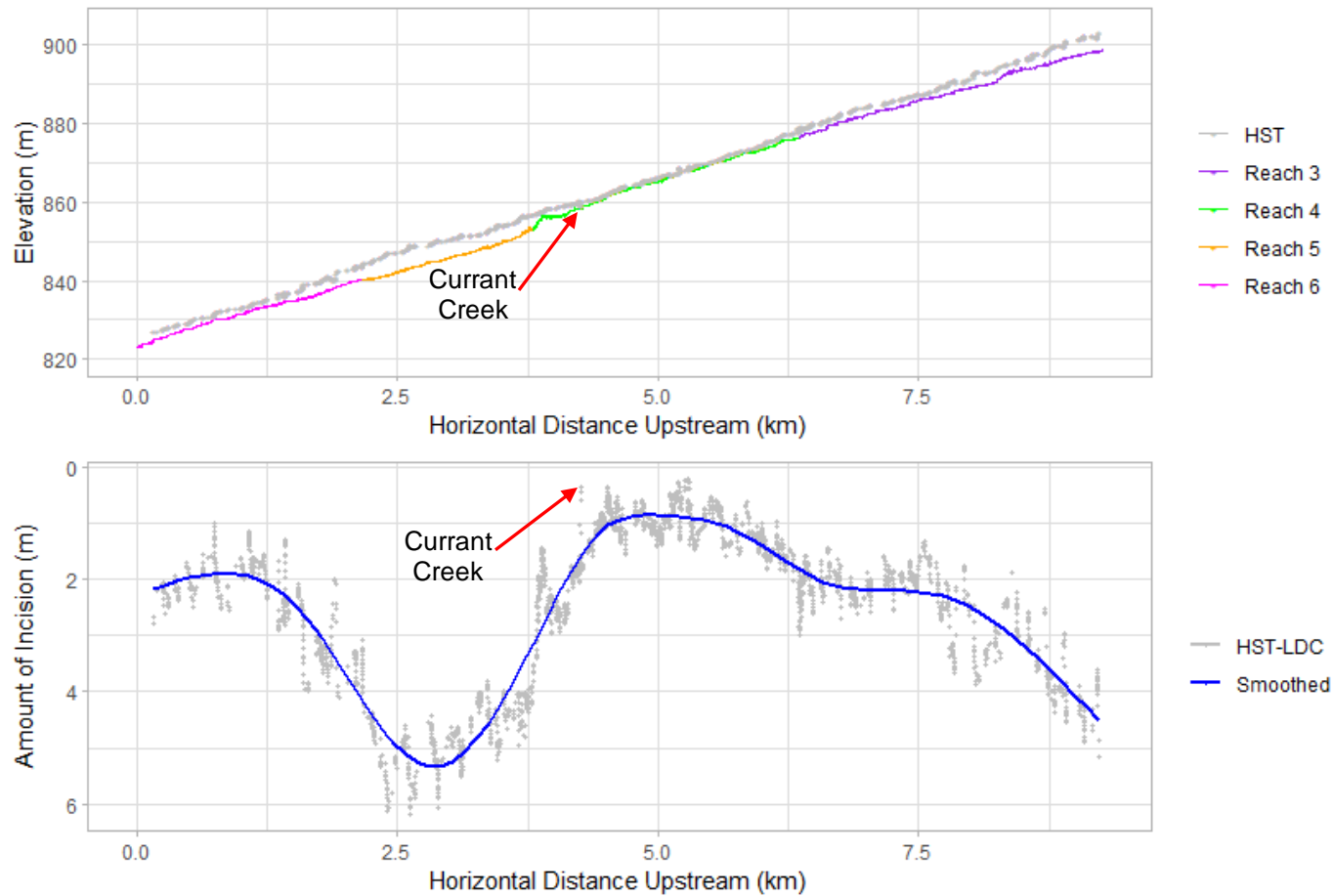
Figure 16 The upper plot is the longitudinal profile from Reach 3 to 6 of Lower Dry Creek (LDC) and the Hidden Spring Terrace (HST) surface. The bottom plot shows the amount of incision in meters between Lower Dry Creek and Hidden Springs Terrace (HST-LDC) and a generalized additive model smoothing line of the data. Observe that the profile is overall a well-behaved concave stream profile. However, the profile is convex through Reach 4 which has a lower amount of incision. Reach 5 has the highest amount of incision, which begins directly downstream of the confluence with Currant Creek.
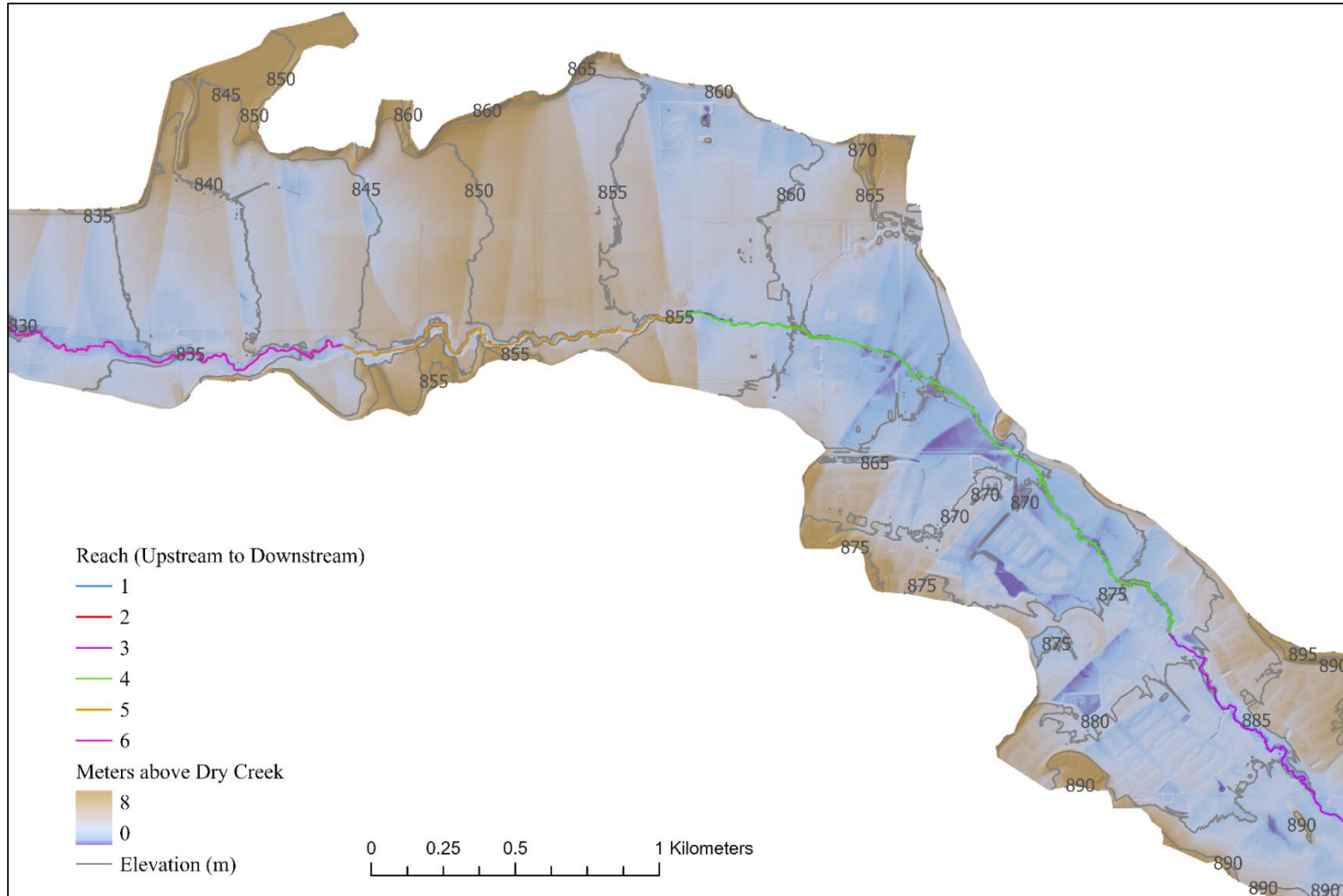
Figure 17   **Relative elevation map showing the height the Lower Dry Creek Valley is above the current stream bottom from Reach 3 to 6. Notice the areas in Reach 3 and 4 that are connected to the Hidden Springs Terrace. We observed flooding on the Hidden Spring Terrace in Reach 4. Reach 5 is not connected to the Hidden Springs Terrace due to recent incision. Relative elevation maps of each reach is in Appendix D.**

5.5 Streambed Grain Size Analysis

Location of each streambed sediment size sample along the longitudinal profile of LDC is shown in figure 18. Sample litthology is primarily granite and basalt in all reaches. The average D_{50} for Reach 1 is 21.6 mm and the D_{84} is 55.4mm. The average D_{50} for Reach 2 is 28.7mm and the D_{84} is 53.2mm. Reach 1 contains more coarse sediment (> 64mm) than Reach 2, as well as more sand sized sediment (< 2mm) (Figure 19). Both Reach 1 and 2 are poorly sorted, with Reach 1 being more poorly sorted than Reach 2. The grain size is substantially reduced between Reach 2 and Reach 3. The D_{50} of Reach 3 is 2.4 mm and D_{50} of Reach 4 is 1.6 mm. Reach 3 and 4 are well sorted. Sediment coarsens in Reach 5 with a D_{50} of 17.9 mm. Reach 5 is poorly sorted. The D_{50} of Reach 6 is 6.5 mm. Reach 6 is well sorted. Photos of each grain size sample location is in Appendix E.
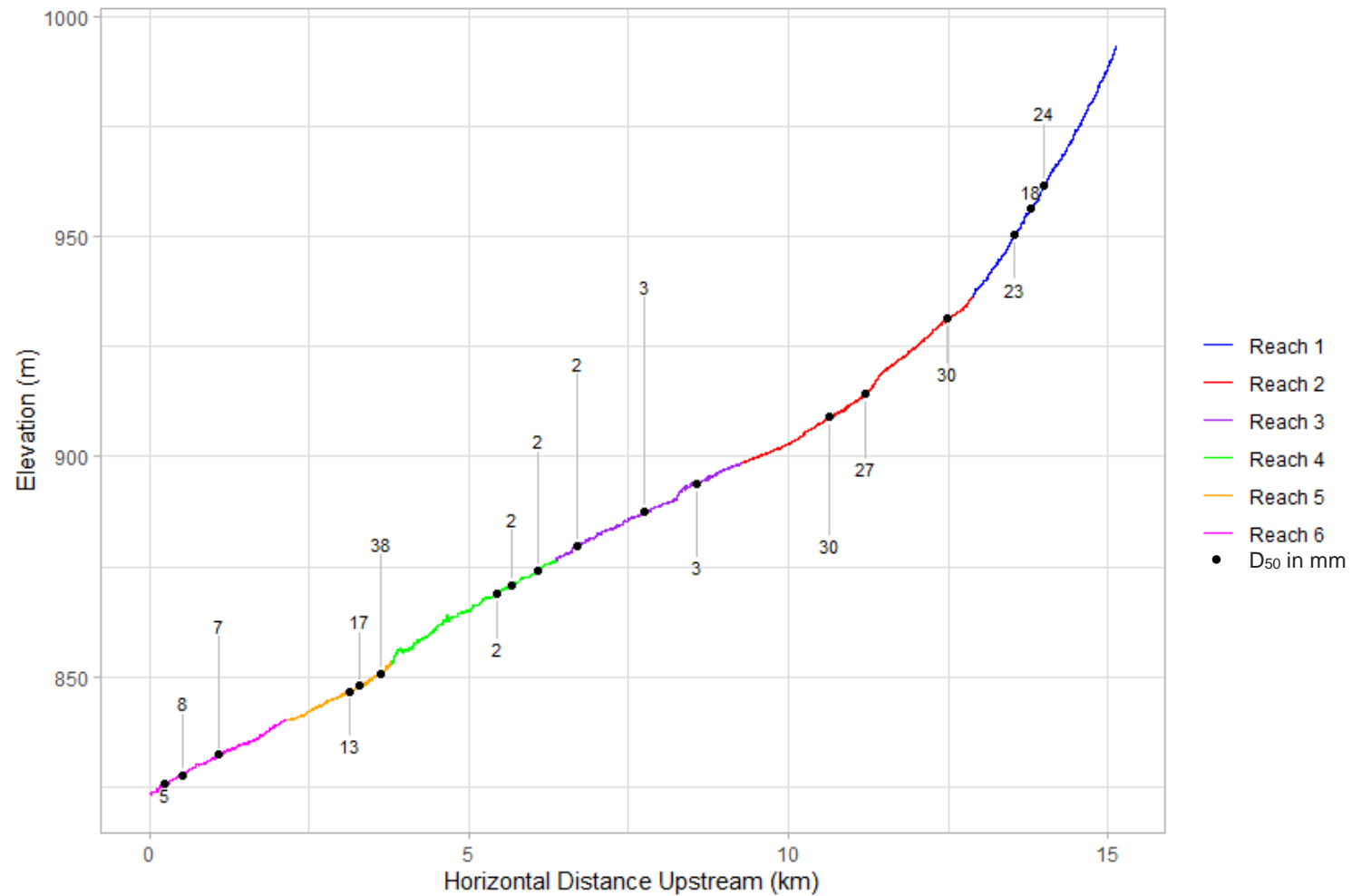
Figure 18 Longitudinal profile of Lower Dry Creek showing locations of grain size samples and the measured median grain size (D_{50}) in mm. The bed sediment fines between Reach 2 and 3 as the profile of Lower Dry Creek switches from concave to convex.
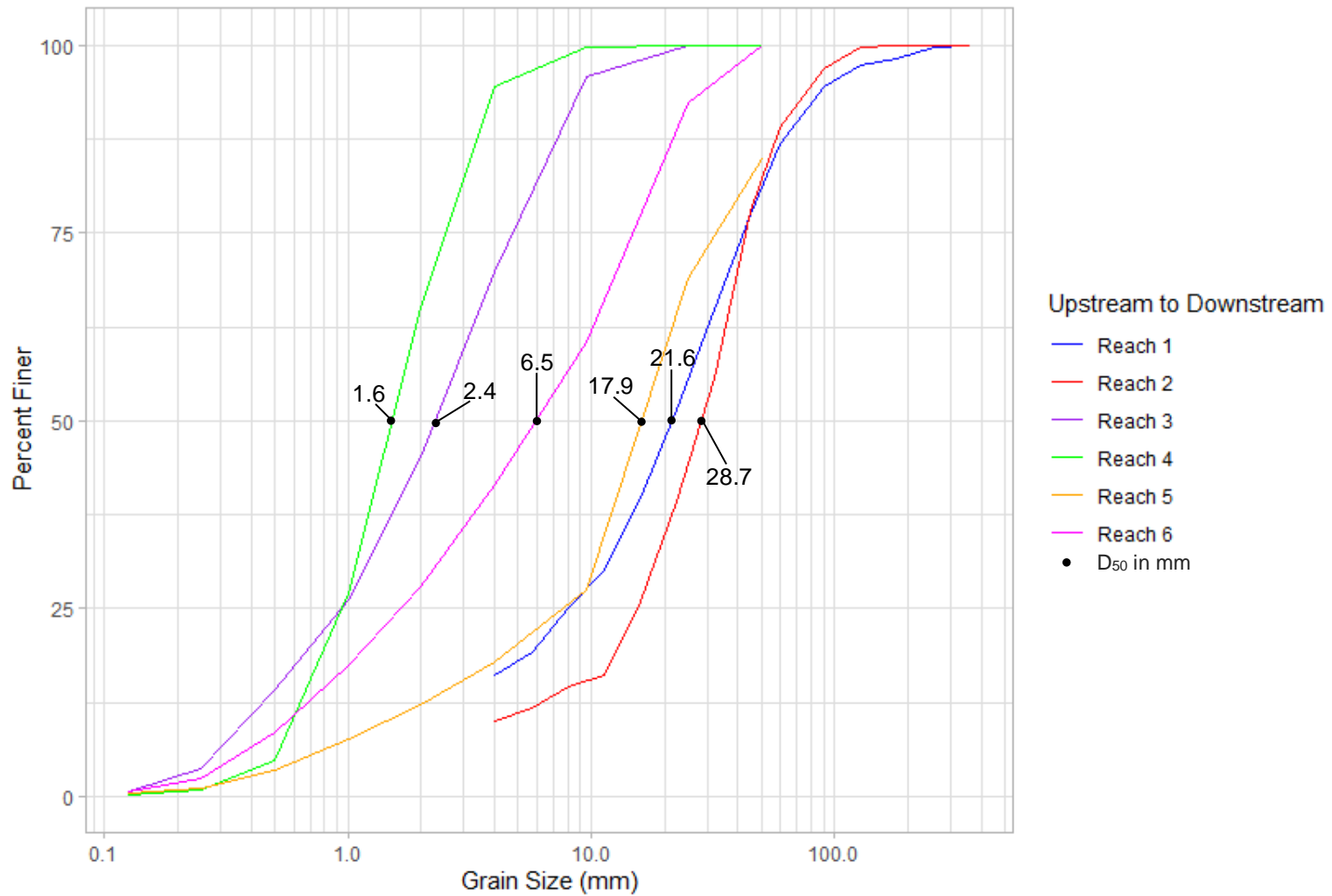
Figure 19 Grain size distribution plot of the average of three stream bed sediment samples from each reach of Lower Dry Creek. The median grain size (D$_{50}$) in mm is annotated on the plot. The grain size substantially fines between Reach 2 and 3. The grain size coarsens in the incised Reach 5.

5.6 HEC-RAS Modeling

The five cross sections of LDC surveyed in the field compare favorably with the DEM cross sections. The average R^2 between the profiles is 0.79, with a low of 0.68 and a high of 0.95. We believe the 1-meter resolution DEM is appropriate for HEC-RAS modeling of a stream of LDC size. Cross section plots are in Appendix F.

DCEW LG 2-year flood is 1.13 m³/s (40 cfs) determined from 21 years of historic discharge (Figure 20). LDC daily average discharge linear relationship with DCEW LG is satisfactory with an R^2 of 0.84 (Moriasi et al., 2015) (Figure 21). Using the 2-year flood from DCEW LG, the comparable 2-year flood at LDC gage is 1.42 m³/s (50 cfs).
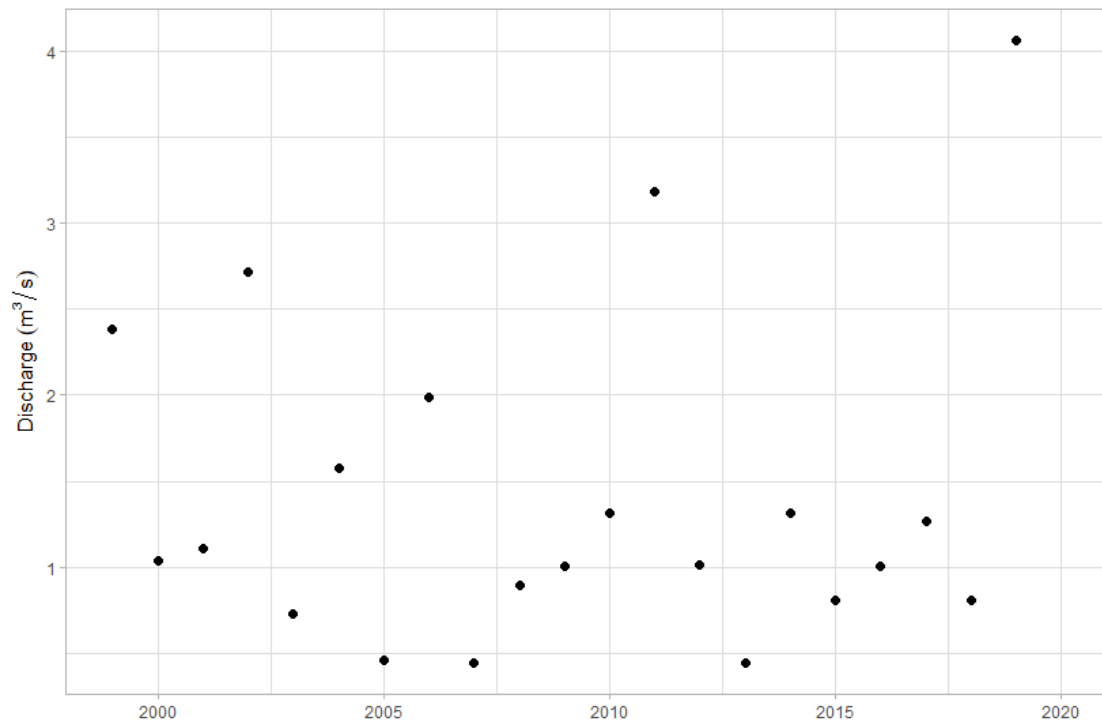
Figure 20   **Plot showing Dry Creek Experimental Watershed Lower Gage annual peak discharge from 1999 to 2019. Estimated 2-year return internal bankfull flow is 1.13 m³/s. All sampling for this project was completed after the highest discharge on record in the spring of 2019.**
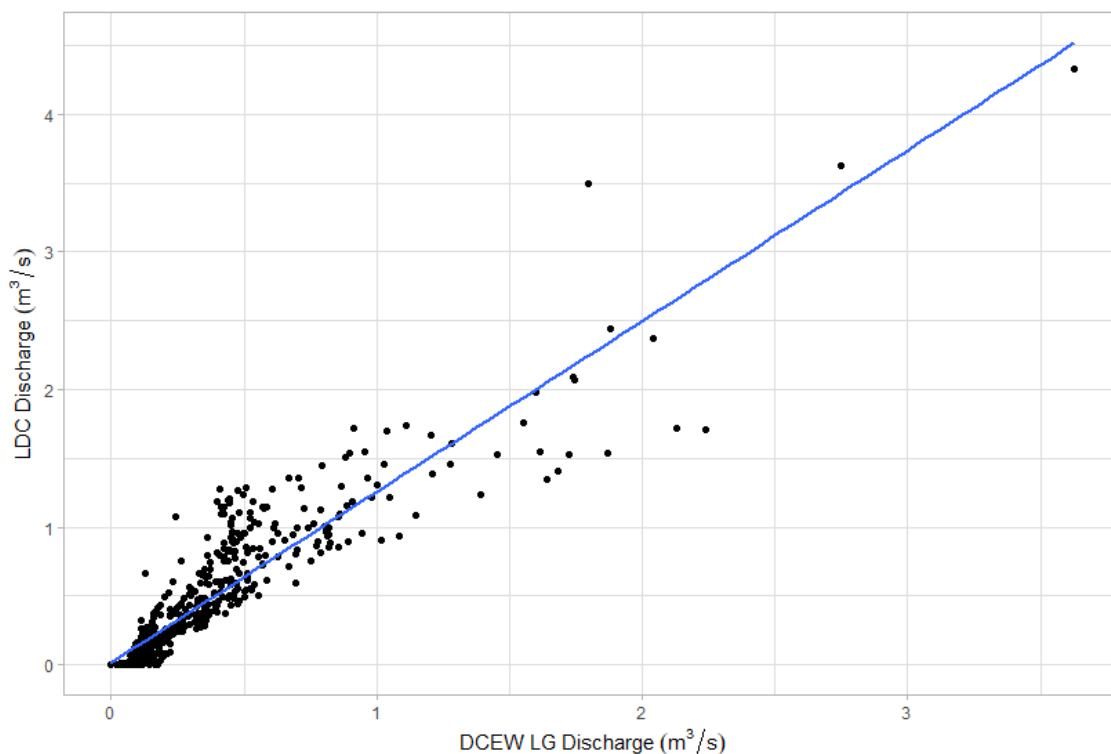
Figure 21   **Dry Creek Experimental Watershed Lower Gage (DCEW LG) discharge plotted against Lower Dry Creek (LDC) discharge. The linear relationship is y=1.24x+16.78 with an R^2=0.84. The 2-year estimated bankfull flow at Dry Creek Experimental Watershed Lower Gage is 1.13 m^3/s and using the linear relationship, the 2-year bankfull flow at Lower Dry Creek is 1.42 m^3/s.**

Results of hydraulic modeling are in table 3 and figure 22. Maps showing depth of water and channel water velocity for each reach and modeling scenario are in Appendix G. Results of the model for the cross sections show the channel filled to its banks in Reach 1 and 2, an indicator of bankfull flow. However, the same flows in areas of Reach 3, 4 and 6 inundate the floodplain. This suggests estimates of Manning's n may not be representative of bankfull flows in these reaches. Keeping the discharge and Manning's n constant between reaches allows for comparison of channel geometry and characteristics.

Table 3 Results of HEC-RAS modeling. Results of each reach are an average of every cross-section in the reach. Manning's n roughness is modified for the three model runs for each reach from 0.03 to 0.1.

	Discharge (m3/s)	Avg Vel Chnl (m/s)	Avg Flow Area (m2)	Avg W.P. (m)	Avg Max Depth (m)	Avg Width (m)	Avg Stream Pwr (N/m s)	Avg Boundary Shear Stress (N/m^2)	Avg Hydr Radius (m)	Avg D$_{50}$ Onset (mm)
R1 n=0.03	1.13	1.65	0.73	3.74	0.33	3.65	81.59	44.67	0.20	63.31
R1 n=0.065	1.13	0.96	1.24	4.74	0.46	4.61	66.12	62.92	0.26	89.17
R1 n=0.1	1.13	0.70	1.69	5.56	0.55	5.40	57.07	74.96	0.31	106.23
R2 n=0.03	1.42	1.15	1.27	5.27	0.42	5.16	29.52	21.16	0.24	29.99
R2 n=0.065	1.42	0.68	2.10	7.03	0.56	6.87	24.93	31.11	0.31	44.09
R2 n=0.1	1.42	0.50	2.86	8.33	0.67	8.14	21.89	37.31	0.36	52.87
R3 n=0.03	1.42	0.99	1.58	6.68	0.46	6.57	19.35	15.65	0.25	22.18
R3 n=0.065	1.42	0.56	2.71	9.73	0.61	9.58	14.45	21.44	0.30	30.38
R3 n=0.1	1.42	0.41	3.74	11.64	0.72	11.46	12.70	25.43	0.35	36.04
R4 n=0.03	1.42	1.08	1.51	7.56	0.44	7.46	25.36	18.97	0.23	26.89
R4 n=0.065	1.42	0.59	2.71	11.77	0.59	11.62	18.45	24.88	0.28	35.27
R4 n=0.1	1.42	0.42	3.86	15.65	0.69	15.46	14.97	28.31	0.31	40.12
R5 n=0.03	1.42	1.15	1.34	4.66	0.49	4.50	27.71	19.69	0.29	27.91
R5 n=0.065	1.42	0.68	2.24	5.71	0.67	5.47	24.45	28.68	0.39	40.65
R5 n=0.1	1.42	0.50	3.03	6.47	0.81	6.16	19.40	33.64	0.47	47.68
R6 n=0.03	1.42	0.97	1.62	7.66	0.40	7.57	18.03	15.48	0.23	21.94
R6 n=0.065	1.42	0.55	2.84	11.58	0.54	11.46	13.49	20.91	0.28	29.64
R6 n=0.1	1.42	0.39	3.95	14.76	0.64	14.61	11.27	24.34	0.32	34.49
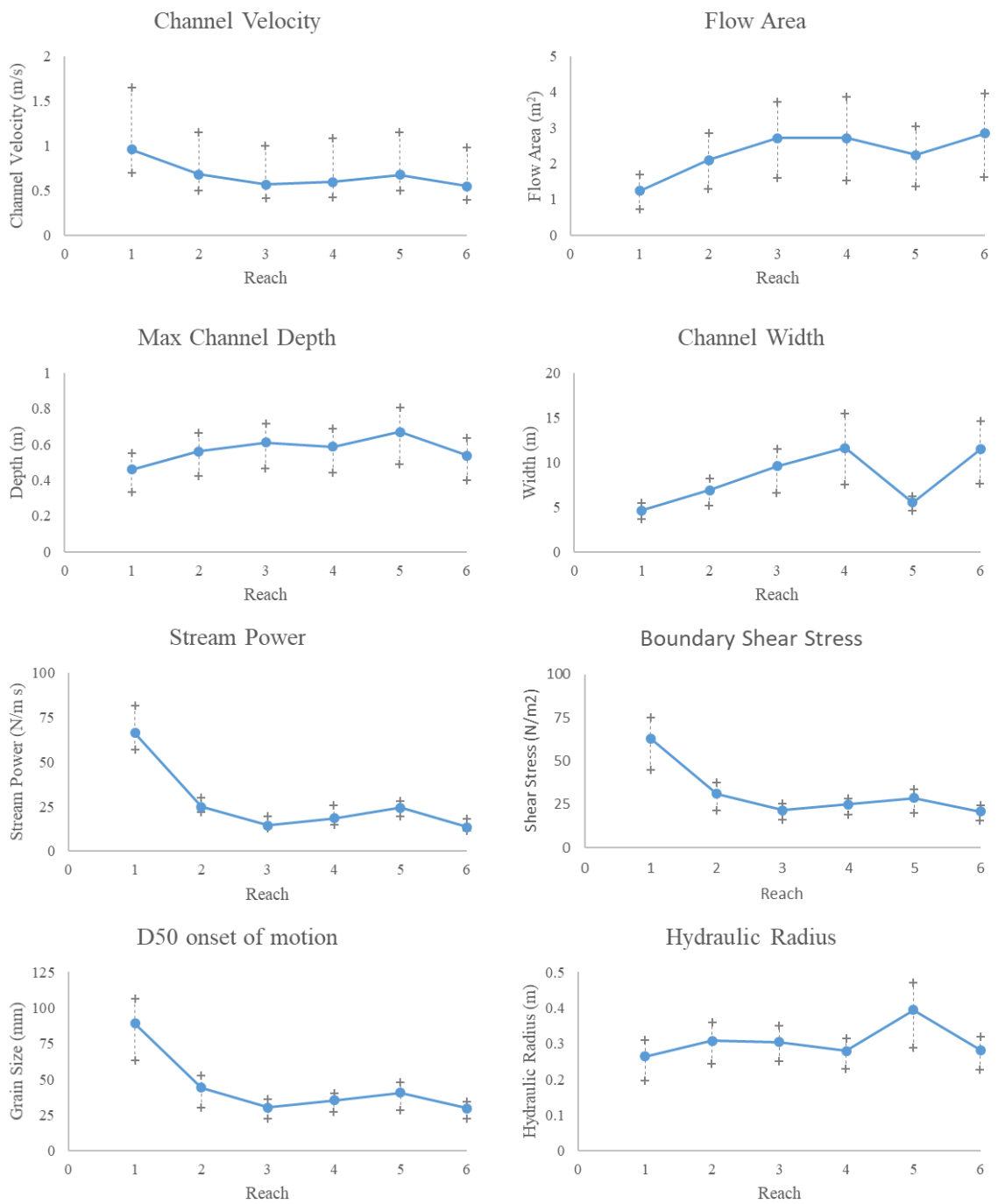
Figure 22   Plots of the results of HEC-RAS modeling divided by reach. Manning's n roughness of 0.065 is the blue dots and upper and lower limits are n=0.03 and 0.1 shown by the gray +. Reach 5 in all plots deviates from the trend due to incision.

5.7 Meander Migration and Land-Use

The georeferencing of the five aerial images for this project is satisfactory when compared with the location of the 2019 NAIP imagery. Measuring distance between identical features, not used as control points, across LDC are within 2 meters. We feel confident using the georeferenced images to measure land-use areas and stream meander migration which moved more than the width of the stream.

Average meander migration rates in meters per year of Reach 2 from upstream (1) to downstream (10) is plotted in figure 23. Meanders 9 and 10 have the highest rate and are located furthest downstream. Meander migration rate is plotted against the distance the meander is from the nearest mining deposit (Figure 23). We didn't observe a trend between distance from mining activity and meander migration rate. We averaged the migration rate for all 10 meanders between each imagery time series (Figure 24). Meander migration is lowest from 1938 to 1992. The rate increased approximately threefold between 1992 and 1998. The rate stays high until between 2011 and 2019 when the rate decreases to approximately the rate before 1992.
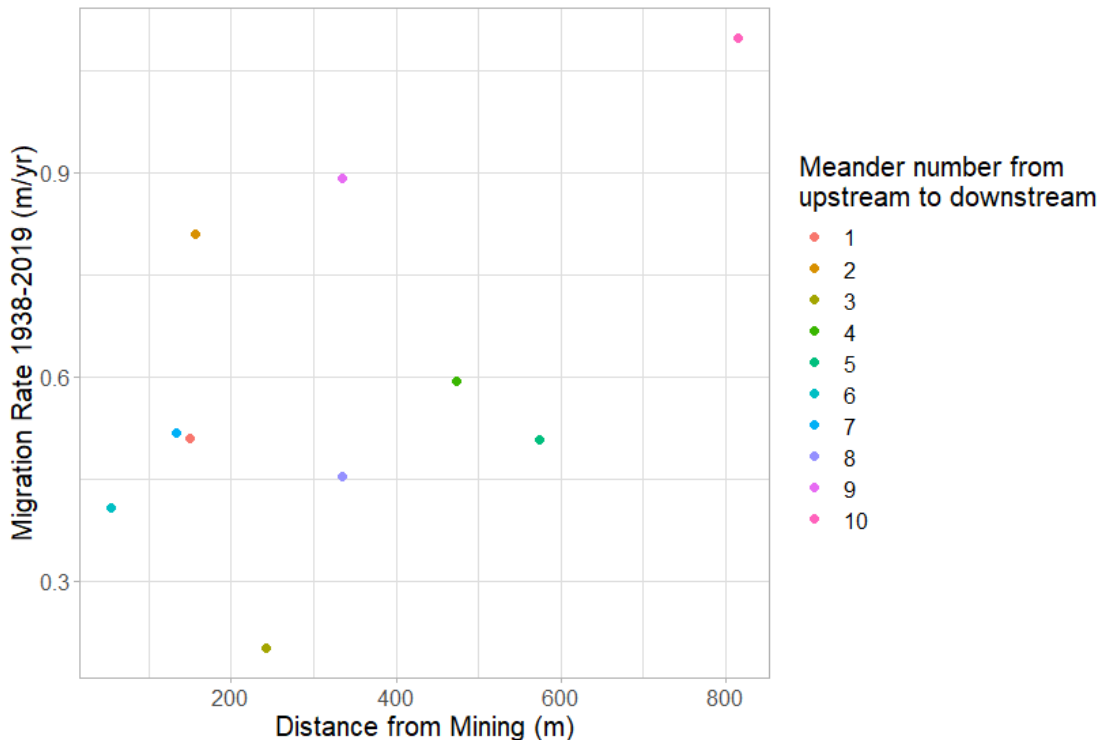
Figure 23   Plot of meander migration rate from 1938 to 2019 (m/yr) by distance from mining in meters from upstream (1) to downstream (10).
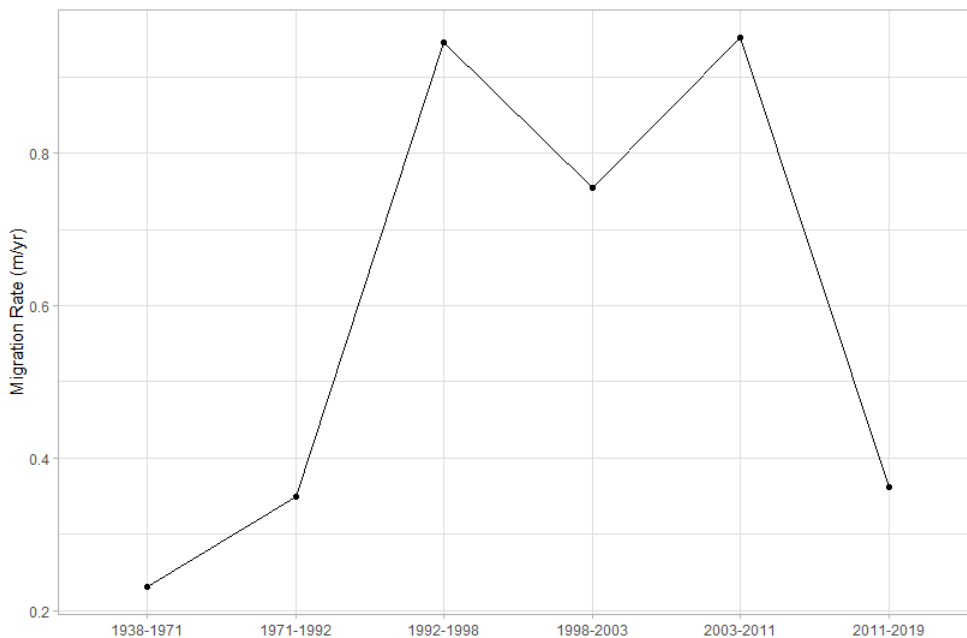
Figure 24   Plot of meander migration rate (m/yr) averaged for all 10 meanders between imagery years. Observe the rate increase between 1992 and 1998, which corresponds temporally to disturbances of the riparian vegetation potentially from a large rain on snow event. The rate stays high until 2011-2019 when the riparian vegetation reestablishes and stabilizes the channel.

LDC land-use is delineated by six researchers. Each researcher was given training to assess the six land-use classes used. After the training, three test boundaries were completed which covered the variation in land-use found in LDC. The 1971 test boundary has two land-uses, farmland and riparian vegetation. The 2003 test boundary contains all six land-uses. Three researchers didn't have any grassland while the other three have an average of 0.7% grassland. The 2019 test boundary has all land-uses except the other category. Three researchers have an average of 0.7% grassland, while the other three had no grassland. Two researchers have an average of 0.3% rural development and the other four have none. Results of the test boundaries are in table 4. Each category has a standard deviation of less than 2.5%.

Results of the land-use designation training show satisfactory comparison with each other. Therefore we believe there is not much bias based on the researcher that is completing the delineations. There is variability in the delineated riparian area, even for the small test squares. This may result in differences between riparian areas measured from different imagery. The discrepancies are potentially due to variability in determining areas to map as riparian vegetation when there are disturbances to the stream and exposed banks. However, the results show significant changes and similarities throughout time and reaches, so we are confident in our conclusions.

Table 4   Results of the three test boundaries (2019, 2003, and 1971) showing land-use percentage by researcher and the average (Avg) and standard deviation (STD) for each land use category. The low standard deviation indicates there is minimal bias based on the researcher completing the delineation.

	Ducar	Pendell	Rozsa	Kidd	Crevier	Arnold	Avg	STD
2019								
Residential	58.8	56.8	58.1	55.2	61.5	58.1	58.1	1.9
Farm	30.0	29.7	31.5	29.1	29.6	30.1	30.0	0.8
Riparian	11.2	13.5	9.3	14.9	8.9	11.3	11.5	2.1
Rural	0.0	0.0	0.3	0.3	0.0	0.0	0.1	0.1
Grass	0.0	0.0	1.1	0.6	0.0	0.5	0.4	0.4
Other	0.0	0.0	0.0	0.0	0.0	0.0	0.0	0.0
2003								
Residential	42.4	38.6	42.2	41.9	42.0	42.3	41.6	1.3
Farm	41.4	44.8	41.5	41.5	41.4	40.6	41.8	1.3
Riparian	3.0	2.9	2.5	2.0	3.7	2.7	2.8	0.5
Rural	6.8	7.9	8.2	8.7	6.8	8.9	7.9	0.8
Grass	0.8	0.6	0.0	0.0	0.7	0.0	0.3	0.3
Other	5.7	5.4	5.6	5.9	5.4	5.4	5.6	0.2
1971								
Farm	88.4	86.9	93.0	93.4	88.1	90.2	90.0	2.4
Riparian	11.6	13.1	7.1	6.6	11.9	9.6	10.0	2.4

The LDC valley is 81.8% farmland in 1971 and 82.6% in 1992 (Table 5 and Figure 25). Farmland in the valley is reduced to 74.4% in 2003. The approximately 7.8% loss in farmland in 2003 is 4.5% residential development and an increase of 2.4% rural development. Farmland is reduced to 57.1% by 2011. Residential development is 13.4% and rural development is 10.3% in 2011. In 2019, farmland is 39.7% of the valley. The loss of 42.1% farmland from 1971 to 2019 became 32.5% residential development and 9.4% rural development.

Table 5   Results of the land-use delineation for the entire Lower Dry Creek Valley through time.

Year	Grass	Farm	Rural	Residential	Riparian	Other
1971	11.2	81.9	1.7	0.0	5.6	0.2
1992	9.8	82.6	2.4	0.0	5.3	0.0
2003	11.1	74.4	4.8	4.5	4.1	1.2
2011	11.3	57.1	10.3	13.4	6.3	1.6
2019	10.6	39.7	9.4	32.5	6.2	1.6
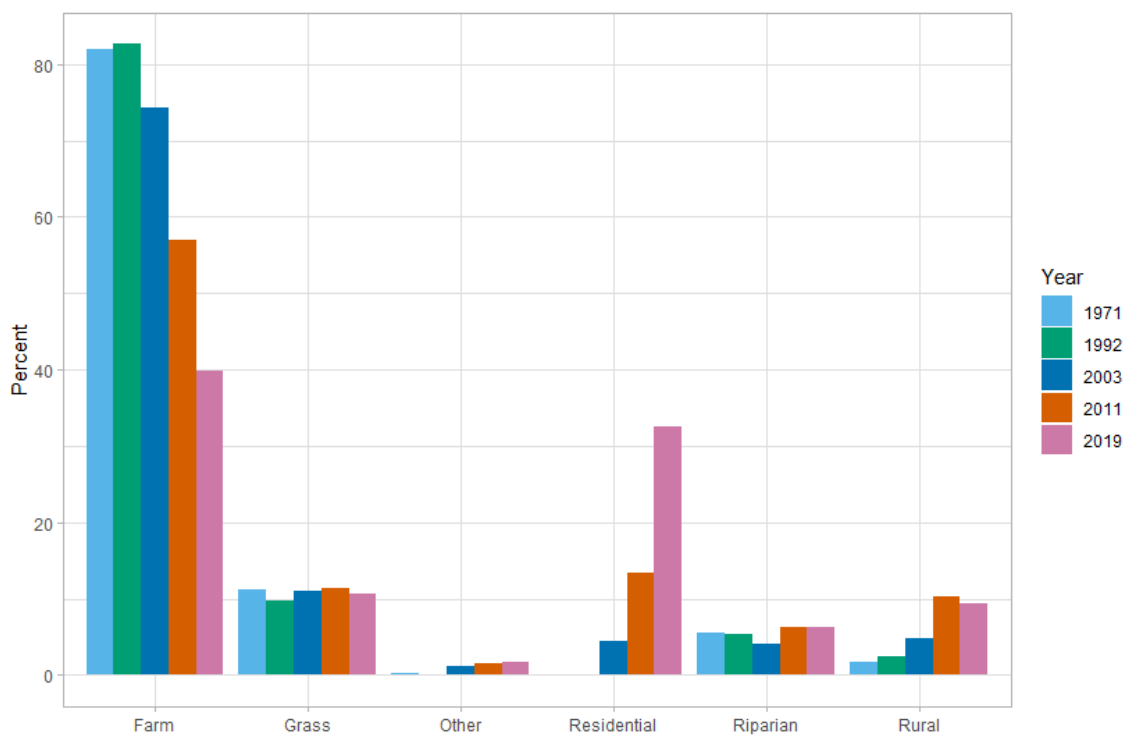
Figure 25   Plot of land-use for the entire Lower Dry Creek Valley through time. The valley has lost 42% of the farmland between 1971 and 2019. The lost farmland is today rural and residential development.

Figure 26 shows land-use change through time divided by reach. Land-use in Reach 1 is only grassland. Reach 2 is grassland with farmland on the downstream end of the reach. The farmland is greater in some-years and less used in others such as 2011. Reach 3 is dominated by farmland until 2011. The Hidden Springs development expanded from Reach 4 to Reach 3 converting more land to residential development. Between 2011 and 2019 the Cartwright Ranch development converted more land to

residential housing in Reach 3. This development project is ongoing. Some rural housing is being converted to residential development. Reach 4 is primarily farmland until the development of the Hidden Spring planned community began in 1997. This is the location of the first phase of the development which later expanded into Reach 3. Reach 4 also saw an increase of rural housing starting in 2003. These homes have large lots which may be irrigated, but are no longer used for agriculture. Reach 5 is primarily farmland which stayed constant from 1971 to 2019. There are a few additional rural homes in 2019. Reach 6 is also primarily farmland, which stayed constant until after 2011. During this time a development project converted farmland to residential housing. This project is ongoing.

We estimated riparian width by dividing the area of riparian vegetation in a reach by the length of stream from the 2015 DEM. The riparian width is plotted by reach with each year delineated in figure 27. The riparian width index is the lowest for each reach in 1938. Riparian width is averaged for each year from Reach 3 to 6 to correlate with changes from farmland to development (Figure 28).
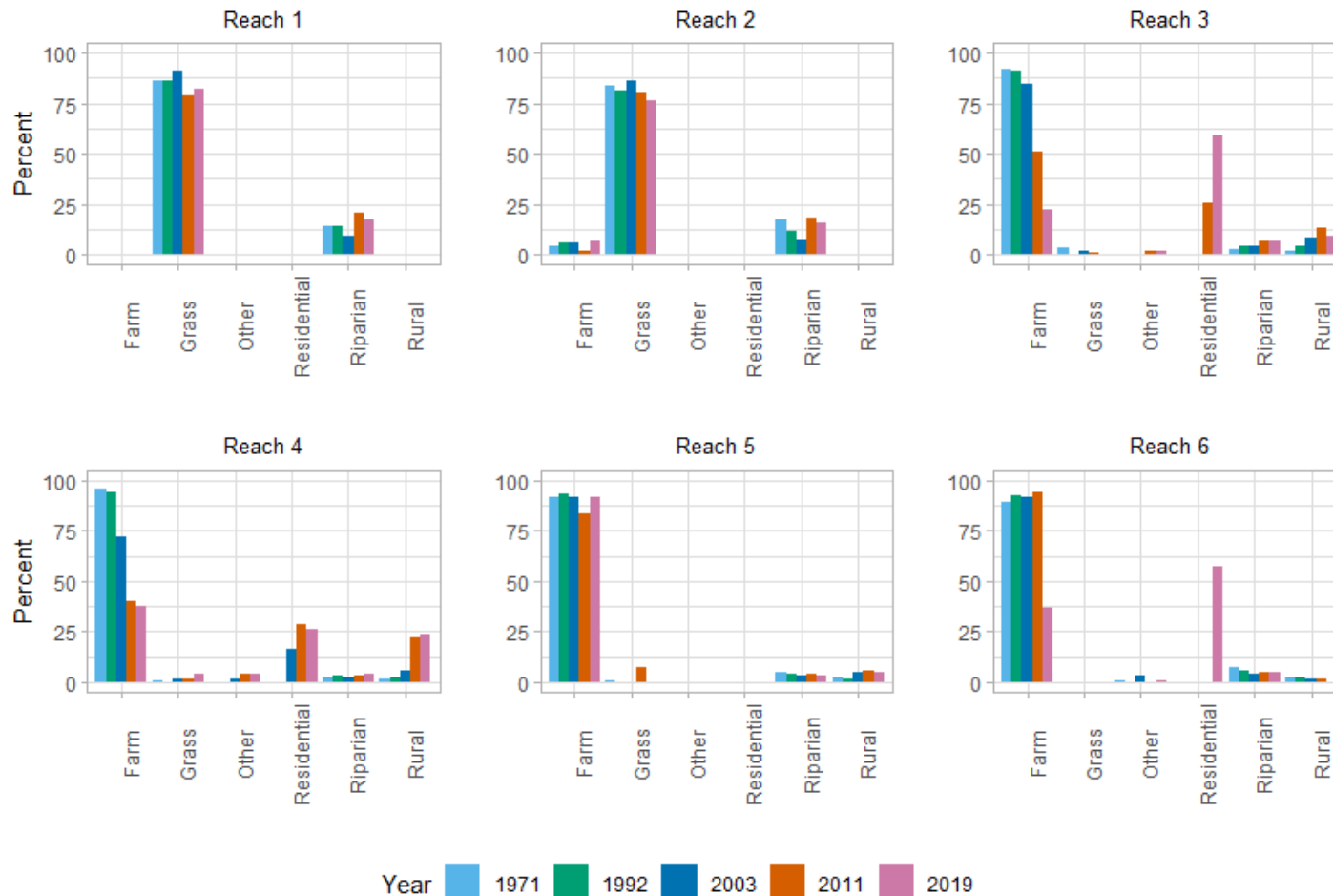
Figure 26 Plot of land-use delineation divided by reach in Lower Dry Creek Valley through time. Reach 1, 2 and 5 land-use has stayed constant through time. Reach 3 and 4 has seen a large amount of farmland converted to rural and residential development. Reach 6 is the site of ongoing development and will continue to see farmland converted to residential development.
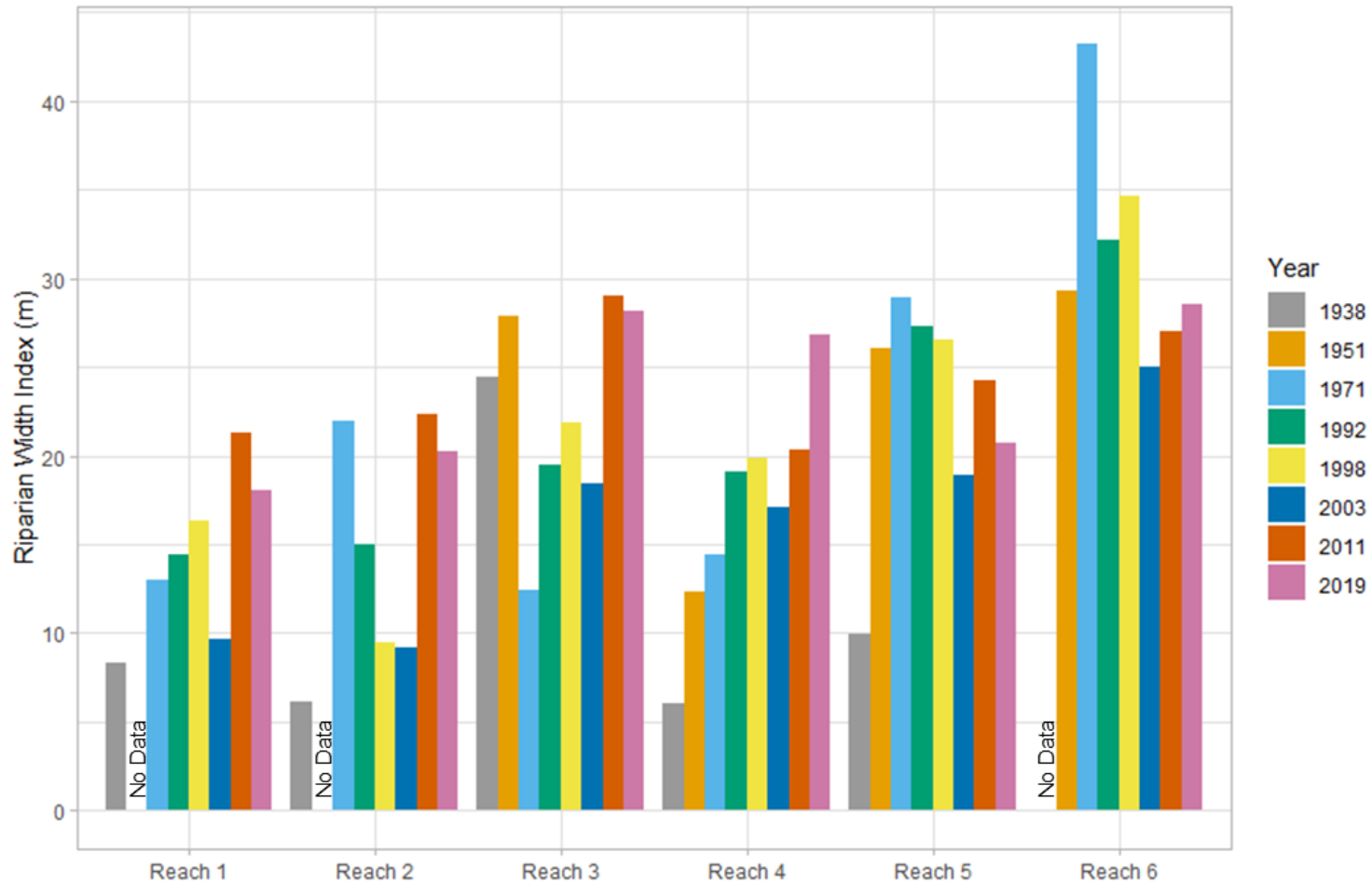
Figure 27 Plot of riparian width index (riparian area divided by stream length) for each reach through time. Reach 2 had a large loss of riparian vegetation after 1992 which corresponds temporally with a 100-year storm in December 1996 to January 1997 and an increase in meander migration rate (Figure 24). Reach 5 has lost riparian vegetation since 1992, which may relate to incision limiting the space for vegetation. Imagery from 2003 is from April, which is before full foliage of riparian vegetation and may have resulted in lower riparian vegetation delineation.
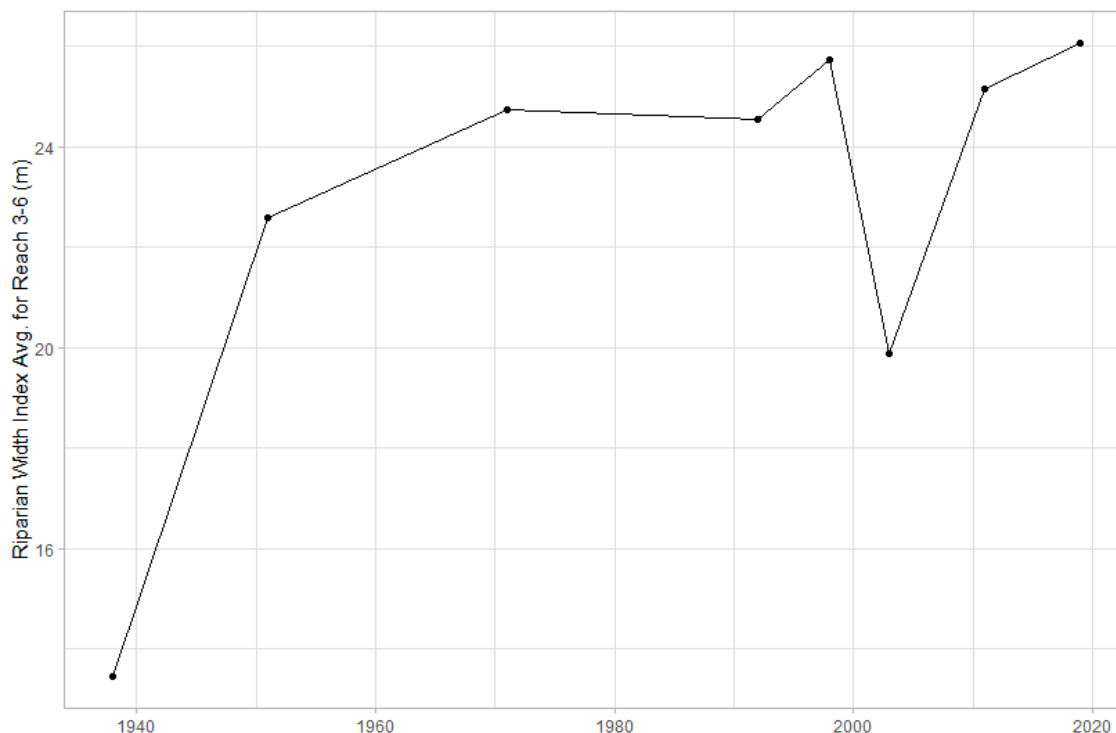
Figure 28 **Plot of riparian width index (riparian area divided by stream length) averaged for Reach 3 to 6 though time. Disregarding 2003, riparian width is approximately constant since 1971 in Reach 3 to 6 despite the conversion of farmland to development. Imagery from 2003 is from April, which is before full foliage of riparian vegetation and may have resulted in lower riparian vegetation delineation.**

Aerial imagery from 1938, 1951, and 1971 show recent deposits of fluvial transported material on Hidden Springs Terrace. Figure 29 shows the confluence of Currant Creek and LDC in 1951 and 2019. Currant Creek drains the Boise foothills and when it reaches the Hidden Springs Terrace, where the gradient decreases, it disperses into several channels. As the energy of Currant Creek dissipates, its sediment is deposited (Figure 29). After 1971, imagery shows remnants of these deposits, but no fresh fluvial deposits are observed. Current Creek has a drainage area of 26.2 km^2 which is 27% of the LDC watershed. Today, Currant Creek is channelized and not hydraulically connected to the Hidden Springs Terrace. Figure 30 shows the channelized path of Currant Creek and

the confluence with LDC. The topography of the confluence shows a fan shape in the

location of the distributaries of Currant Creek visible in the 1951 imagery (Figure 29 and

30).
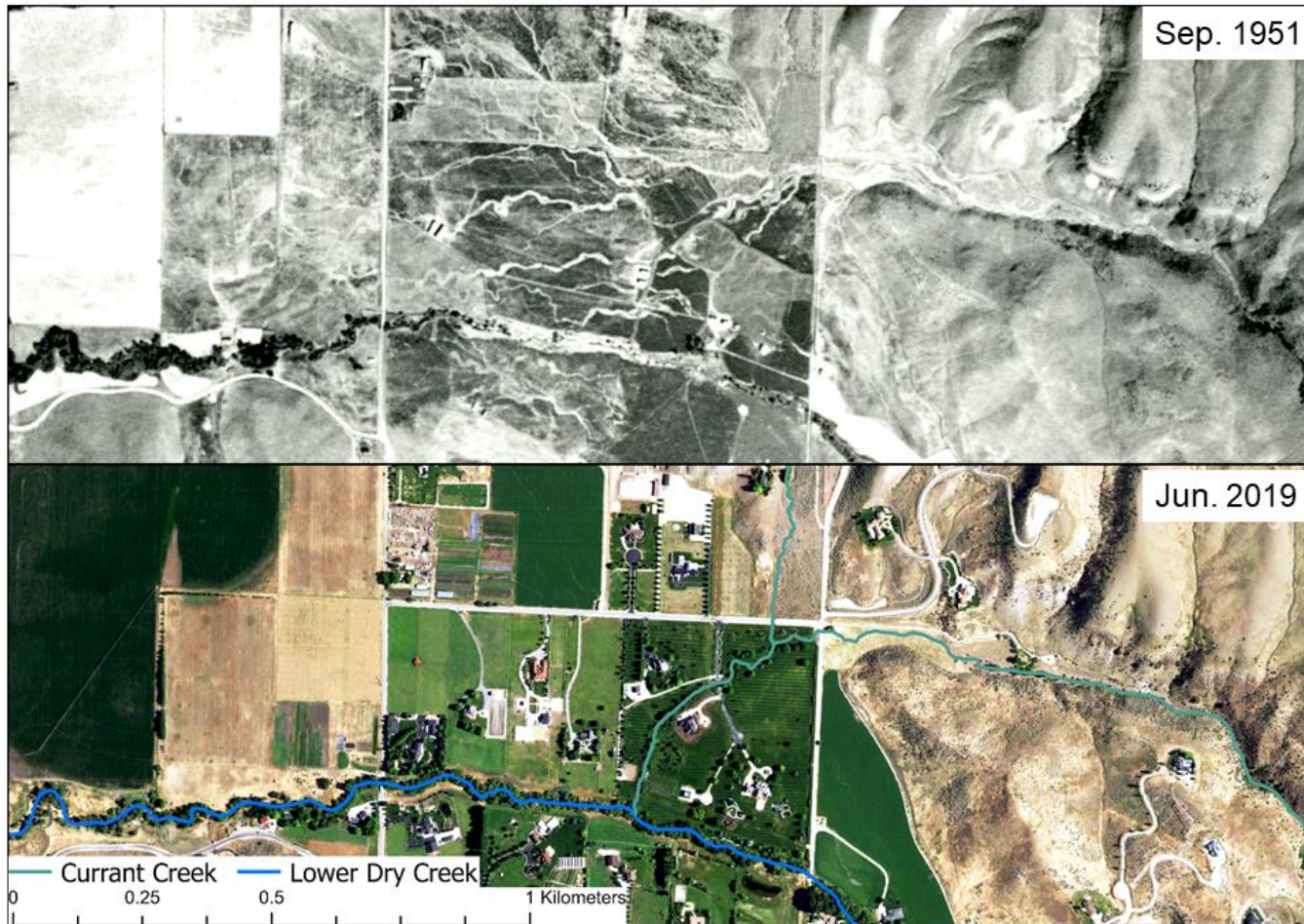
Figure 29 **Imagery showing Currant Creek confluence with Lower Dry Creek in 1951 and 2019. In 1951 Currant Creek transitioned to a series of distributaries across the Hidden Springs Terrace. Observe the amount of sediment deposition on the floodplain in 1951. In 2019, Currant Creek is channelized to prevent flooding of rural housing. Flow paths of Currant and Lower Dry Creek are delineated in 2019 imagery.**
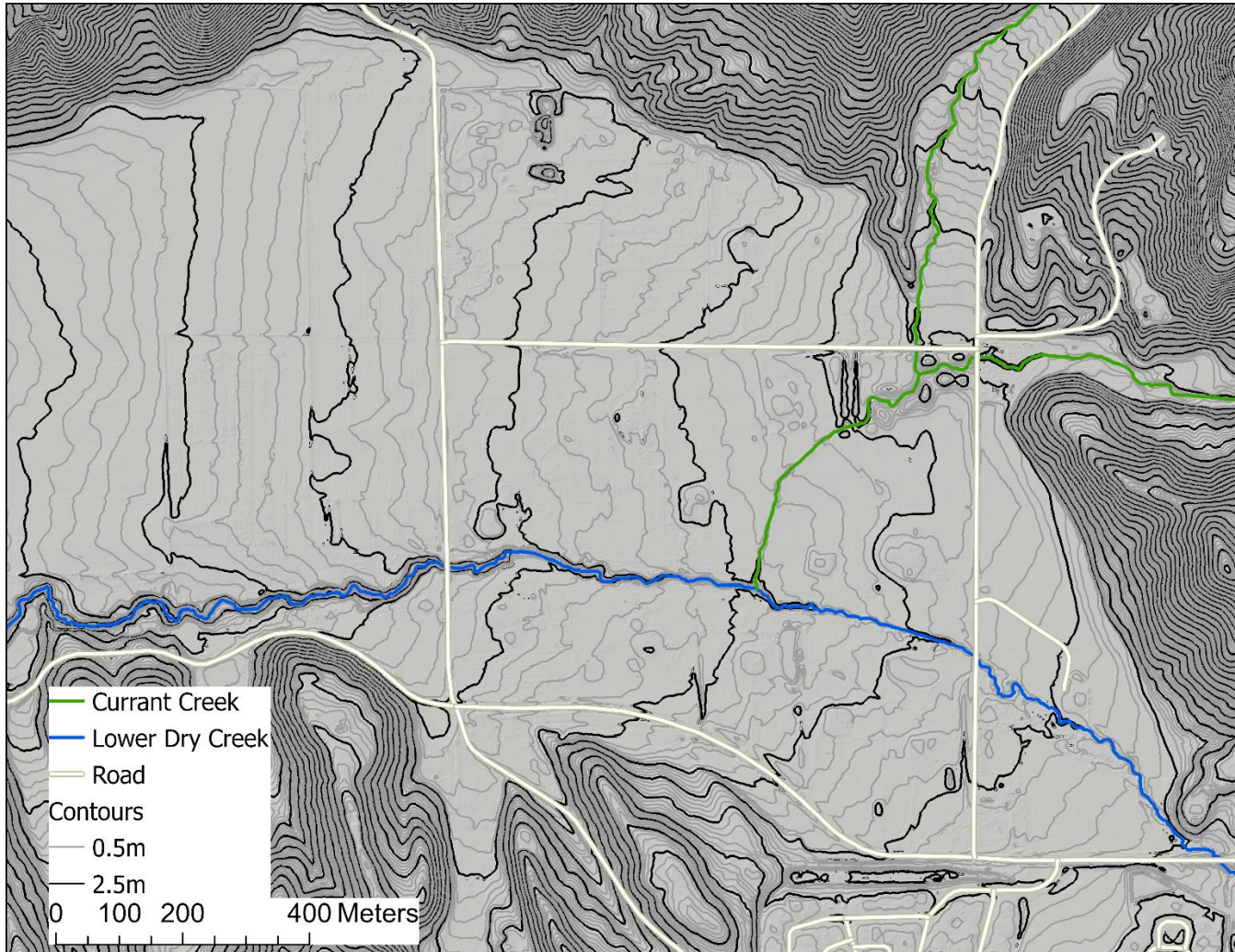
Figure 30 Hillshade map showing the confluence of Currant Creek with Lower Dry Creek. Contour lines at an interval 0.5 meters show a fan shape at the location of distributaries of Currant Creek visible in the 1951 imagery in figure 29.

CHAPTER 6: DISCUSSION

This study examines stream and sediment characteristics in order to 1) characterize the geomorphic history of the reaches of LDC, 2) compare the long-term geomorphic history with recent channel changes and 3) determine possible driving forces resulting in high reach-scale variability in lateral and vertical adjustment of LDC.

Geomorphic mapping, dated stratigraphic sequences, and soil pits in Reach 2 indicate episodic incision and aggradation throughout the Holocene. OSL dates provide evidence of cut and fill in Reach 2 corresponding temporally to increased fire activity during a climatic change (Poulos and Pierce, 2018). Historic aerial photos and riparian width changes in Reach 2, indicate high lateral channel adjustment in the last approximately 100 years. The presence of dredge piles, historic records, and stream sediment size distribution all indicate historic placer mining profoundly impacted the channel. This evidence suggests Reach 2 shifted from vertical to lateral channel adjustment due to mobilization of fine-grained sediment from placer mining.

Geomorphic mapping and a dated stratigraphic sequence in Reach 5 indicate recent (<1950 AD) incision of 3.9 meters. While the presence of the Hidden Springs Terrace indicates long term aggradation; historic photos and land-use change shows channelization of tributaries greatly changed the sediment and hydrology of Reach 5. This evidence suggests Reach 5 shifted from an aggrading to incising reach from channelization of Currant Creek to prevent flooding of housing developments after approximately 1992.

6.1 Modern Land-use Impacts on Lower Dry Creek

Land-use influences the hydrology and sediment supply of LDC. We observed and measured localized channel change in LDC of high lateral adjustment in Reach 2 and recent incision in Reach 5. We do not find these changes throughout the watershed allowing us to disentangle the localized drivers from the watershed wide drivers. Beavers were extirpated in the region during the 19th century. We observed beavers in DCEW and Reach 5 during this study. Beavers continue to occupy incised Reach 5 today because the confined channel is excellent habitat. Beaver extirpation is presented and prevalent in LDC, but we assume beavers were trapped throughout the watershed. Therefore, it is unlikely the channel response we observe in Reach 2 and 5 are associated with only beaver removal. Farming over time modified the soil of the Hidden Springs Terrace due to tillage and irrigation. We observed from aerial photos land-owners farmed up to the banks in sections of LDC. Farming activity increases runoff and sediment supply to streams and likely LDC (Waters, 1995; Le Bissonnais et al. 2005). Early settlers in the Boise area farmed Reach 3 through 6 since the 1850's; therefore farming is not likely the driver of incision in Reach 5. Grazing causes compaction of the floodplain and bank failures resulting in channel changes and increased sedimentation (Leopold, 1974). Studies found that grazing causes localized stream modification near a location frequently used by the herd for water or crossing the stream (Kauffman and Krueger, 1984; Fitch and Adams, 1998). We observed meander migration throughout Reach 2, which is not likely attributed with localized grazing activity. The forests in the headwaters of Dry Creek have a history of logging. We did not assess the impact of logging in the watershed. However, we believe logging is not likely the cause of the channel response in LDC because Reach 1, which is closest to logging activity, shows

limited impact. Climate change is known to impact streams due to changes in the timing

and magnitude of precipitation (Cayan et al., 2001; Salathe et al., 2014; Tennant et al.,

2015; Lee et al., 2018). Changes to the timing and magnitude of precipitation in the Dry

Creek watershed impact the entire watershed and likely cannot explain the complex

channel response in certain reaches of LDC and not others. We found placer mining and

development influenced LDC the greatest.

6.2 Holocene Channel Response in the Upper Reaches of Lower Dry Creek and the Modern Channel Change Linked to Placer Mining

Terraces mapped in Reach 2 show episodic incision from 8.7 meters above the

current channel (Figure 11). Overall, Reach 2 of LDC incised during the Holocene.

However, the dated streambank exposures shows a complex response from 4.79 ka to

present day (Figure 15). The upstream terrace surface was stable around 4.79 ka allowing

for the accumulation of colluvium on fluvial deposits and the development of carbonates

and a mollic A-horizon. At some point after 4.79 ka, LDC incised in Reach 2. This was

followed by aggradation of the downstream bank exposure terrace (T2) around 0.79 to

0.67 ka. High discharge events caused the accumulation of the sediment in sheet flood

and cross bedded deposits. This correlates to a period of increased alluvial fan deposits in

DCEW related to increased fire activity (Poulos and Pierce, 2018). After accumulation of

approximately 2.4 meters of sediment above current bankfull, the stream incised to its

current level. The reach incised after 0.67 ka and additional dating is needed to constrain

the timing and rate of incision. The Holocene complex response in Reach 2 is before

human influence and may be a response to a climatic change. Poulos and Pierce (2018)

linked the increased in alluvial fan deposits in DCEW to the Medieval Climate Anomaly.

The Medieval Climate Anomaly is a period of warming and more frequent and persistent

droughts throughout the Western United States from 900-1300 AD (1050-650 cal yr BP) (Cook et al., 2004). The warming and increased fire activity increased erosion in the watershed and potential is the cause of the aggradation in the downstream Peggy's Trail bank (Figure 15).

Historic mining activity was concentrated in Reach 2 of LDC (Figure 11). Placer mining ceased in the area prior to the earliest aerial photos of 1938, however, we suspect mining concluded in the watershed before 1900 AD (Figure 12) (Druss, 2015). Since 1938, Reach 2 has laterally migrated. Measurable lateral migration is not observed in any other reach of LDC. In the 1938 imagery, freshly deposited sand bars are scattered throughout Reach 2 (Figure 12). In the 1971 and 1992 imagery, a riparian zone developed which stabilized the channel (Figure 27). However, between 1992 and 1998 riparian vegetation width index decreased from 15.0 m to 9.4 m. Also, the lateral migration rate increased from 0.35 m/yr to 0.95 m/yr. Using aerial photos, we observe disturbed riparian vegetation and in several areas vegetation is completely removed. The Boise region experienced high amounts of rain and snow during the end of December 1996 and the first week of January 1997. Several weather stations in southwest Idaho recorded precipitation with storm return intervals of greater than 100 years (Shaub, 2001). The 1997 New Year Storm caused widespread flooding and slope failures in southwest Idaho. The flood event corresponds temporally to the increase in meander migration and removal of riparian vegetation. We only see this disturbance around the placer mining deposits of Reach 2, indicating the channel was unstable potentially due to the mining activity. The meander migration rate continues to be high until after 2011, when the riparian vegetation returned and the migration rate is similar as it was prior to the 1997

New Year Storm (Figure 27). The impact of placer mining is still being seen today in the watershed even though mining ceased over 100 years ago. This suggests that riparian vegetation is able to stabilize fine-grain placer mining outwash, but large flood events have the potential to reactivate the instability of the fine-grained material and remove riparian vegetation. The reactivation in Reach 2 persisted for approximately 13 years and 15 meters of lateral movement. We estimate the modern lateral migration is greater than LDC experienced throughout the Holocene, otherwise we would expect a wider valley (Grant and Swanson, 1995).

Lateral migration depends on the size and environmental characteristics of the basin and therefore it is not useful to compare rates between streams, but rather within the same system (Downs and Gregory, 2014). Few studies have documented meander migration rates of small alluvial streams as compared to large rivers, because resolution of aerial images to determine stream position. A study on placer mining of the Middle Fork of the South Platte River in Colorado found greater channel migration in mined reaches, but a lower sinuosity (Hilmes and Wohl, 1995). We did not compare sinuosity changes for each reach through time, but mined Reach 2 has the highest sinuosity in LDC in 2015 (Table 2). The South Platte River study found the channel has not recovered from placer mining impacts in 67-82 years, which is comparable to this study (Himes and Wohl, 1995). A study on placer gold mining impacts on a second order stream in Alaska, found after mining ceased the stream abandoned its channelized course and formed a new channel (Gilvear et al., 1995). The study also suggested the recovery of the geomorphology and habitat of the stream will take a number of large flood events.

Knighton (1989) predicted it would take ~150 years for a stream to regain dynamic equilibrium in his study reach.

Placer mining is known to mobilize fine-grained material which causes downstream aggradation (Gilbert, 1917). The increased fine-grained material causes sedimentation issues which are detrimental for aquatic species (Gilvear et al, 1995; Pentz and Kostaschuk, 1999). Downstream of Reach 2, Reach 3 has the lowest riparian vegetation width in 1971 (Figure 27). We attribute the lack of riparian vegetation to a potential slug of fine-grained sediment that is moving from Reach 2 to Reach 3 and 4. Today, LDC median bed sediment size fines from 28.7 mm in Reach 2 to 2.4 mm in Reach 3 (Figure 19). We expect fining of sediment moving downstream in LDC (Leopold et al., 1964). However after Reach 4, bed sediment coarsens in Reach 5 and 6 (Figure 19). We attribute the coarsening to two potential hypotheses. The median sediment size in Reach 3 and 4 is the natural deposition. Incision in Reach 5 increased the unit stream power, due to smaller width-depth ratio and additional discharge from Currant Creek (Figure 22 and Table 3). The increased stream power moved the majority of the fine grained material being transported from Reach 4 further downstream of Reach 5 and 6, resulting in coarser median bed sediment. However, we believe the fining in Reach 3 and 4 is from the mining activity in Reach 2. The longitudinal profile of LDC in Reach 4 is convex instead of the idealized concave stream profile (Figure 16). We attribute the convexity to deposition of fine-grained material when the slope of LDC decreased in Reach 3. In addition to the fine-grained deposition in Reach 3 and 4, Reach 5 is coarsened due to incision. We believe Reach 6 median grain size of 6.5mm is the expected grain size in LDC for Reach 3 to 6. All streambed grain size samples were

collected in the summer of 2020 after the largest discharge event on record at DCEW LG in spring of 2019 (Figure 20).

Small scale placer mining impacts on streams has not been well studied (Rohe, 1986). However, larger-scale placer mining studies (Gilbert, 1917, James, 1999), demonstrate that mining results in sediment slugs causing downstream aggradation (Nelson and Church, 2012). A long term study in Tasmania saw a 75 km study reach impacted by a slug of sediment for over 110 year (Knighton, 1989). Gilbert (1917) found sediment moved rapidly downstream, but some sediment remained stored in overbank deposits and likely will continue to affect the rivers (James, 2010). A study in Canada on the Frasier River found the slug of sediment could continue to move downstream for an estimated 300 years (Nelson and Church, 2012). We concluded that the historic and current geomorphic processes in Reach 2 of LDC as well as downstream aggradation in Reach 3 and 4 are impacted by historical placer mining.

6.3 Holocene Channel Response in the Lower Reaches of Lower Dry Creek and the Modern Channel Change Linked to Development and Channelization of Tributaries

The broad, low gradient Hidden Springs Terrace is evidence of long-term aggradation throughout Reach 3 to 6 during the Holocene (Figure 13). Also, well-developed soils on the Hidden Springs Terrace indicate a long record of stability. The radiocarbon dates in Reach 5 provide evidence of rapid aggradation (0.75 cm/yr) near the current channel during the last 300 years. The aggradation is episodic as indicated by the debris flow and sheet flood deposits in the stratigraphy (Figure 14). The Hidden Springs Terrace continues to form when large amounts of sediment from both the upper basin and tributaries contribute sediment to this major aggradational surface. Figure 29 shows in 1951 Currant Creek depositing sediment in distributaries on the Hidden Springs Terrace.

The modern topography shows remnants of an alluvial fan in the location of the distributaries of Currant Creek before it was channeled (Figure 30).

LDC Valley was primarily agricultural land until the development of the planned Hidden Springs community in 1997 (Figure 25). Post-1997, residential development continued and in 2019 represented 32.5% of the valley. Rural development also increased after 1992. Several of these homes contain large lots with land that is converted farmland. The largest amount of rural development in 2019 is in Reach 4 which accounts for 23.6% of the land (Figure 26). Currant Creek is in this reach, which provides large amount of discharge and sediment to the Hidden Springs Terrace and LDC during flood events (Figure 29). Homes are now located on abandoned distributaries of Current Creek.

Aerial imagery shows that Currant Creek was channelized sometime between 1971 and 1992. Historically, Currant Creek transitioned to a series of distributaries across the Hidden Springs Terrace (Figure 29). Directly downstream of the confluence with Currant Creek begins the incision in Reach 5 (Figure 16). HEC-RAS modeling shows LDC is wide and shallow in Reach 3, 4, and 6 and connected to the floodplain (Figure 17 and 22). LDC dissipates the energy over the floodplain throughout these reaches; however, modeling shows flows in Reach 5 are confined with a lower width/depth ratio. The confined flows and additional discharge from Currant Creek increase the stream power and sediment transport downstream, resulting in downcutting. We do not have direct discharge measurements of Currant Creek discharge, but the tributary's drainage area is 27% of the LDC watershed. Based on the drainage area we believe Currant Creek may provide enough discharge during flood events to have triggered the incision. The time period during which Currant Creek was channelized coincides with local's reports of

when incision in Reach 5 began. Channelization is a known contributor to channel incision (Gregory et al., 1992; Simon, 1989). As LDC incised, it reached unconsolidated sands and gravels (Figure 14). The unconsolidated material is easily eroded and transported potentially resulting in the rapid 4.7 meters of incision.

Stream incision is known to propagate upstream and/or downstream because of the changes in hydraulics and slope of the incised channel (Summerfield, 1991; Darby and Simon, 1999). The complex response caused by incision may impact downstream and upstream reaches because of changes in sediment supply and stream power. Incised Reach 5 may follow the channel evolution model (Figure 5) (Simon and Hupp, 1986). The reach is currently in the channelized, degraded stage 3. Going forward the streambank may pass a critical height and fail resulting in widening of the channel. This will result in increased width-depth ratio and a decreased shear stress allowing sediment to aggrade. However, the timeline for this process is unknown. This model is only one possible channel response and land-use may continue to impact LDC.

From 1971 to 2019, riparian vegetation in Reach 3 to 6 stayed similar, except for in 2003 (Figure 28). We attribute the decrease in 2003 to the timing of the imagery. The 2003 imagery is during April, while the other years are between June and September. The riparian trees haven't reached full foliage, which potentially resulted in less area delineation in 2003. The width stayed constant despite land-use change from farmland to development along LDC banks. Therefore, residential development didn't influence riparian width in LDC. Development near riparian zones is documented to cause a significant decrease in the extent of riparian vegetation and often the removal of vegetation (Lussier et al., 2006). We believe we did not see a decrease in riparian

vegetation because development is leaving a buffer between homes and the riparian zone, as well as riparian vegetation was removed before development for farmland. However, there is a decrease in riparian vegetation width in Reach 5 after 2003 (Figure 27). We believe this is associated with incision in Reach 5 which restricted the area for riparian vegetation to grow. Therefore, there is a correlation between rural development and concurrent channelization of Currant Creek with incision and loss of riparian vegetation in Reach 5.

6.4 Implications of Holocene to Modern Complex Response in Lower Dry Creek

LDC illustrates textbook complex response of Holocene cut and fill, lateral migration, and recent incision and sedimentation (Figure 31, Table 6). LDC, like many small western streams in developing areas, is sensitive to changes in land use. This study showed channelization of a tributary to reduce flooding caused rapid incision in an area which aggraded over the Holocene. We also observed mining activity shift the behavior of Reach 2 from episodic incision to lateral adjustment. This implies that not all reaches of a stream will respond to land-use disturbances the same. We found through hydraulic modeling and grain size analysis, LDC's median grain size is mobile at estimated bankfull flow for all reaches (Table 2). This mobility allows the stream to rapidly adjust both vertically and laterally.

During the Holocene from approximately 4790 to 700 years BP, Reach 2 incised while Reach 3 to 5 aggraded and laterally migrated building the Hidden Springs Terrace (Figure 31). Around approximately 700 years BP, during and after the Medieval Climate Anomaly, Reach 2 experienced increased sediment transport into the reach which caused aggradation. Meanwhile, Reach 3 to 5 continued to aggrade and laterally migrate, but had episodic aggradation from fire-related debris flows. During modern time (1940 to 2020

AD), Reach 2 experienced increased lateral migration caused by placer mining land-use. The placer mining also mobilized fine-grained sediment resulting in increased sediment transport to Reach 3 and 4. Reach 3 and 4 experienced fining of the grain size and increased aggradation due to the increased sediment transport into the reach. Reach 5 saw the channelization of Currant Creek which caused incision and an increase in sediment transport downstream.

We hypothesize a simple channel response LDC may follow in the short-term future (Figure 31). Reach 2 may have flood events remove leftover placer mining tailings from the channel and floodplains. Over time the sediment transport from Reach 2 to Reach 3 and 4 will decrease. Reach 3 and 4 may continue to transport the slug of placer mining sediment downstream. This will result in an increase in sediment transport downstream to Reach 5 and equilibrium with the decreased sediment transport into the reach. Finally, Reach 5 may follow the channel evolution model and widen its channel allowing aggradation of sediment from upstream until equilibrium is reached. Described here is a potential channel response of LDC in the future. However, as discussed, channel response of streams is complex and takes time to reach equilibrium. In addition, land-use may continue to impact LDC.
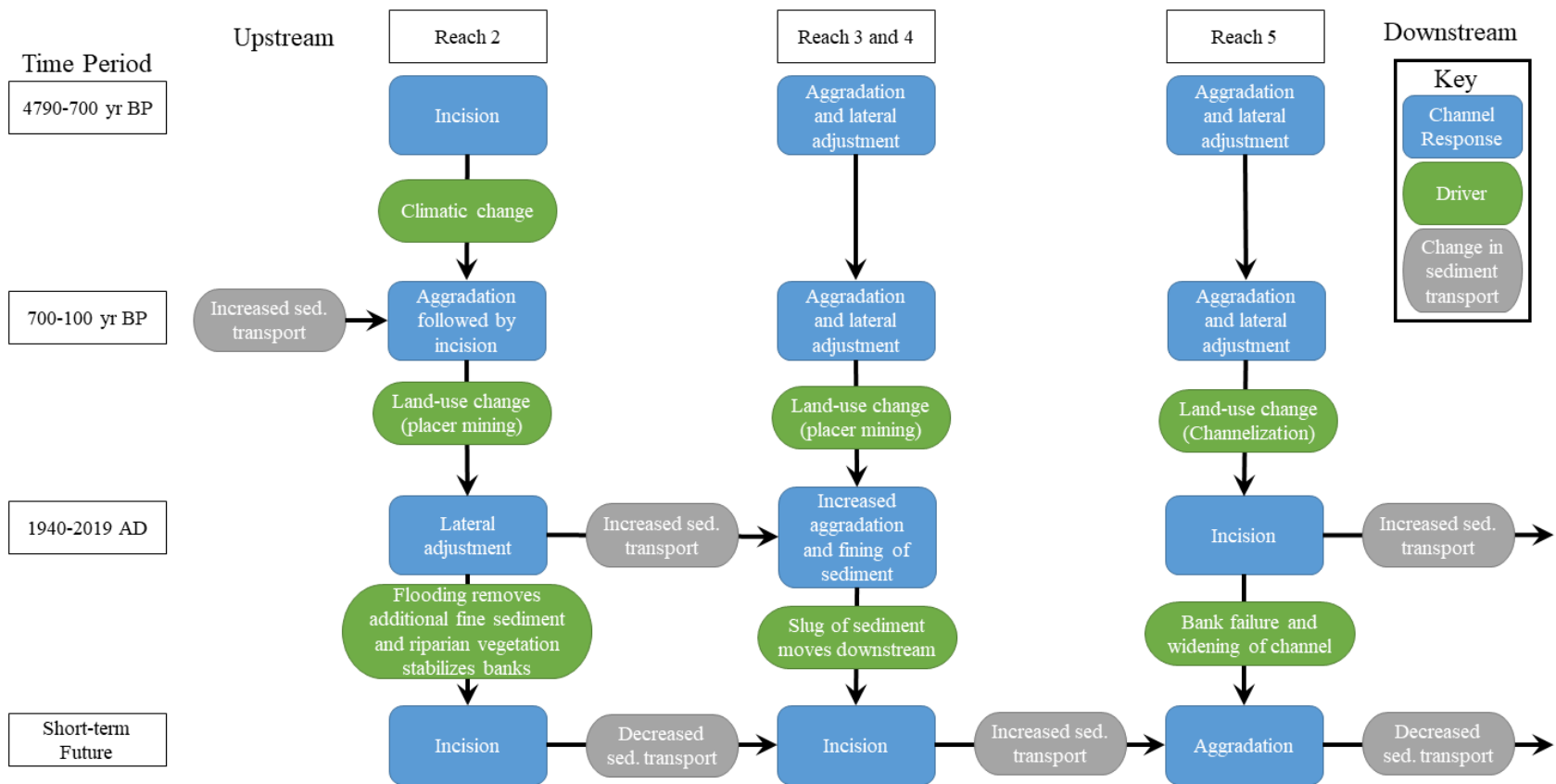
Figure 31 Flow chart of channel responses, drivers, and sediment transport changes of Lower Dry Creek. Time periods are from the earliest Quaternary date from this study to modern time. We hypothesize channel response Lower Dry Creek may experience in the short-term future. Blue boxes are channel responses we interpreted or observed during the time period. Green boxes are interpreted drivers which caused the channel response. Gray boxes are interpreted changes of sediment transport between reaches. Where there is no green or gray box we were unable to interpret a driver or change in sediment transport.

Table 6   Summary of channel response from Holocene to Modern time of Lower Dry Creek Reach 2 through 5.

Time Period	Reach 2	Reach 3 and 4	Reach 5
4790 - 700 BP	- Complex response of cut and fill initiated by a climatic change - Alluvial fan building	- Aggradation of Hidden Spring Terrace surface	- Aggradation of Hidden Springs Terrace surface
700 - 100 years BP	- Incision - Followed by aggradation from placer mining ~150-100 years BP	- Aggradation of Hidden Springs Terrace surface	- ^{14}C dates show rapid aggradation of Hidden Springs Terrace and lateral channel movement - Fire related debris flows
1940-2019 AD	- Increased lateral migration - Riparian vegetation changes potentially caused by unstable banks from mining sediment and 1997 flood	- Increased aggradation shown in convex longitudinal profile - Fining of bed substrate potentially due to placer mining mobilizing sediment	- Rapid incision - Increased input of discharge and sediment from channelization of Currant Creek

CHAPTER 7: CONCLUSION

We used remote sensing, hydraulic modeling, grain size analysis, and field observations to quantify how the distinct reaches of LDC are changing over human time scales; we use Quaternary dating methods and geomorphic mapping to examine how LDC has changed over centennial to millennial time scales. We found LDC has adjusted vertically and laterally compared to the longitudinal profile of the Hidden Springs Terrace. Quaternary dating, historic photos, and land use change suggest the primary drivers of aggradation (Reach 2) and incision (Reach 5) are likely due to impacts from placer mining and channelization of tributaries. This represents a shift from long-term aggradation and large-scale formation of the Hidden Springs Terrace observed over Holocene timescales.

While we cannot quantify (and therefore cannot discount) the influence of beaver trapping, logging, farming, grazing, and climate change on reach-scale channel change in LDC, these factors are likely not the main drivers of modern channel change in Reach 2 and 5. While several land-uses impact the stream, mining and channelization caused the most drastic response. It is useful to place modern channel changes into a longer geomorphic context to understand the stream's response to other external variables of technics, base-level, and climate. We found evidence of cut and fill potentially caused by climatic change in Reach 2. We believe that recent channel changes in Reach 2 are associated with placer mining impacts, but there may be a legacy complex response causing the channel to continue adjusting from the climatic change. Historical analysis of

fluvial changes is useful for designing, restoring, and maintaining a sustainable river or stream system (Kondolf and Larson, 1995; Gregory, 2006).

We believe results of this study can support stakeholders as they strive to understand the characteristics and response of small alluvial streams to anthropogenic land-use, and best options for restoration of degraded systems. Understanding the past geomorphic behavior of a stream allows restoration efforts to work with the stream instead of against it. For example, instead of channeling Currant Creek to prevent flooding, an alternative is to divert Currant Creek's flood discharge to farmland or wetland to allow for dissipation of the energy. This would allow for a more "natural" solution to flooding and would provide irrigation and habitat for aquatic species. A similar study as this has the potential to help stakeholders mitigate and restore alluvial streams more effectively in developing areas throughout the west because of the knowledge gained by understanding past fluvial conditions.

LDC illustrates textbook complex response as the stream both incises and aggrades in different locations due to differing drivers. This study shows that determining the drivers of modern channel change need to be placed within a longer more complete context. Results of this study can support stakeholders as they strive to understand the characteristics and response of small alluvial streams to anthropogenic land-use, and best options for restoration of degraded systems.

REFERENCES

Aitken, M.J., (1998). An introduction to optical dating: The dating of Quaternary sediments by the use of photon-stimulated luminescence. *Oxford University Press*, 267.

Antevs, E. (1952). Arroyo-cutting and filling. *The Journal of Geology*, *60*(4), 375-385.

Birkeland, P.W. (1984). Soils and geomorphology. *Oxford University Press.*

Birt, S.J. (2002). Quaternary stream and fan terraces in the Boise Foothills of the Idaho Batholith Mountains. *Geological Society of America Abstracts with Programs. 33*(4), 57

Booth, D. B. (1990). Stream channel incision following drainage basin urbanization. *Journal of the American Water Resources Association, 26*(3), 407-417.

Brunner, G. W. (2010). HEC-RAS river analysis system: hydraulic reference manual. *US Army Corps of Engineers, Institute for Water Resources, Hydrologic Engineering Center.*

Bryan, K. (1925). Date of channel trenching (arroyo cutting) in the arid southwest. *Science, 62*(1607), 338-344.

Cayan, D. R., Kammerdiener, S. A., Dettinger, M. D., Caprio, J. M., & Peterson, D. H. (2001). Changes in the onset of spring in the western United States. *Bulletin of the American Meteorological Society, 82*(3), 399-416.

Charlton, R. (2008). Fundamentals of fluvial geomorphology. *Routledge.*

Chow, V. T. (1959). Open-channel hydraulics. *McGraw-Hill Book Co.*

Cook, E. R., Woodhouse, C. A., Eakin, C. M., Meko, D. M., & Stahle, D. W. (2004). Long-term aridity changes in the western United States. *Science*, *306*(5698), 1015-1018.

Dahal, K. R., Benner, S., & Lindquist, E. (2017). Urban hypotheses and spatiotemporal characterization of urban growth in the Treasure Valley of Idaho, USA. *Applied Geography, 79,* 11-25.

Darby, S., & Simon, A. (1999). Incised river channels: processes, forms, engineering, and management. *Wiley.*

Downs, P., & Gregory, K. (2014). River channel management: towards sustainable catchment hydrosystems. *Routledge.*

Druss, C. (2015). The creek chronicles: nineteenth century Idaho farm life. *Basin & Range Publishing.*

Fitch, L., & Adams, B. W. (1998). Can cows and fish co-exist?. *Canadian Journal of Plant Science, 78*(2), 191-198.

Galbraith, R. F., & Roberts, R. G. (2012). Statistical aspects of equivalent dose and error calculation and display in OSL dating: an overview and some recommendations. *Quaternary Geochronology, 11,* 1-27.

Gilbert, G. K. (1917). Hydraulic-mining debris in the Sierra Nevada. *U.S. Geological Survey Professional Paper (105). U.S. Government Printing Office.*

Gilvear, D. J., Waters, T. M., & Milner, A. M. (1995). Image analysis of aerial photography to quantify changes in channel morphology and instream habitat following placer mining in interior Alaska. *Freshwater Biology, 34*(2), 389-398.

Grant, G. E., & Swanson, F. J. (1995). Morphology and processes of valley floors in mountain streams, western Cascades, Oregon. *Geophysical Monograph-American Geophysical Union*, *89*, 83-101.

Gregory, K. J. (2006). The human role in changing river channels. *Geomorphology, 79*(3-4), 172-191.

Gregory, K. J., Davis, R. J., & Downs, P. W. (1992). Identification of river channel change to due to urbanization. *Applied Geography, 12*(4), 299-318.

Gregory, K. J., Starkel, L., & Baker, V. (1995). Global continental palaeohydrology. *Global continental palaeohydrology. Wiley.*

Guérin, G., Mercier, N., & Adamiec, G. (2011). Dose-rate conversion factors: update. *Ancient TL, 29*(1), 5-8.

Hardison, E. C., O'Driscoll, M. A., DeLoatch, J. P., Howard, R. J., & Brinson, M. M. (2009). Urban land use, channel incision, and water table decline along coastal plain streams, North Carolina 1. *Journal of the American Water Resources Association, 45*(4), 1032-1046.

Hilmes, M. M., & Wohl, E. E. (1995). Changes in channel morphology associated with placer mining. *Physical Geography, 16*(3), 223-242.

Hutchins, M. G., Cowan, E. A., & Badurek, C. A. (2012). Identification and Geomorphometric assessment of stream terraces along the North and South Fork of the New River, Blue Ridge Physiographic Province. *Journal of Student Research in Environmental Science at Appalachian, 2*

Interagency Advisory Committee on Water Data. (1982). Guidelines for determining flood flow frequency. *Bulletin 17B of the Hydrology Subcommittee.*

James, A. (1999). Time and the persistence of alluvium: River engineering, fluvial geomorphology, and mining sediment in California. *Geomorphology, 31*(1-4), 265-290.

James, A. L. (2010). Secular sediment waves, channel bed waves, and legacy sediment. *Geography Compass, 4*(6), 576-598.

Kauffman, J. B., & Krueger, W. C. (1984). Livestock impacts on riparian ecosystems and streamside management implications... a review. *Rangeland Ecology & Management/Journal of Range Management Archives, 37*(5), 430-438.

Knighton, A. D. (1989). River adjustment to changes in sediment load: the effects of tin mining on the Ringarooma River, Tasmania, 1875–1984. *Earth Surface Processes and Landforms, 14*(4), 333-359.

Kondolf, G. M., & Larson, M. (1995). Historical channel analysis and its application to riparian and aquatic habitat restoration. *Aquatic Conservation: Marine and Freshwater Ecosystems, 5*(2), 109-126.

Kondolf, G. M., & Piégay, H. (2003). Tools in fluvial geomorphology: problem statement and recent practice. *Tools in Fluvial Geomorphology,* 1-22.

Lane, E. W. (1955). Design of stable channels. *Transaction of American Society of Civil Engineers, 120,* 1234-1260.

Le Bissonnais, Y., Daroussin, J., Jamagne, M., Lambert, J. J., Le Bas, C., King, D., Cerdan, O., Leonard, J., Bresson, L.-M., & Jones, R. J. A. (2005). Pan-European soil crusting and erodibility assessment from the European Soil Geographical Database using pedotransfer rules. *Advances in Environmental Modelling and Monitoring, 2*(1), 1-15.

Lee, S.-Y., Mauger, G.S., & Won. J.S. (2018). Effect of climate change on flooding in King County Rivers: Using new regional climate model simulations to quantify changes in flood risk. *Report prepared for King County. Climate Impacts Group, University of Washington.*

Leopold, A. S. (1974). Ecosystem deterioration under multiple use. *In Proceedings of the Wild Trout Symposium,* 96-98.

Leopold, L.B., Emmett, W.W., & Myrick, R.M. (1954). Channel and Hillslope Processes in a Semiarid Area, New Mexico. *U.S.G.S. Professional Paper 352-G,* 193-253.

Leopold, L. B., Wolman, M. G., & Miller, J. P. (1964). Fluvial processes in geomorphology. *Dover Publications, INC.*

Lewis, R. S., Kiilsgaard, T. H., Bennett, E. H., Hall, W. E., Vallier, T. L., & Brooks, H. C. (1987). Lithologic and chemical characteristics of the central and southeastern part of the southern lobe of the Idaho Batholith. *Geology of the Blue Mountains region of Oregon, Idaho, and Washington,* 171-196.

Love, D. W., & Rhodes, D. D. (1979). Quaternary fluvial geomorphic adjustments in Chaco Canyon, New Mexico. *Adjustments of the fluvial system,* 277-308.

Lussier, S. M., Enser, R. W., Dasilva, S. N., & Charpentier, M. (2006). Effects of habitat disturbance from residential development on breeding bird communities in riparian corridors. *Environmental management, 38*(3), 504-521.

Martz, L. W., & Garbrecht, J. (1992). Numerical definition of drainage network and subcatchment areas from digital elevation models. *Computers & Geosciences, 18*(6), 747-761.

Montgomery, D. R., & Buffington, J. M. (1997). Channel-reach morphology in mountain drainage basins. *Geological Society of America Bulletin*, *109*(5), 596-611.

Moriasi, D. N., Gitau, M. W., Pai, N., & Daggupati, P. (2015). Hydrologic and water quality models: Performance measures and evaluation criteria. *Transactions of the ASABE, 58*(6), 1763-1785.

Murray, A. S., & Wintle, A. G. (2000). Luminescence dating of quartz using an improved single-aliquot regenerative-dose protocol. *Radiation measurements, 32*(1), 57-73.

Nelson, A. D., & Church, M. (2012). Placer mining along the Fraser River, British Columbia: the geomorphic impact. *Geological Society of America Bulletin, 124*(7-8), 1212-1228.

Othberg, K. L. (1994). Geology and geomorphology of the Boise Valley and adjoining areas, western Snake River Plain, Idaho. *Idaho Geological Survey, 29.*

Othberg, K. L., & Stanford, L. R. (1992). Geologic map of the Boise Valley and adjoining area, western Snake River Plain. Idaho. *Idaho Geological Survey Geologic Map, 18.*

Pentz, S. B., & Kostaschuk, R. A. (1999). Effect of placer mining on suspended sediment in reaches of sensitive fish habitat. *Environmental Geology, 37*(1-2), 78-89.

Peterson, H. V. (1950). The problem of gullying in western valleys. *Applied sedimentation. Wiley,* 407-434.

Pierce, J. L., Meyer, G. A., & Jull, A. T. (2004). Fire-induced erosion and millennial-scale climate change in northern ponderosa pine forests. *Nature*, *432*(7013), 87-90.

Pollock, M. M., Beechie, T. J., Wheaton, J. M., Jordan, C. E., Bouwes, N., Weber, N., & Volk, C. (2014). Using beaver dams to restore incised stream ecosystems. *Bioscience, 64*(4), 279-290.

Poulos, M. J. (2016). Feedbacks Among Climate, Soils, Vegetation, and Erosion Drive Valley Asymmetry Development in the Mountains of Central Idaho. *Boise State University Theses and Dissertations. 1190*

Poulos, M. J., & Pierce, J. L. (2018). Alluvial fan depositional records from north and south-facing catchments in semi-arid montane terrain. *Quaternary Research, 89*(1), 237.

Quantum Spatial Inc. (2015). Ada County Enhanced Wildfire Risk Map: LiDAR Technical Data Report (RFP 15045).

Reimer, P. J., Bard, E., Bayliss, A., Beck, J. W., Blackwell, P. G., Ramsey, C. B., ... & Grootes, P. M. (2013). IntCal13 and Marine13 radiocarbon age calibration curves 0–50,000 years cal BP. *Radiocarbon, 55*(4), 1869-1887.

Rinaldi, M., Gurnell, A. M., Belletti, B., Berga Cano, M. I., Bizzi, S., Bussettini, M., & Vezza, P. (2015). Final report on methods, models, tools to assess the hydromorphology of rivers, Deliverable 6.2, Part 1, of REFORM (REstoring rivers FOR effective catchment Management), a Collaborative project (large-scale integrating project) funded by the European Commission within the 7th Framework Programme under Grant Agreement 282656.

Richards, K. S. (1982). Rivers: form and process in alluvial channels *(Vol. 358). London: Methuen.*

Riley, K. E., Rittenour, T. M., Pederson, J. L., & Belmont, P. (2019). Erosion rates and patterns in a transient landscape, Grand Staircase, southern Utah, USA. *Geology, 47*(9), 811-814.

Rohe, R. (1986). Man and the land: Mining's impact in the far West. *Arizona and the West, 28*(4), 299-338.

Salathé Jr, E. P., Hamlet, A. F., Mass, C. F., Lee, S. Y., Stumbaugh, M., & Steed, R. (2014). Estimates of twenty-first-century flood risk in the Pacific Northwest based on regional climate model simulations. *Journal of Hydrometeorology, 15*(5), 1881-1899.

Schilling, K. E., Zhang, Y. K., & Drobney, P. (2004). Water table fluctuations near an incised stream, Walnut Creek, Iowa. *Journal of Hydrology, 286*(1-4), 236-248.

Schumm, S. A. (1973). Geomorphic thresholds and complex response of drainage systems. *Fluvial geomorphology, 6,* 69-85.

Schumm, S.A. (1977). The fluvial system. *John Wiley and Sons, New York.*

Schumm, S. A., & Hadley, R. F. (1957). Arroyos and the semiarid cycle of erosion. *American Journal of Science, 255*(3), 161-174.

Schumm, S. A., Harvey, M. D., & Watson, C. C. (1984). Incised channels: morphology, dynamics, and control. *Water Resources Publications.*

Schumm, S. A., & Parker, R. S. (1973). Implications of complex response of drainage systems for Quaternary alluvial stratigraphy. *Nature Physical Science, 243*(128), 99-100.

Shaub, S. (2001). Landslides and wildfire: an example from the Boise National Forest. *Boise State University Theses and Dissertations. 792*

Simon, A. (1989). A model of channel response in disturbed alluvial channels. *Earth surface processes and landforms, 14*(1), 11-26.

Simon, A., & Hupp, C. R. (1986). Channel evolution in modified Tennessee channels. *In Proceedings of the Fourth Federal Interagency Sedimentation Conference March 24-27, 1986, Las Vegas, Nevada, 2.*

Stine, S. (1994). Extreme and persistent drought in California and Patagonia during mediaeval time. *Nature, 369(6481),* 546-549.

Strahler, A. N. (1957). Quantitative analysis of watershed geomorphology. *Eos, Transactions American Geophysical Union, 38*(6), 913-920.

Stuiver, M., & Reimer, P. J. (1993). Extended ^{14}C database and revised CALIB radiocarbon calibration program, *Radiocarbon, 35,* 215-230.

Summerfield, M. A. (1991). Global Geomorphology, An introduction to the study of landforms. *Longman, Harlow*

Tennant, C. J., Crosby, B. T., & Godsey, S. E. (2015). Elevation-dependent responses of streamflow to climate warming. *Hydrological Processes, 29*(6), 991-1001.

Turnipseed, D. P., & Sauer, V. B. (2010). Discharge measurements at gaging stations. *US Geological Survey. No. 3-A8.*

Waters, T. F. (1995). Sediment in streams: sources, biological effects, and control. *American Fisheries Society.*

Wheeler, H. E., & Cook, E. F. (1954). Structural and stratigraphic significance of the Snake River capture, Idaho-Oregon. *The Journal of Geology, 62*(6), 525-536.

Williams, G. P. (1978). Bank-full discharge of rivers. *Water resources research, 14*(6), 1141-1154.

Wohl, E. (2017). The significance of small streams. *Frontiers of Earth Science, 11*(3), 447-456.

Wohl, E., Allen, A.O., Mersel, M.K., Kichefski, S.L., Fritz, K.M., Lichvar, R.W., Nadeau, T.L., Topping, B.J., Trier, P.H. and Vanderbilt, F.B., (2016). Synthesizing the scientific foundation for ordinary high water mark delineation in fluvial systems (No. ERDC/CRREL SR-16-5). *US Army Engineer Research and Development Center (ERDC) Hanover United States.*

Wolman, M. G. (1954). A method of sampling coarse river-bed material. *EOS, Transactions American Geophysical Union, 35*(6), 951-956.

Womack, W. R., & Schumm, S. A. (1977). Terraces of Douglas Creek, northwestern Colorado: an example of episodic erosion. *Geology, 5*(2), 72-76.

Wood, S. H. (1994). Seismic expression and geological significance of a lacustrine delta in Neogene deposits of the western Snake River plain, Idaho. *AAPG bulletin, 78*(1), 102-121.

Wood, S. H., & Burnham, W. L. (1983). Boise, Idaho geothermal system. *Geothermal Resources Council, Transactions, 7,* 215-223.

Wood, S. H., & Clemens, D. M. (2002). Geologic and tectonic history of the western
Snake River Plain, Idaho and Oregon. Tectonic and Magmatic Evolution of the
Snake River Plain Volcanic Province. *Idaho Geological Survey Bulletin.*

APPENDIX A

Representative Photos of Each Reach

Appendix A includes a representative photo of each of the six distinct reaches of

Lower Dry Creek from upstream (Reach 1) to downstream (Reach 6).
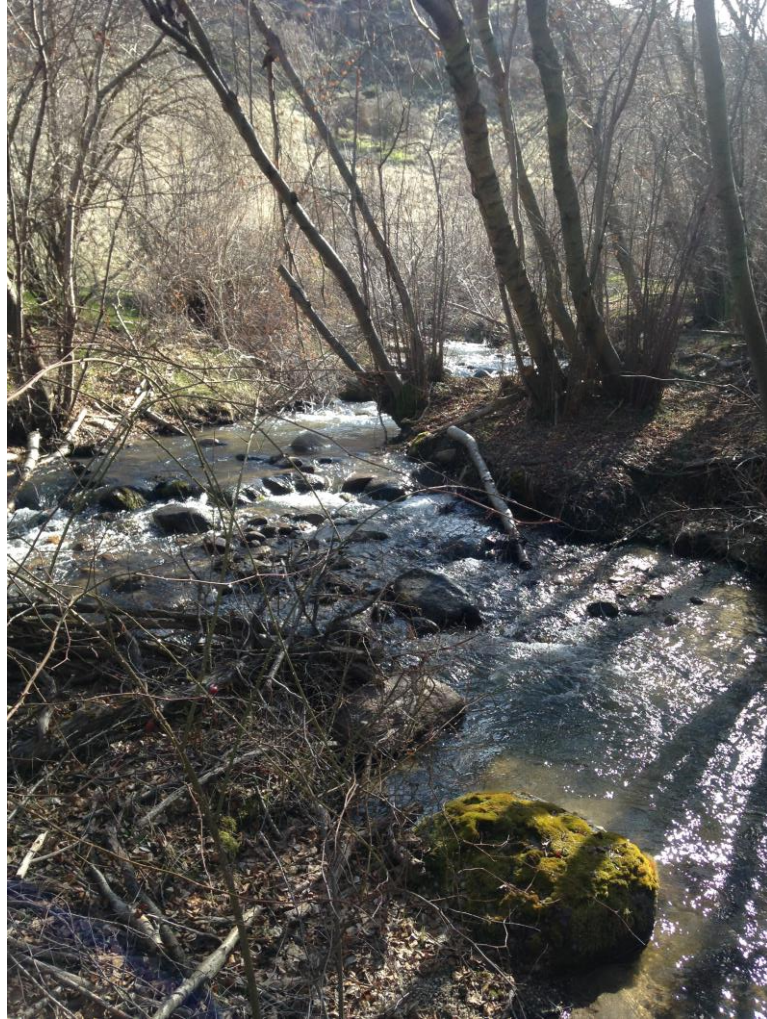
Figure A1   **Representative photo of Reach 1.**

Figure A2   Representative photo of Reach 2.

Figure A3   Representative photo of Reach 3.

Figure A4   Representative photo of Reach 4.

Figure A5   Representative photo of Reach 5.

Figure A6   Representative photo of Reach 6.

APPENDIX B

Soil Pit Photos, Soil Descriptions, and Geomorphic Maps

Appendix B includes photos of soil pits from this study. Soil characteristics and descriptions are available in tables found in this appendix. Soil descriptions follow the methods and naming outlined in the appendix of Birkeland (1984). Appendix B also includes geomorphic maps of Lower Dry Creek divided by reach from upstream (Reach 1) to downstream (Reach 6).

Figure B1   **Photo of DC-Terrace 1 soil pit on terrace 0.6m above current Lower Dry Creek bankfull.**

Figure B2 **Photo of DC-Terrace 2 soil pit on terrace 6.3m above current Lower Dry Creek bankfull.**

Figure B3 **Photo of DC-Terrace 3 soil pit on terrace 5.7m above current Lower Dry Creek bankfull.**

Figure B4   Photo of DC-Terrace 4 soil pit on terrace 4.75m above current Lower Dry Creek bankfull.

Figure B5   Photo of DC-Terrace 5 soil pit on terrace 1.85m above current Lower Dry Creek bankfull.

Figure B6   Photo of DC-Terrace 6 soil pit on terrace 0.6m above current Lower Dry Creek bankfull.

Figure B7   Photo of DC-Terrace 7 soil pit on terrace 1.85m above current Lower Dry Creek bankfull.

Figure B8   **Photo of DC-Terrace 8 soil pit on terrace 4.75m above current Lower Dry Creek bankfull.**

Figure B9   **Photo of DC-Terrace 9 soil pit on terrace 1.8m above current Lower Dry Creek bankfull.**

Figure B10   Photo of DC-Terrace 10 soil pit on terrace 3.6m above current Lower Dry Creek bankfull.

Figure B11   Photo of DC-Terrace 11 soil pit on terrace 3.4m above current Lower Dry Creek bankfull.

Figure B12   Photo of DC-Terrace 12 soil pit on terrace 4.75m above current Lower Dry Creek bankfull.

Figure B13   Photo of DC-Terrace 13 soil pit on terrace 1.05m above current Lower Dry Creek bankfull.

Figure B14   Photo of DC-Terrace 14 soil pit on terrace 7.5m above current Lower Dry Creek bankfull.
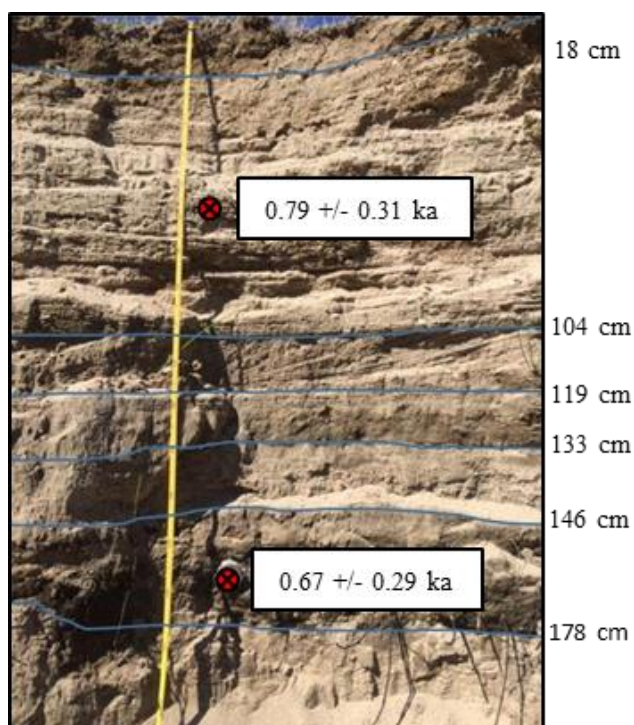
Figure B15   Photo of DC-Terrace 15 soil pit on terrace 2.4m above current Lower Dry Creek bankfull.
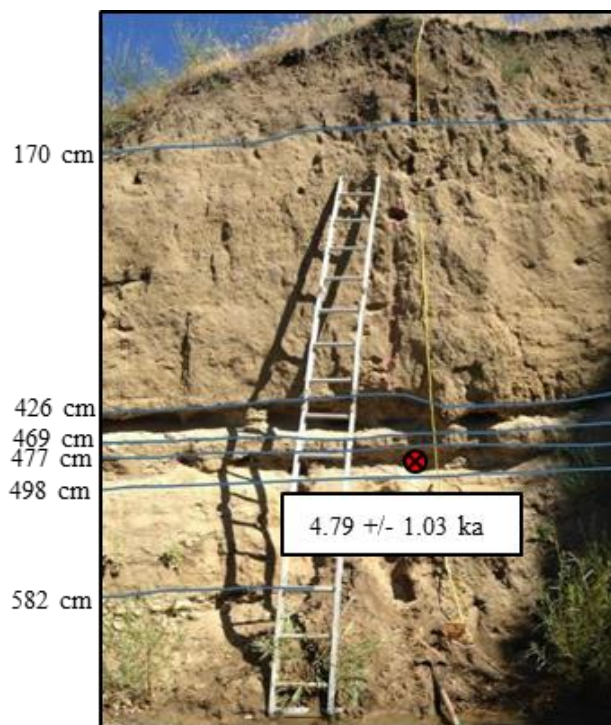
Figure B16   **Photo of DC-Bank 1 soil pit on terrace 2.44m above current Lower Dry Creek bankfull.**

Figure B17   **Photo of soil pit DC-Pit 1 on Peggy's Trail high surface.**

Figure B18   Photo of soil pit on landslide high surface.

Table B1 DC-Terrace 1 soil properties.

Soil Desc. Location : DC-Terrace 1 (11T 562998N 4839141E)

Date 5/23/2019 Time 12:35 Geomorphic Surface Stream terrace ~0.6m above bankfull

Elev. 910 Slope 5° Aspect North Vegetation Grasses and sage brush

Parent Material(s) Fluvial

Depth (cm)	Horizon	Color moist	Structure			Gravel %		Consistence Wet		Moist	Dry	Texture		pH	Clay Films			Bound-aries		Notes
0-6	A	7.5 YR 2.5/2	m	vf	gr	0	50	so	po	lo	lo	S	SiCL		v1	f	pf	a	s	
			sg	f	pl	<10	75	ss	ps	vfr	so	LS	SiL		1		po	c	w	
			1	m	pr	10	>75	s	p	fr	sh	SL	Si		2	d	br	g	i	
			2	c	cpr	25		vs	vp	fi	h	SCL	SiC		3		co	d	b	
			3	vc	abk					vfi	vh	L	C			p	cobr			
					sbk					efi	eh	CL	SC							
2-25	C	10YR 5/4	m	vf	gr	0	50	so	po	lo	lo	S	SiCL		v1	f	pf	a	s	Well sorted sands
			sg	f	pl	<10	75	ss	ps	vfr	so	LS	SiL		1		po	c	w	
			1	m	pr	10	>75	s	p	fr	sh	SL	Si		2	d	br	g	i	
			2	c	cpr	25		vs	vp	fi	h	SCL	SiC		3		co	d	b	
			3	vc	abk					vfi	vh	L	C			p	cobr			
					sbk					efi	eh	CL	SC							
25-35	A	7.5YR 3/2	m	vf	gr	0	50	so	po	lo	lo	S	SiCL		v1	f	pf	a	s	Roots
			sg	f	pl	<10	75	ss	ps	vfr	so	LS	SiL		1		po	c	w	
			1	m	pr	10	>75	s	p	fr	sh	SL	Si		2	d	br	g	i	
			2	c	cpr	25		vs	vp	fi	h	SCL	SiC		3		co	d	b	
			3	vc	abk					vfi	vh	L	C			p	cobr			
					sbk					efi	eh	CL	SC							

Table B2   DC-Terrace 2 soil properties.

Soil Desc.   Location :   DC-Terrace 2 (11T 562924N 489136E)

Date   5/23/2019   Time   13:00   Geomorphic Surface   Fan terrace ~6.3m above bankfull

Elev.   916   Slope   10°   Aspect   North   Vegetation   Grasses and sage brush

Parent Material(s)   Fluvial

Depth (cm)	Horizon	Color moist	Structure			Gravel %		Consistence Wet		Moist	Dry	Texture		pH	Clay Films				Bound-aries		Notes
0-60	?	10YR 2/2	m	vf	gr	0	50	so	po	lo	lo	S	SiCL		v1	f	pf		a	s	Sand with some gravel and silt.
			sg	f	pl	<10	75	ss	ps	vfr	so	LS	SiL		1		po		c	w	
			1	m	pr	10	>75	s	p	fr	sh	SL	Si		2	d	br		g	i	
			2	c	cpr	25		vs	vp	fi	h	SCL	SiC		3		co		d	b	
			3	vc	abk					vfi	vh	L	C				p	cobr			
					sbk					efi	eh	CL	SC								
60-78	C	7.5YR 3/3	m	vf	gr	0	50	so	po	lo	lo	S	SiCL		v1	f	pf		a	s	Less silt
			sg	f	pl	<10	75	ss	ps	vfr	so	LS	SiL		1		po		c	w	
			1	m	pr	10	>75	s	p	fr	sh	SL	Si		2	d	br		g	i	
			2	c	cpr	25		vs	vp	fi	h	SCL	SiC		3		co		d	b	
			3	vc	abk					vfi	vh	L	C				p	cobr			
					sbk					efi	eh	CL	SC								
78-95	C	10 YR 2/1	m	vf	gr	0	50	so	po	lo	lo	S	SiCL		v1	f	pf		a	s	More cohesive
			sg	f	pl	<10	75	ss	ps	vfr	so	LS	SiL		1		po		c	w	
			1	m	pr	10	>75	s	p	fr	sh	SL	Si		2	d	br		g	i	
			2	c	cpr	25		vs	vp	fi	h	SCL	SiC		3		co		d	b	
			3	vc	abk					vfi	vh	L	C				p	cobr			
					sbk					efi	eh	CL	SC								

Table B3 DC-Terrace 3 soil properties.

Soil Desc. Location : DC-Terrace 3 (11T 563064N 4839135E)

Date 5/30/2019 Time 9:40 Geomorphic Surface Stream terrace ~5.7m above bankfull

Elev. 915 Slope 5° Aspect North Vegetation Grasses and sage brush

Parent Material(s) Fluvial

Depth (cm)	Horizon	Color moist	Structure			Gravel %		Consistence Wet		Moist	Dry	Texture		pH	Clay Films			Bound-aries		Notes
0-30	A	10 YR 2/2	m	vf	**gr**	0	50	so	po	lo	lo	S	SiCL		v1	f	pf	a	s	
			sg	f	pl	<10	75	ss	ps	**vfr**	so	LS	SiL		1		po	c	**w**	
			1	m	pr	10	>75	s	p	fr	sh	**SL**	Si		2	d	br	**g**	i	
			2	c	cpr	25		vs	vp	fi	h	SCL	SiC		3		co	d	b	
			3	vc	abk					vfi	vh	L	C			p	cobr			
					sbk					efi	eh	CL	SC							
30-60	C	7.5YR 5/3	m	vf	gr	0	50	so	po	lo	lo	**S**	SiCL		v1	f	pf	a	**s**	Sandy gravel, not weathered
			sg	f	pl	<10	75	ss	ps	vfr	so	LS	SiL		1		po	**c**	w	
			1	m	pr	10	>75	s	p	fr	sh	SL	Si		2	d	br	g	i	
			2	c	cpr	25		vs	vp	fi	h	SCL	SiC		3		co	d	b	
			3	vc	abk					vfi	vh	L	C			p	cobr			
					sbk					efi	eh	CL	SC							
60-75	C	7.5YR 3/2	m	vf	gr	0	50	so	po	lo	lo	S	SiCL		v1	f	pf	a	**s**	Overbank silt and clay
			sg	f	pl	<10	75	ss	ps	vfr	so	LS	SiL		1		po	**c**	w	
			1	m	pr	10	>75	s	p	fr	sh	SL	Si		2	d	br	g	i	
			2	c	cpr	25		vs	vp	fi	h	**SCL**	SiC		3		co	d	b	
			3	vc	abk					vfi	vh	L	C			p	cobr			
					sbk					efi	eh	CL	SC							
75-105	C	7.5YR 6/4	m	vf	gr	0	50	so	po	lo	lo	**S**	SiCL		v1	f	pf	a	s	Similar to parent material from 30-60 cm, coarser then unit above.
			sg	f	pl	<10	75	ss	ps	vfr	so	LS	SiL		1		po	c	w	
			1	m	pr	10	>75	s	p	fr	sh	SL	Si		2	d	br	g	i	
			2	c	cpr	25		vs	vp	fi	h	SCL	SiC		3		co	d	b	
			3	vc	abk					vfi	vh	L	C			p	cobr			
					sbk					efi	eh	CL	SC							

Table B4   DC-Terrace 4 soil properties.

Soil Desc.   Location :   DC-Terrace 4 (11T 563240N 4839072E)

Date   5/30/2019   Time   10:58   Geomorphic Surface   Stream terrace ~4.75m above bankfull

Elev.   918   Slope   5°   Aspect   South   Vegetation   Grasses and sage brush

Parent Material(s)   Fluvial

Depth (cm)	Horizon	Color moist	Structure			Gravel %		Consistence Wet		Moist	Dry	Texture		pH	Clay Films			Bound-aries		Notes
0-50	A	7.5YR 2.5/2	m	vf	gr	0	50	so	po	lo	lo	S	SiCL		v1	f	pf	a	s	Boundary is wavy with sand lens below.
			sg	f	pl	<10	75	ss	ps	vfr	so	LS	SiL		1		po	c	w	
			1	m	pr	10	>75	s	p	fr	sh	SL	Si		2	d	br	g	i	
			2	c	cpr	25		vs	vp	fi	h	SCL	SiC		3		co	d	b	
			3	vc	abk					vfi	vh	L	C			p	cobr			
					sbk					efi	eh	CL	SC							
50-65	C	7.5YR 6/3	m	vf	gr	0	50	so	po	lo	lo	S	SiCL		v1	f	pf	a	s	Sand, Areas of coarser gravels that are weathering in place.
			sg	f	pl	<10	75	ss	ps	vfr	so	LS	SiL		1		po	c	w	
			1	m	pr	10	>75	s	p	fr	sh	SL	Si		2	d	br	g	i	
			2	c	cpr	25		vs	vp	fi	h	SCL	SiC		3		co	d	b	
			3	vc	abk					vfi	vh	L	C			p	cobr			
					sbk					efi	eh	CL	SC							

Table B5   DC-Terrace 5 soil properties.

Soil Desc.   Location : DC-Terrace 5 (11T 5632740N 4839088E)

Date 5/30/2019   Time 11:42   Geomorphic Surface Stream terrace ~1.85m above bankfull

Elev. 915 Slope 5°   Aspect South   Vegetation Grasses, aspen, russian olive

Parent Material(s) Fluvial

Depth (cm)	Horizon	Color moist	Structure			Gravel %		Consistence Wet		Moist	Dry	Texture		pH	Clay Films			Bound-aries		Notes
0-10	A	7.5YR 3/4	m	vf	gr	0	50	so	po	lo	lo	S	SiCL		v1	f	pf	a	s	Very thin soil with not much silt.
			sg	f	pl	<10	75	ss	ps	vfr	so	LS	SiL		1		po	c	w	
			1	m	pr	10	>75	s	p	fr	sh	SL	Si		2	d	br	g	i	
			2	c	cpr	25		vs	vp	fi	h	SCL	SiC		3		co	d	b	
			3	vc	abk					vfi	vh	L	C			p	cobr			
					sbk					efi	eh	CL	SC							
10-35	Bw	7.5YR 5/3	m	vf	gr	0	50	so	po	lo	lo	S	SiCL		v1	f	pf	a	s	Possibly a very weakly developed B horizon
			sg	f	pl	<10	75	ss	ps	vfr	so	LS	SiL		1		po	c	w	
			1	m	pr	10	>75	s	p	fr	sh	SL	Si		2	d	br	g	i	
			2	c	cpr	25		vs	vp	fi	h	SCL	SiC		3		co	d	b	
			3	vc	abk					vfi	vh	L	C			p	cobr			
					sbk					efi	eh	CL	SC							
35-65	C	7.5YR 7/3	m	vf	gr	0	50	so	po	lo	lo	S	SiCL		v1	f	pf	a	s	Sandy parent material.
			sg	f	pl	<10	75	ss	ps	vfr	so	LS	SiL		1		po	c	w	
			1	m	pr	10	>75	s	p	fr	sh	SL	Si		2	d	br	g	i	
			2	c	cpr	25		vs	vp	fi	h	SCL	SiC		3		co	d	b	
			3	vc	abk					vfi	vh	L	C			p	cobr			
					sbk					efi	eh	CL	SC							

Table B6   DC-Terrace 6 soil properties.

Soil Desc.   Location :   DC-Terrace 6 (11T 563308N 4839063E)

Date   5/30/2019   Time   12:30   Geomorphic Surface   Stream terrace ~0.6m above bankfull

Elev.   915   Slope   5°   Aspect   South   Vegetation   Grasses, aspen

Parent Material(s)   Fluvial

Depth (cm)	Horizon	Color moist	Structure			Gravel %		Consistence Wet		Moist	Dry	Texture		pH	Clay Films			Bound-aries		Notes
0-4	A	7.5 YR 2.5/2	m	vf	gr	0	50	so	po	lo	lo	S	SiCL		v1	f	pf	a	s	Thin soil w/ abundant gravels
			sg	f	pl	<10	75	ss	ps	vfr	so	LS	SiL		1		po	c	w	
			1	m	pr	10	>75	s	p	fr	sh	SL	Si		2	d	br	g	i	
			2	c	cpr	25		vs	vp	fi	h	SCL	SiC		3		co	d	b	
			3	vc	abk					vfi	vh	L	C			p	cobr			
					sbk					efi	eh	CL	SC							
4-30	C	7.5YR 5/3	m	vf	gr	0	50	so	po	lo	lo	S	SiCL		v1	f	pf	a	s	Sand w gravels and cobbles
			sg	f	pl	<10	75	ss	ps	vfr	so	LS	SiL		1		po	c	w	
			1	m	pr	10	>75	s	p	fr	sh	SL	Si		2	d	br	g	i	
			2	c	cpr	25		vs	vp	fi	h	SCL	SiC		3		co	d	b	
			3	vc	abk					vfi	vh	L	C			p	cobr			
					sbk					efi	eh	CL	SC							

Table B7 DC-Terrace 7 soil properties.

Soil Desc. Location : DC-Terrace 7 (11T 563226N 4839058E)

Date 6/3/2019 Time 10:30 Geomorphic Surface Stream terrace ~2.0m above bankfull

Elev. 915 Slope 5° Aspect South Vegetation Grasses (cheat and native), sagebrush

Parent Material(s) Fluvial

Depth (cm)	Horizon	Color moist	Structure			Gravel %		Consistence Wet	Moist	Dry	Texture		pH	Clay Films			Bound-aries		Notes
0-20	A	7.5YR 3/3	m	vf	gr	0	50	so po	lo	lo	S	SiCL		v1	f	pf	a	s	Very sandy soil, thin w/ wavy boundary above fluvial stratigraphy, 90 cm coble near surface.
			sg	f	pl	<10	75	ss ps	vfr	so	LS	SiL		1		po	c	w	
			1	m	pr	10	>75	s p	fr	sh	SL	Si		2	d	br	g	i	
			2	c	cpr	25		vs vp	fi	h	SCL	SiC		3		co	d	b	
			3	vc	abk				vfi	vh	L	C			p	cobr			
					sbk				efi	eh	CL	SC							
20-32	C	10YR 5/4	m	vf	gr	0	50	so po	lo	lo	S	SiCL		v1	f	pf	a	s	Fluvial sand
			sg	f	pl	<10	75	ss ps	vfr	so	LS	SiL		1		po	c	w	
			1	m	pr	10	>75	s p	fr	sh	SL	Si		2	d	br	g	i	
			2	c	cpr	25		vs vp	fi	h	SCL	SiC		3		co	d	b	
			3	vc	abk				vfi	vh	L	C			p	cobr			
					sbk				efi	eh	CL	SC							
32-39	C	10YR 3/3	m	vf	gr	0	50	so po	lo	lo	S	SiCL		v1	f	pf	a	s	
			sg	f	pl	<10	75	ss ps	vfr	so	LS	SiL		1		po	c	w	
			1	m	pr	10	>75	s p	fr	sh	SL	Si		2	d	br	g	i	
			2	c	cpr	25		vs vp	fi	h	SCL	SiC		3		co	d	b	
			3	vc	abk				vfi	vh	L	C			p	cobr			
					sbk				efi	eh	CL	SC							
39-80	C	10YR 6/4	m	vf	gr	0	50	so po	lo	lo	S	SiCL		v1	f	pf	a	s	Coarsen upwards, larger gravels.
			sg	f	pl	<10	75	ss ps	vfr	so	LS	SiL		1		po	c	w	
			1	m	pr	10	>75	s p	fr	sh	SL	Si		2	d	br	g	i	
			2	c	cpr	25		vs vp	fi	h	SCL	SiC		3		co	d	b	
			3	vc	abk				vfi	vh	L	C			p	cobr			
					sbk				efi	eh	CL	SC							

Table B8   DC-Terrace 8 soil properties.

Soil Desc.   Location :   DC-Terrace 8 (11T 563288N 4839041E)

Date   6/3/2019   Time   11:40   Geomorphic Surface   Stream terrace ~4.75m above bankfull

Elev.   918   Slope   5°   Aspect   North   Vegetation   Grasses, sagebrush

Parent Material(s)   Fluvial

Depth (cm)	Horizon	Color moist	Structure			Gravel %		Consistence Wet		Moist	Dry	Texture		pH	Clay Films			Bound-aries		Notes
0-80	A	10YR 2/2	m	vf	gr	0	50	so	po	lo	lo	S	SiCL		v1	f	pf	a	s	Thick A, no color change, sampled every 20 cm. Bed rock appears to be 1.5 m below terrace.
			sg	f	pl	<10	75	ss	ps	vfr	so	LS	SiL		1		po	c	w	
			1	m	pr	10	>75	s	p	fr	sh	SL	Si		2	d	br	g	i	
			2	c	cpr	25		vs	vp	fi	h	SCL	SiC		3		co	d	b	
			3	vc	abk					vfi	vh	L	C			p	cobr			
					sbk					efi	eh	CL	SC							

Table B9   DC-Terrace 9 soil properties.

Soil Desc.	Location :	DC-Terrace 9 (11T 563415N 4838888E)		
Date	6/12/2019	Time	8:30	Geomorphic Surface	Stream terrace ~1.8m above bankfull
Elev.	921	Slope	5°	Aspect	North	Vegetation	Grasses, sagebrush
Parent Material(s)		Fluvial		

Depth (cm)	Horizon	Color moist	Structure			Gravel %		Wet	Moist	Dry	Texture		pH	Clay Films			Boundaries		Notes
0-27	A	7.5YR 2.5/3	m / sg / 1 / 2 / 3	vf / f / m / c / vc	**gr** / pl / pr / cpr / abk / sbk	0 / <10 / 10 / 25	50 / 75 / >75	so / ss / s / vs	po / ps / p / vp	lo / vfr / fr / fi / vfi / efi	lo / so / sh / h / vh / eh	S / **LS** / SL / SCL / L / CL	SiCL / SiL / Si / SiC / C / SC		v1 / 1 / 2 / 3 / p	f / d	pf / po / br / co / cobr	a / c / **g** / d	s / **w** / i / b	Weathered gravels granite and basalt.
27-34	C	7.5YR 4/4	m / sg / 1 / 2 / 3	vf / f / m / c / vc	gr / pl / pr / cpr / abk / sbk	0 / <10 / 10 / 25	50 / 75 / >75	so / ss / s / vs	po / ps / p / vp	lo / vfr / fr / fi / vfi / efi	lo / so / sh / h / vh / eh	**S** / LS / SL / SCL / L / CL	SiCL / SiL / Si / SiC / C / SC		v1 / 1 / 2 / 3 / p	f / d	pf / po / br / co / cobr	a / **c** / g / d	s / **w** / i / b	Sand lens
34-42	C	7.5YR 3/4	m / sg / 1 / 2 / 3	vf / f / m / c / vc	gr / pl / pr / cpr / abk / sbk	0 / <10 / 10 / 25	50 / 75 / >75	so / ss / s / vs	po / ps / p / vp	lo / vfr / fr / fi / vfi / efi	lo / so / sh / h / vh / eh	S / **LS** / SL / SCL / L / CL	SiCL / SiL / Si / SiC / C / SC		v1 / 1 / 2 / 3 / p	f / d	pf / po / br / co / cobr	**a** / c / g / d	s / **w** / i / b	More silt content, overbank deposit.
42-46	C	7.5YR 4/2	m / sg / 1 / 2 / 3	vf / f / m / c / vc	gr / pl / pr / cpr / abk / sbk	0 / <10 / 10 / 25	50 / 75 / >75	so / ss / s / vs	po / ps / p / vp	lo / vfr / fr / fi / vfi / efi	lo / so / sh / h / vh / eh	**S** / LS / SL / SCL / L / CL	SiCL / SiL / Si / SiC / C / SC		v1 / 1 / 2 / 3 / p	f / d	pf / po / br / co / cobr	**a** / c / g / d	s / **w** / i / b	Sand lens.
46-70	C	7.5YR 3/3	m / sg / 1 / 2 / 3	vf / f / m / c / vc	gr / pl / pr / cpr / abk / sbk	0 / <10 / **10** / 25	50 / 75 / >75	so / ss / s / vs	po / ps / p / vp	lo / vfr / fr / fi / vfi / efi	lo / so / sh / h / vh / eh	S / **LS** / SL / SCL / L / CL	SiCL / SiL / Si / SiC / C / SC		v1 / 1 / 2 / 3 / p	f / d	pf / po / br / co / cobr	a / c / g / d	s / w / i / b	Weathered gravels and overbank deposit, few roots.

Table B10   DC-Terrace 10 soil properties.

Soil Desc.   Location: DC-Terrace 10 (11T 563593N 4838730E)
Date 6/12/2019   Time 9:00   Geomorphic Surface: Stream terrace ~3.6m above bankfull
Elev. 926   Slope 5°   Aspect North   Vegetation: Grasses, sagebrush, wild flowers
Parent Material(s): Fluvial

Depth (cm)	Horizon	Color moist	Structure			Gravel %		Consistence Wet		Moist	Dry	Texture		pH	Clay Films			Boundaries		Notes
0-10	A	7.5YR 3/2	m	vf	**gr**	0	50	so	po	lo	lo	S	SiCL		v1	f	pf	a	s	Sampled A horizon every 10 cm.
			sg	f	pl	<10	75	ss	ps	vfr	**so**	**LS**	SiL		1		po	c	w	
			1	m	pr	10	>75	s	p	**fr**	sh	SL	Si		2	d	br	g	i	
			2	c	cpr	25		vs	vp	fi	h	SCL	SiC		3		co	d	b	
			3	vc	abk					vfi	vh	L	C			p	cobr			
					sbk					efi	eh	CL	SC							
10-20	A	7.5YR 3/2	m	vf	**gr**	0	50	so	po	lo	lo	S	SiCL		v1	f	pf	a	s	
			sg	f	pl	<10	75	ss	ps	vfr	so	**LS**	SiL		1		po	c	w	
			1	m	pr	10	>75	s	p	**fr**	sh	SL	Si		2	d	br	g	i	
			2	c	cpr	25		vs	vp	fi	h	SCL	SiC		3		co	d	b	
			3	vc	abk					vfi	vh	L	C			p	cobr			
					sbk					efi	eh	CL	SC							
20-30	A	7.5YR 3/2	m	vf	**gr**	0	50	so	po	lo	lo	S	SiCL		v1	f	pf	a	s	
			sg	f	pl	<10	75	ss	ps	vfr	so	**LS**	SiL		1		po	c	w	
			1	m	pr	10	>75	s	p	**fr**	sh	SL	Si		2	d	br	g	i	
			2	c	cpr	25		vs	vp	fi	h	SCL	SiC		3		co	d	b	
			3	vc	abk					vfi	vh	L	C			p	cobr			
					sbk					efi	eh	CL	SC							
30-45	A	7.5YR 4/2	m	vf	**gr**	0	50	so	po	lo	lo	S	SiCL		v1	f	pf	a	s	
			sg	f	pl	<10	75	ss	ps	vfr	so	**LS**	SiL		1		po	c	**w**	
			1	m	pr	10	>75	s	p	**fr**	sh	SL	Si		2	d	br	**g**	i	
			2	c	cpr	25		vs	vp	fi	h	SCL	SiC		3		co	d	b	
			3	vc	abk					vfi	vh	L	C			p	cobr			
					sbk					efi	eh	CL	SC							
45-60	C	7.5YR 4/2	m	vf	gr	0	50	so	po	lo	**lo**	S	SiCL		v1	f	pf	**a**	s	Sand lens
			sg	f	pl	<10	75	ss	ps	vfr	so	LS	SiL		1		po	c	**w**	
			1	m	pr	10	>75	s	p	fr	sh	SL	Si		2	d	br	g	i	
			2	c	cpr	25		vs	vp	fi	h	SCL	SiC		3		co	d	b	
			3	vc	abk					vfi	vh	L	C			p	cobr			
					sbk					efi	eh	CL	SC							
60-80	C	7.5YR 2.5/3	m	vf	gr	0	50	so	po	lo	lo	S	SiCL		v1	f	pf	a	s	Increased silt content.
			sg	f	pl	<10	75	ss	ps	**vfr**	so	LS	SiL		1		po	c	w	
			1	m	pr	10	>75	s	p	fr	sh	**SL**	Si		2	d	br	g	i	
			2	c	cpr	25		vs	vp	fi	h	SCL	SiC		3		co	d	b	
			3	vc	abk					vfi	vh	L	C			p	cobr			
					sbk					efi	eh	CL	SC							

Table B11   DC-Terrace 11 soil properties.

Soil Desc.   Location :   DC-Terrace 11 (11T 563549N 4838825E)

Date   6/12/2019   Time   12:05   Geomorphic Surface   Stream terrace ~3.4m above bankfull

Elev.   925   Slope   5°   Aspect   South   Vegetation   Grasses

Parent Material(s)   Fluvial

Depth (cm)	Horizon	Color moist	Structure			Gravel %		Consistence Wet		Moist	Dry	Texture		pH	Clay Films			Bound-aries		Notes
0-80	A	7.5YR 2.5/2	m	vf	gr	0	50	so	po	lo	lo	S	SiCL		v1	f	pf	a	s	Gravel content increases with depth, no horizons observed.
			sg	f	pl	<10	75	ss	ps	vfr	so	LS	SiL		1		po	c	w	
			1	m	pr	10	>75	s	p	fr	sh	SL	Si		2	d	br	g	i	
			2	c	cpr	25		vs	vp	fi	h	SCL	SiC		3		co	d	b	
			3	vc	abk					vfi	vh	L	C			p	cobr			
					sbk					efi	eh	CL	SC							

Table B12   DC-Terrace 12 soil properties.

Soil Desc. Location : DC-Terrace 12 (11T 563172N 4839115E)

Date 6/13/2019 Time 8:40 Geomorphic Surface Stream terrace ~4.75m above bankfull

Elev. 917 Slope 5° Aspect South Vegetation Grasses and sagebrush

Parent Material(s) Fluvial

Depth (cm)	Horizon	Color moist	Structure			Gravel %		Consistence Wet		Moist	Dry	Texture		pH	Clay Films			Bound-aries		Notes
0-10	A	7.5YR 2.5/3	m	vf	gr	0	50	so	po	lo	lo	S	SiCL		v1	f	pf	a	s	No boundary designation. Sampled every 10 cm.
			sg	f	pl	<10	75	ss	ps	vfr	so	LS	SiL		1		po	c	w	
			1	m	pr	10	>75	s	p	fr	sh	SL	Si		2	d	br	g	i	
			2	c	cpr	25		vs	vp	fi	h	SCL	SiC		3		co	d	b	
			3	vc	abk					vfi	vh	L	C			p	cobr			
					sbk					efi	eh	CL	SC							
10-50	A	7.5YR 2.5/3	m	vf	gr	0	50	so	po	lo	lo	S	SiCL		v1	f	pf	a	s	
			sg	f	pl	<10	75	ss	ps	vfr	so	LS	SiL		1		po	c	w	
			1	m	pr	10	>75	s	p	fr	sh	SL	Si		2	d	br	g	i	
			2	c	cpr	25		vs	vp	fi	h	SCL	SiC		3		co	d	b	
			3	vc	abk					vfi	vh	L	C			p	cobr			
					sbk					efi	eh	CL	SC							
50-65	C		m	vf	gr	0	50	so	po	lo	lo	S	SiCL		v1	f	pf	a	s	Sand lens
			sg	f	pl	<10	75	ss	ps	vfr	so	LS	SiL		1		po	c	w	
			1	m	pr	10	>75	s	p	fr	sh	SL	Si		2	d	br	g	i	
			2	c	cpr	25		vs	vp	fi	h	SCL	SiC		3		co	d	b	
			3	vc	abk					vfi	vh	L	C			p	cobr			
					sbk					efi	eh	CL	SC							

Table B13   DC-Terrace 13 soil properties.

Soil Desc. Location : DC-Terrace 13 (11T 562906N 4839220E)

Date 6/13/2019 Time 9:20 Geomorphic Surface Stream terrace ~1.05m above bankfull

Elev. 909 Slope 5° Aspect South Vegetation Grasses and willows

Parent Material(s) Fluvial

Depth (cm)	Horizon	Color moist	Structure			Gravel %		Consistence Wet	Moist	Dry	Texture		pH	Clay Films			Bound-aries		Notes
0-15	A	7.5YR 4/3	m	vf	gr	0	50	so po	lo	lo	S	SiCL		v1	f	pf	a	s	
			sg	f	pl	<10	75	ss ps	vfr	so	LS	SiL		1		po	c	w	
			1	m	pr	10	>75	s p	fr	sh	SL	Si		2	d	br	g	i	
			2	c	cpr	25		vs vp	fi	h	SCL	SiC		3		co	d	b	
			3	vc	abk				vfi	vh	L	C			p	cobr			
					sbk				efi	eh	CL	SC							
15-55	C	7.5YR 5/4	m	vf	gr	0	50	so po	lo	lo	S	SiCL		v1	f	pf	a	s	Coarse sands and gravels.
			sg	f	pl	<10	75	ss ps	vfr	so	LS	SiL		1		po	c	w	
			1	m	pr	10	>75	s p	fr	sh	SL	Si		2	d	br	g	i	
			2	c	cpr	25		vs vp	fi	h	SCL	SiC		3		co	d	b	
			3	vc	abk				vfi	vh	L	C			p	cobr			
					sbk				efi	eh	CL	SC							
55-85	C	7.5YR 4/6	m	vf	gr	0	50	so po	lo	lo	S	SiCL		v1	f	pf	a	s	Sand lens
			sg	f	pl	<10	75	ss ps	vfr	so	LS	SiL		1		po	c	w	
			1	m	pr	10	>75	s p	fr	sh	SL	Si		2	d	br	g	i	
			2	c	cpr	25		vs vp	fi	h	SCL	SiC		3		co	d	b	
			3	vc	abk				vfi	vh	L	C			p	cobr			
					sbk				efi	eh	CL	SC							
85-105	C		m	vf	gr	0	50	so po	lo	lo	S	SiCL		v1	f	pf	a	s	Bottom is at bankfull. Cobble layer.
			sg	f	pl	<10	75	ss ps	vfr	so	LS	SiL		1		po	c	w	
			1	m	pr	10	>75	s p	fr	sh	SL	Si		2	d	br	g	i	
			2	c	cpr	25		vs vp	fi	h	SCL	SiC		3		co	d	b	
			3	vc	abk				vfi	vh	L	C			p	cobr			
					sbk				efi	eh	CL	SC							

Table B14   DC-Terrace 14 soil properties.

Soil Desc.   Location :   DC-Terrace 14 (11T 562784N 4839308E)

Date   6/13/2019   Time   10:15   Geomorphic Surface   Stream terrace ~7.5m above bankfull

Elev.   914   Slope   5°   Aspect   South   Vegetation   Sagebrush and grasses

Parent Material(s)   Fluvial

Depth (cm)	Horizon	Color moist	Structure		Gravel %		Consistence Wet		Moist	Dry	Texture		pH	Clay Films			Bound-aries		Notes
0-10	A	7.5YR 3/3	m	vf	gr	0	50	so	po	lo	lo	S	SiCL		v1	f	pf	a	s	Compacted due to grazing.
			sg	f	pl	<10	75	ss	ps	vfr	so	LS	SiL		1		po	c	w	
			1	m	pr	10	>75	s	p	fr	sh	SL	Si		2	d	br	g	i	
			2	c	cpr	25		vs	vp	fi	h	SCL	SiC		3		co	d	b	
			3	vc	abk					vfi	vh	L	C			p	cobr			
					sbk					efi	eh	CL	SC							
10-20	A	7.5YR 3/3	m	vf	gr	0	50	so	po	lo	lo	S	SiCL		v1	f	pf	a	s	15-20 cm sand lens
			sg	f	pl	<10	75	ss	ps	vfr	so	LS	SiL		1		po	c	w	
			1	m	pr	10	>75	s	p	fr	sh	SL	Si		2	d	br	g	i	
			2	c	cpr	25		vs	vp	fi	h	SCL	SiC		3		co	d	b	
			3	vc	abk					vfi	vh	L	C			p	cobr			
					sbk					efi	eh	CL	SC							
20-60	A	7.5YR 4/6	m	vf	gr	0	50	so	po	lo	lo	S	SiCL		v1	f	pf	a	s	
			sg	f	pl	<10	75	ss	ps	vfr	so	LS	SiL		1		po	c	w	
			1	m	pr	10	>75	s	p	fr	sh	SL	Si		2	d	br	g	i	
			2	c	cpr	25		vs	vp	fi	h	SCL	SiC		3		co	d	b	
			3	vc	abk					vfi	vh	L	C			p	cobr			
					sbk					efi	eh	CL	SC							
60-75	C		m	vf	gr	0	50	so	po	lo	lo	S	SiCL		v1	f	pf	a	s	
			sg	f	pl	<10	75	ss	ps	vfr	so	LS	SiL		1		po	c	w	
			1	m	pr	10	>75	s	p	fr	sh	SL	Si		2	d	br	g	i	
			2	c	cpr	25		vs	vp	fi	h	SCL	SiC		3		co	d	b	
			3	vc	abk					vfi	vh	L	C			p	cobr			
					sbk					efi	eh	CL	SC							

Table B15   DC-Pit 1 Peggy's trail high surface soil properties.

Soil Desc.   Location :   DC-Pit1 Peggy's Trail High Surface (11T 562784N 4839308E)

Date   5/23/2019   Time   10:00   Geomorphic Surface   Old Stream terrace

Elev.   1072   Slope   5°   Aspect   North   Vegetation   Sagebrush and grasses

Parent Material(s)   Fluvial

Depth (cm)	Horizon	Color moist	Structure			Gravel %		Consistence Wet		Moist	Dry	Texture		pH	Clay Films			Bound-aries		Notes
0-25	A	10YR 4/3	m	vf	gr	0	50	so	po	lo	lo	S	SiCL		v1	f	pf	a	s	Sampled
			sg	f	pl	<10	75	ss	ps	vfr	so	LS	SiL		1		po	c	w	
			1	m	pr	10	>75	s	p	fr	sh	SL	Si		2	d	br	g	i	
			2	c	cpr	25		vs	vp	fi	h	SCL	SiC		3		co	d	b	
			3	vc	abk					vfi	vh	L	C			p	cobr			
					sbk					efi	eh	CL	SC							
25-40	Cox	7.5YR 5/6	m	vf	gr	0	50	so	po	lo	lo	S	SiCL		v1	f	pf	a	s	Saprolite, wavy boundary of granite from 25-40 cm.
			sg	f	pl	<10	75	ss	ps	vfr	so	LS	SiL		1		po	c	w	
			1	m	pr	10	>75	s	p	fr	sh	SL	Si		2	d	br	g	i	
			2	c	cpr	25		vs	vp	fi	h	SCL	SiC		3		co	d	b	
			3	vc	abk					vfi	vh	L	C			p	cobr			
					sbk					efi	eh	CL	SC							

Figure B19   Geomorphic map of Reach 1.

Figure B20   Geomorphic map of Reach 2.
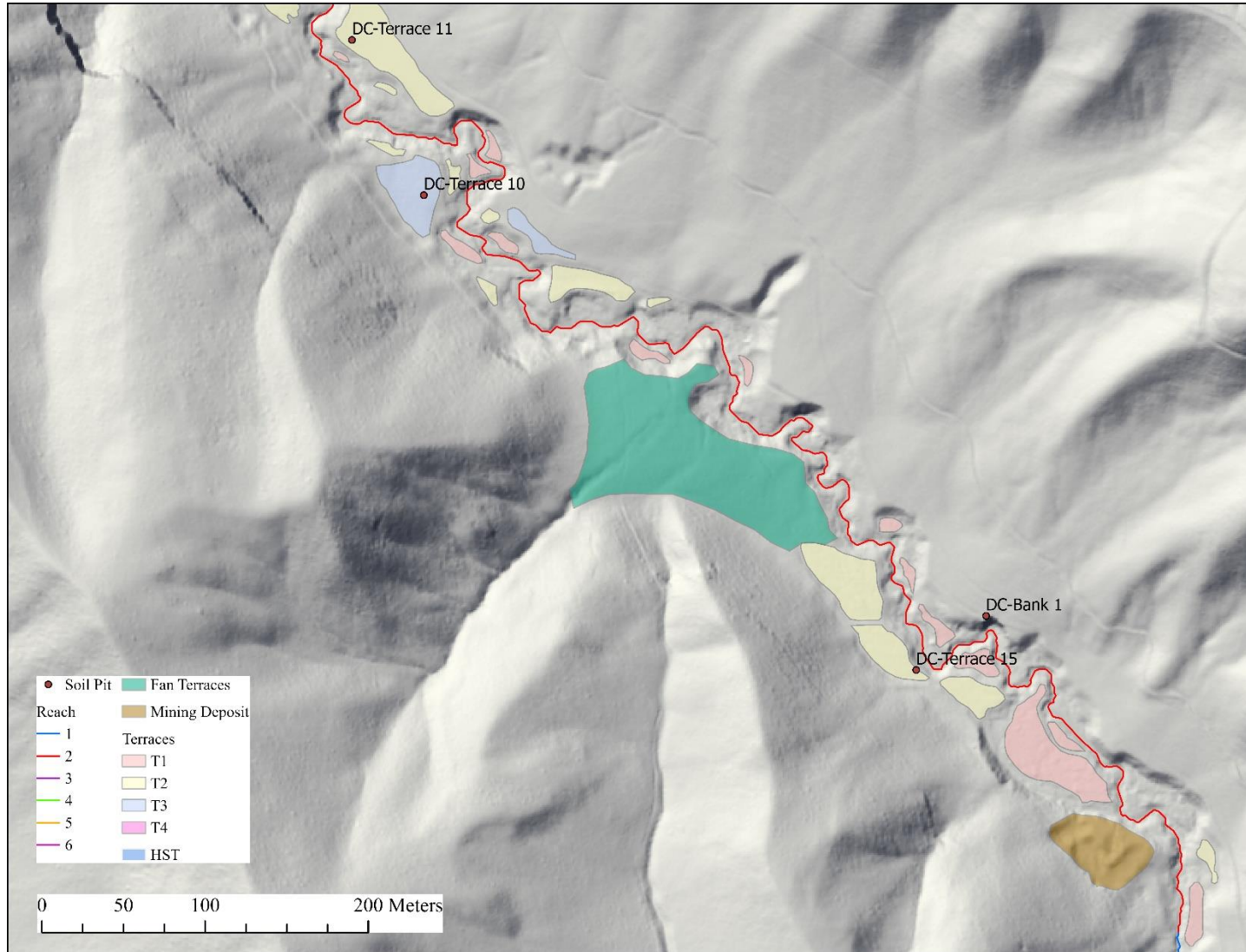
Figure B21   Geomorphic map of upper Reach 2.
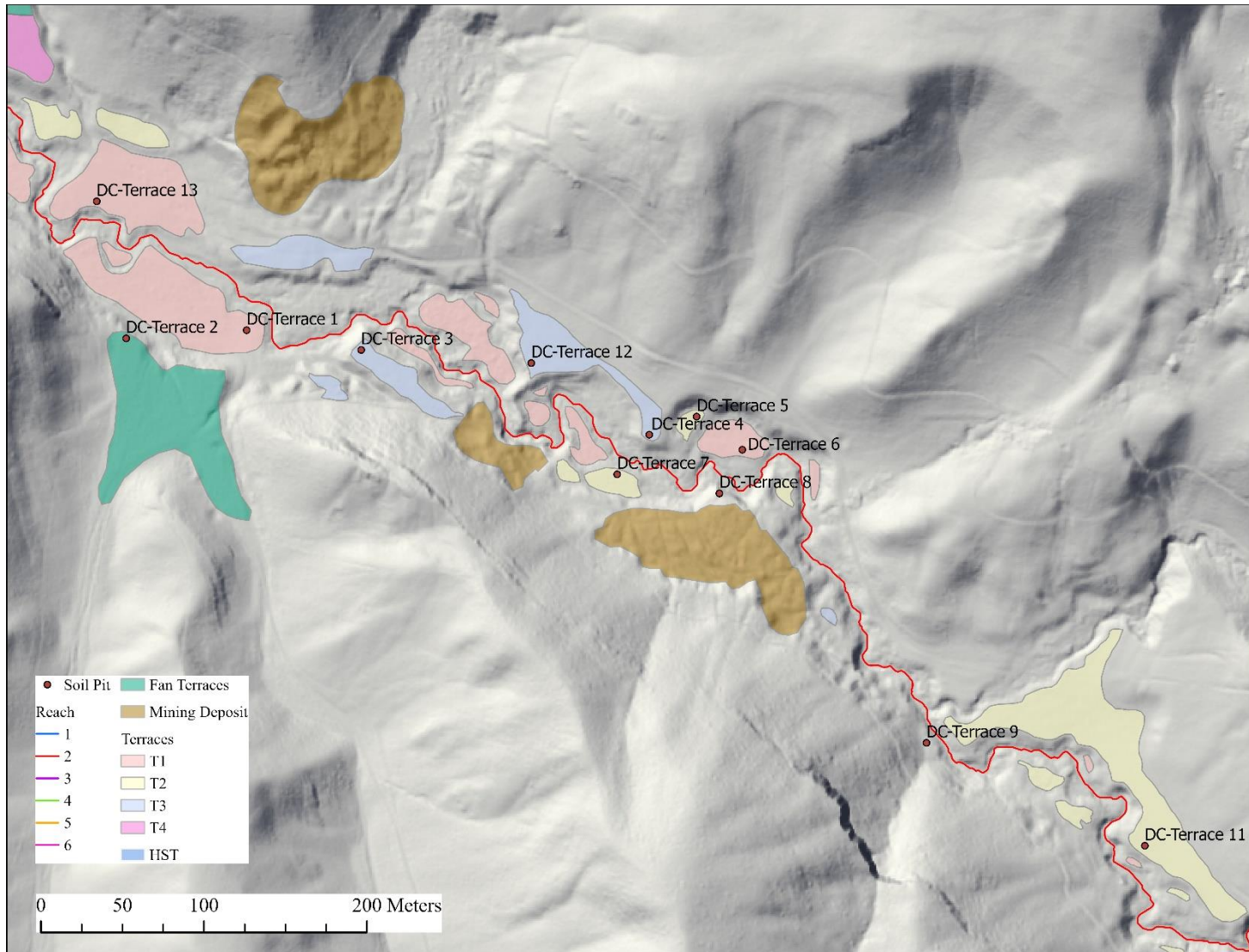
Figure B22   Geomorphic map of middle Reach 2.
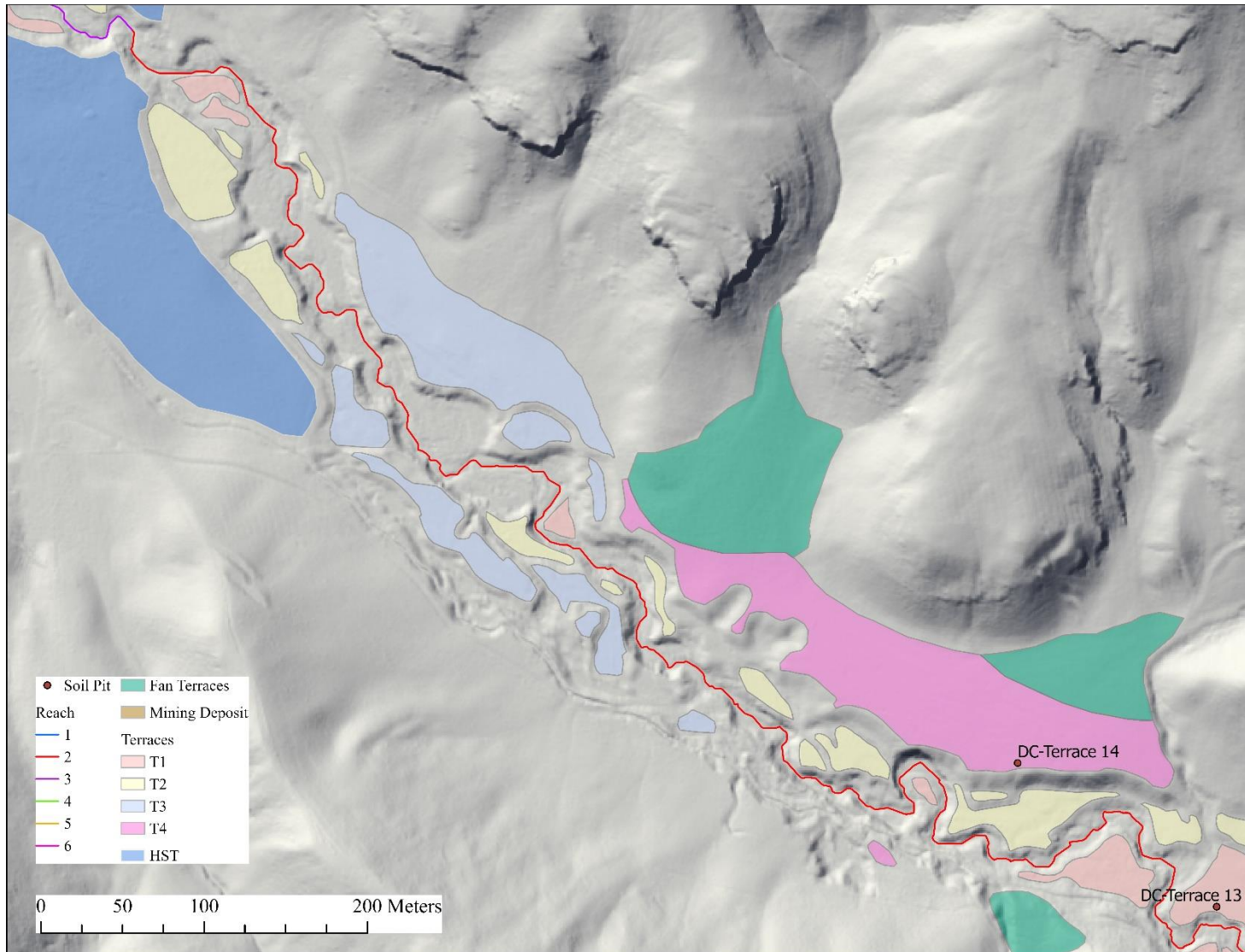
Figure B23   Geomorphic map of lower Reach 2.
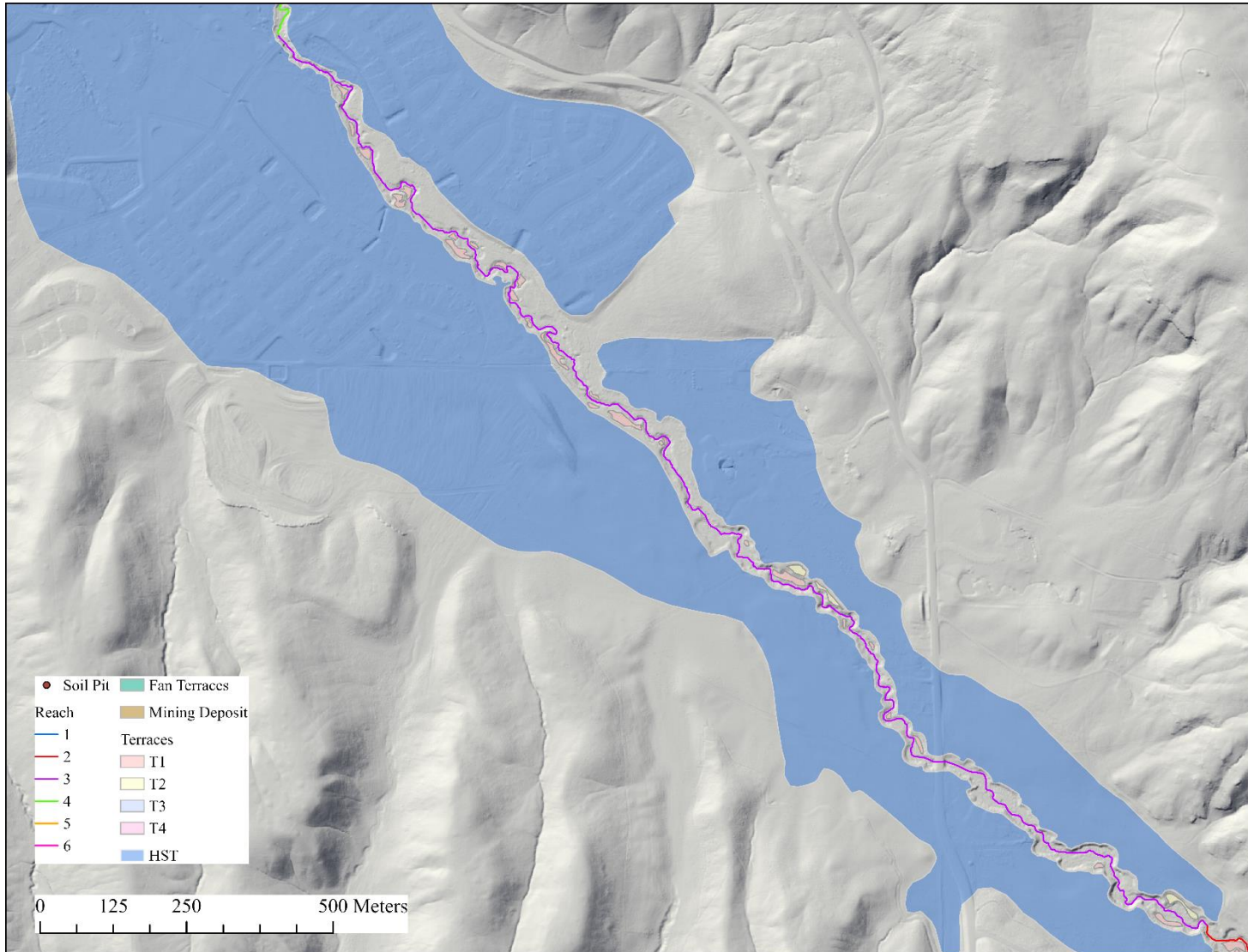
Figure B24   Geomorphic map of Reach 3.
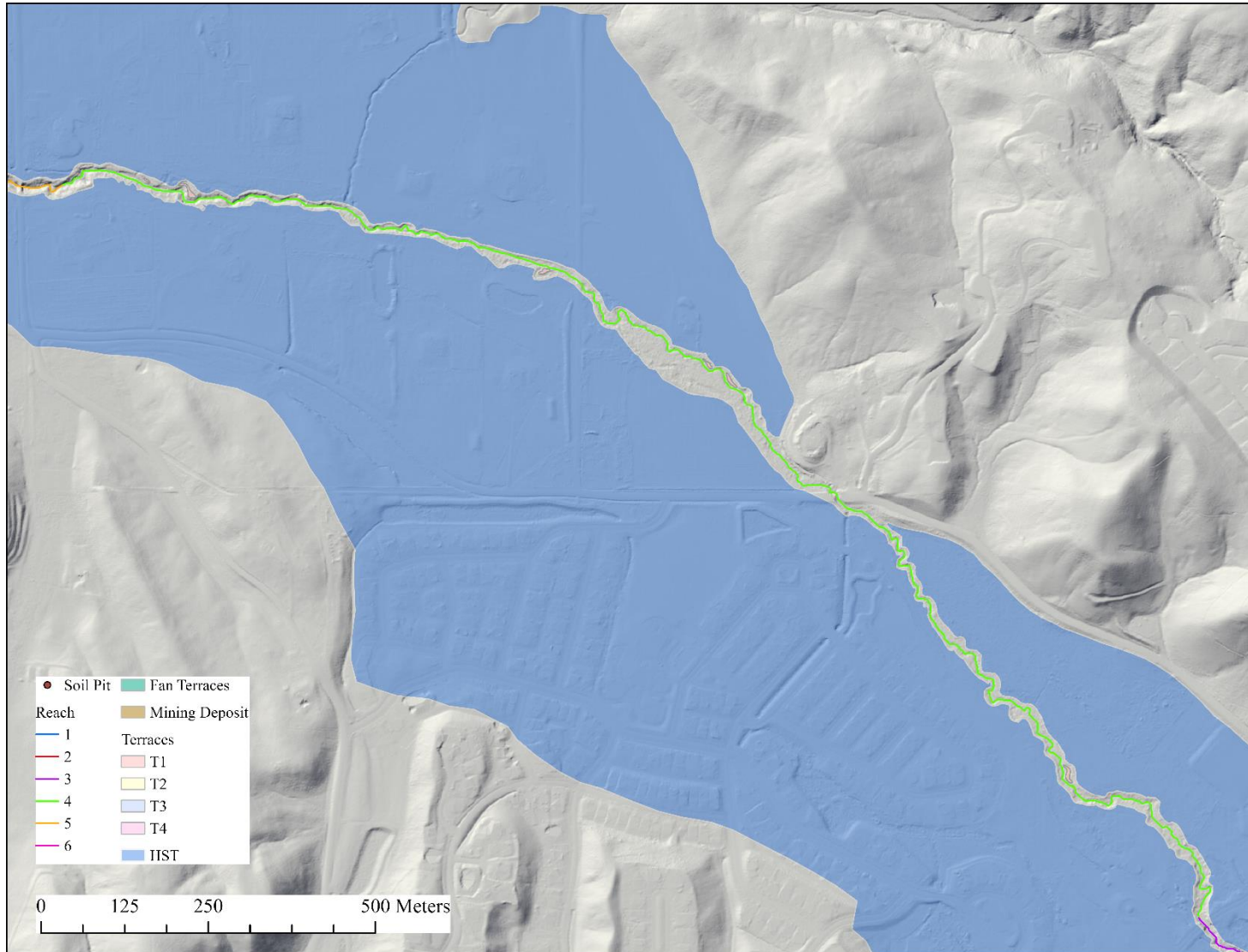
Figure B25   Geomorphic map of Reach 4.
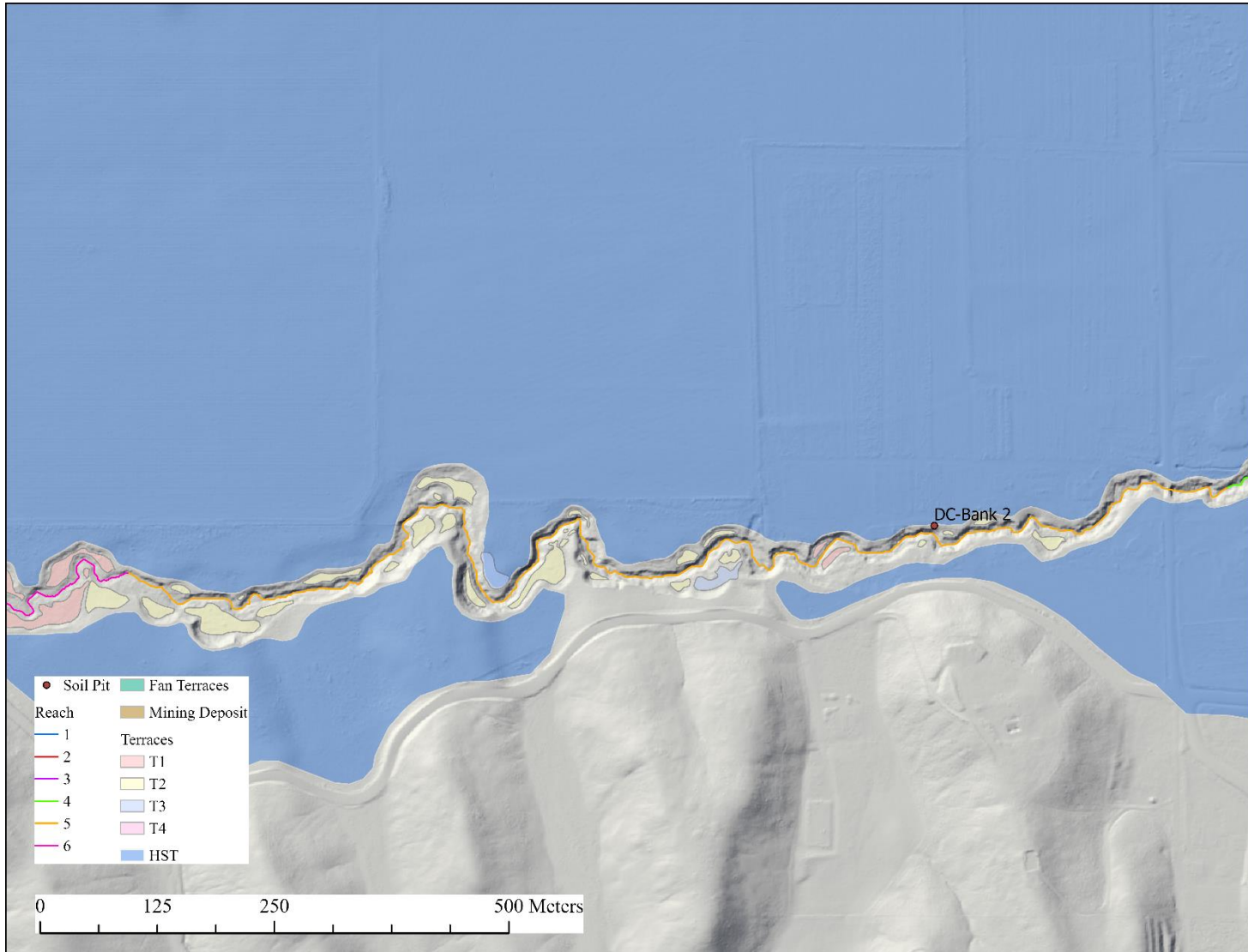
Figure B26   Geomorphic map of Reach 5.

Figure B27   Geomorphic map of Reach 6.

APPENDIX C

Radiocarbon and Optically Stimulated Luminescence Dating Laboratory Reports

Appendix C includes the complete laboratory reports from radiocarbon and

Optically Stimulated Luminescence (OSL) dating from Lawrence Livermore National

Laboratory and Utah State Luminescence Laboratory.

Table C1   **Radiocarbon dating results from Lawrence Livermore National Laboratory.**

CAMS #	Sample Name	d^{13}C	Fraction Modern	±	D^{14}C	±	^{14}C age	±
183612	OC 1 65-67 *	-28	0.9987	0.0027	-1.3	2.7	Modern	
183613	OC1 18 295-296	-28	0.9649	0.0029	-35.1	2.9	285	25

1) d^{13}C values are the assumed values according to Stuiver and Polach (Radiocarbon, v. 19, p.355, 1977) when given samples with an (*) were large enough, and as requested, to take a sample specific split for IRMS d13C analysis.

2) The quoted age is in radiocarbon years using the Libby half life of 5568 years and following the conventions of Stuiver and Polach (ibid.).

3) Radiocarbon concentration is given as fraction Modern, D^{14}C, and conventional radiocarbon age.

4) Sample preparation backgrounds have been subtracted, based on measurements of samples of ^{14}C-free coal. Backgrounds were scaled relative to sample size.

USU LUMINESCENCE LABORATORY

https://usu.edu/geo/luminlab

1770 North Research Parkway, Suite 123, North Logan, Utah 84341

Project: Lower Dry Creek, 10km North of Boise, ID   Project #: 339

Scientists: Scott Ducar and Jen Pierce, Boise State University

Report by: Tammy Rittenour   Report date: May 13, 2020

Final Luminescence Age Report

Table 1. Optically Stimulated Luminescence Age Information

Sample num.	USU num.	Depth (m)	Num. of aliquots[1]	Dose rate (Gy/ka)	Equivalent Dose ± 2σ (Gy)	OSL age ± 2σ (ka)	Age Model[2]
DC-Terr15-1	USU-3118	1.55-1.58	17 (36)	4.41 ± 0.18	2.94 ± 1.27 [3]	0.67 ± 0.29	MAM
DC-Terr15-2	USU-3119	0.55-0.57	21 (30)	3.34 ± 0.13	2.64 ± 1.02 [3]	0.79 ± 0.31	MAM
DC-Bank1-2	USU-3122	4.92-4.95	17 (30)	2.44 ± 0.09	11.68 ± 2.34	4.79 ± 1.03	CAM

[1] Age analysis using the single-aliquot regenerative-dose procedure of Murray and Wintle (2000) on 1-mm small-aliquots of quartz sand. Number of aliquots used in age calculation and number of aliquots analyzed in parentheses.

[2] Equivalent dose (D_E) calculated using the Minimum Age Model (MAM) or Central Age Model (CAM) of Galbraith and Roberts (2012).

[3] Overestimate on D_E is possible due to averaging of signals from grains on small aliquots. Single-grain dating is a tool that may minimize this effect.

Table 2. Dose Rate Information

Sample num.	USU num.	In-situ H_2O (%)[1]	Grain size (μm)	K (%)[2]	Rb (ppm)[2]	Th (ppm)[2]	U (ppm)[2]	Cosmic (Gy/ka)
DC-Terr15-1	USU-3118	33%	90-150	2.30±0.06	126.0±5.0	15.4±1.4	4.2±0.3	0.20±0.02
DC-Terr15-2	USU-3119	0.3%	150-250	2.25±0.06	66.6±2.7	12.3±1.1	0.9±0.1	0.23±0.02
DC-Bank1-2	USU-3122 [3]	0.2%	150-250	1.90±0.05	61.6±2.5	4.53±0.4	0.6±0.1	0.14±0.01
				1.74±0.04	80.5±3.2	11.2±1.0	1.6±0.2	
				1.99±0.05	57.6±2.3	4.1±0.4	1.6±0.2	

[1] Assumed 5.0 ± 2.0% as moisture content over burial history.

[2] Radioelemental concentrations determined using ICP-MS and ICP-AES techniques; dose rate is derived from concentrations by conversion factors from Guérin et al. (2011).

[3] Dose rate subsamples include the main sample (top values, 55%), upper unit (middle values, 20%), and lower unit (bottom values, 25%). Gamma dose rate uses percent of contribution based on distance from OSL unit for 3 subsamples, beta dose rate uses chemistry from main sample only.

USU LUMINESCENCE LABORATORY
https://usu.edu/geo/luminlab
1770 North Research Parkway, Suite 123, North Logan, Utah 84341

<u>Equivalent dose (D_E) Distributions:</u> Probability density function, radial plot, overdispersion (OD)

1. DC-Terr15-1, USU-3118

MAM
OD = 46 ± 11 %

2. DC-Terr15-2, USU-3119

MAM
OD = 48 ± 10 %
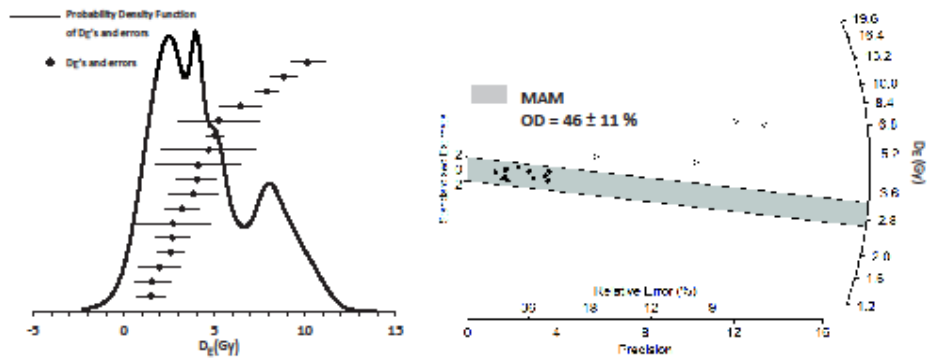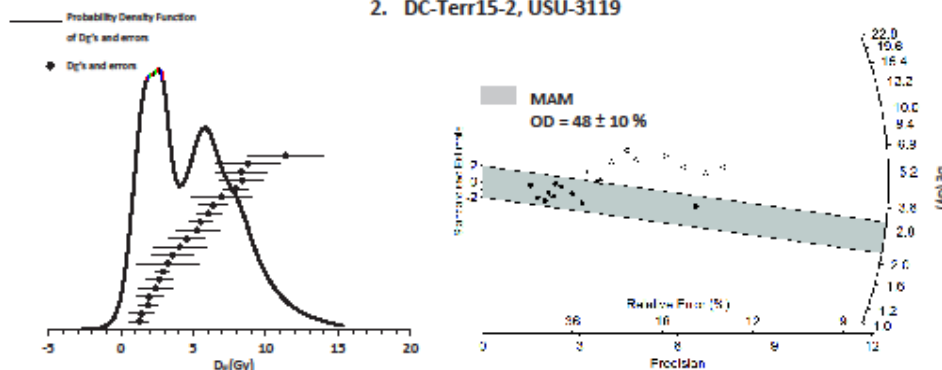
3. DC-Bank1-2, USU-3122

CAM
OD = 37 ± 8 %
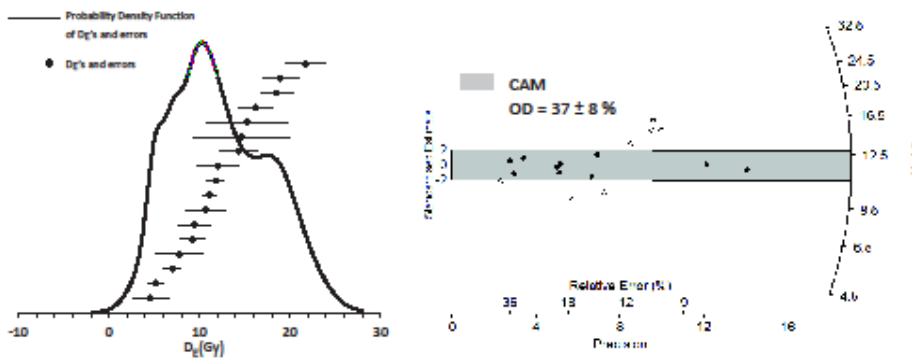
Project: Lower Dry Creek, 10km North of Boise, ID
Scientists: Scott Ducar and Jen Pierce, Boise State University
Report by: Tammy Rittenour

Project #: 339

Report date: May 13, 2020

2

USU LUMINESCENCE LABORATORY

http://usu.edu/geo/luminlab

1770 North Research Parkway, Suite 123, North Logan, Utah 84341

Procedures for sample processing and small-aliquot OSL age analysis:

All samples were opened and processed under dim amber safelight conditions within the lab. Sample processing for quartz optically stimulated luminescence (OSL) dating followed standard procedures involving sieving, HCl and bleach treatments, heavy mineral separation at 2.72 g/cm^3, and acid treatments with HCl and HF to isolate the quartz component of a narrow grain-size range, usually 90-150 μm*. The purity of the quartz samples was checked by measurement with infra-red stimulation to detect the presence of feldspar.

The USU Luminescence Lab follows the latest single-aliquot regenerative-dose (SAR) procedures for OSL dating of quartz sand (Murray and Wintle, 2000, 2003; Wintle and Murray, 2006). The SAR protocol includes tests for sensitivity correction and brackets the equivalent dose (D_E) the sample received during burial by irradiating the sample at three to five different doses (below, at, and above the D_E, plus a zero dose and a repeated dose to check for recuperation of the signal and sensitivity correction). The resultant data are fit with a linear or saturating exponential curve from which the D_E is calculated on the Central Age Model (CAM) or the Minimum Age Model (MAM) of Galbraith and Roberts (2012), depending on the distribution of D_E results and evidence for partial bleaching*. In cases where the samples have significant positive skew, ages are calculated based on a MAM. The OSL age is reported at 2σ standard error and is calculated by dividing the D_E (in grays, gy) by the environmental dose rate (gy/ka) that the sample has been exposed to during burial.

Dose-rate calculations were determined by chemical analysis of the U, Th, K and Rb content using ICP-MS and ICP-AES techniques and conversion factors from Guérin et al. (2011). The contribution of cosmic radiation to the dose rate was calculated using sample depth, elevation, and latitude/longitude following Prescott and Hutton (1994). Dose rates are calculated based on water content, sediment chemistry, and cosmic contribution (Aitken and Xie, 1990; Aitken, 1998).

Under the collaborative agreement to analyze samples at the USU Luminescence Lab, please consider including Dr. Rittenour as a co-author on resultant publications. Contact me for additional information and help with describing the OSL technique when you plan your publication.

Dr. Tammy Rittenour

Director
USU Luminescence Lab
1770 N Research parkway, suite 123
North Logan, UT 84341

Associate Professor
Department of Geology, Utah State University
4505 Old Main Hill
Logan, UT 84322-4505

tammy.rittenour@usu.edu

http://www.usu.edu/geo/luminlab/

* These parameters are sample dependent, see first page of report for specific sample information

3

USU **LUMINESCENCE LABORATORY** http://usu.edu/geo/luminlab

1770 North Research Parkway, Suite 123, North Logan, Utah 84341

References cited:

Aitken, M.J. 1998: An Introduction to Optical Dating: The dating of Quaternary sediments by the use of photon-stimulated luminescence. New York, Oxford University Press, 267 p.

Aitken, M.J., Xie, J., 1990. Moisture correction for annual gamma dose. Ancient TL 8 (2), 6-9.

Galbraith, R.F., Roberts, R.G., 2012. Statistical aspects of equivalent dose and error calculation and display in OSL dating: An Overview and some recommendations. Quaternary Geochronology 11, 1-27.

Guérin, G., Mercier, N., Adamiec, G., 2011. Dose-rate conversion factors: update: Ancient TL 29, 5-8.

Murray, A.S., Wintle, A.G., 2000. Luminescence dating of quartz using an improved single aliquot regenerative-dose protocol. Radiation Measurements 32, 57-73.

Murray, A.S., Wintle, A.G., 2003. The single aliquot regenerative dose protocol: potential for improvements in reliability. Radiation Measurements 37, 377-381.

Prescott, J. R., Hutton, J.T., 1994. Cosmic ray contributions to dose rates for luminescence and ESR dating: Radiation Measurements 23, 497-500.

Wintle, A.G. Murray, A.S., 2006. A review of quartz optically stimulated luminescence characteristics and their relevance in single-aliquot regenerative protocols: Radiation Measurements, v. 41, p. 369-391.

APPENDIX D

Relative Elevation Maps by Reach

Appendix D contains relative elevation maps of Lower Dry Creek divided by reach from upstream (Reach 1) to downstream (Reach 6).
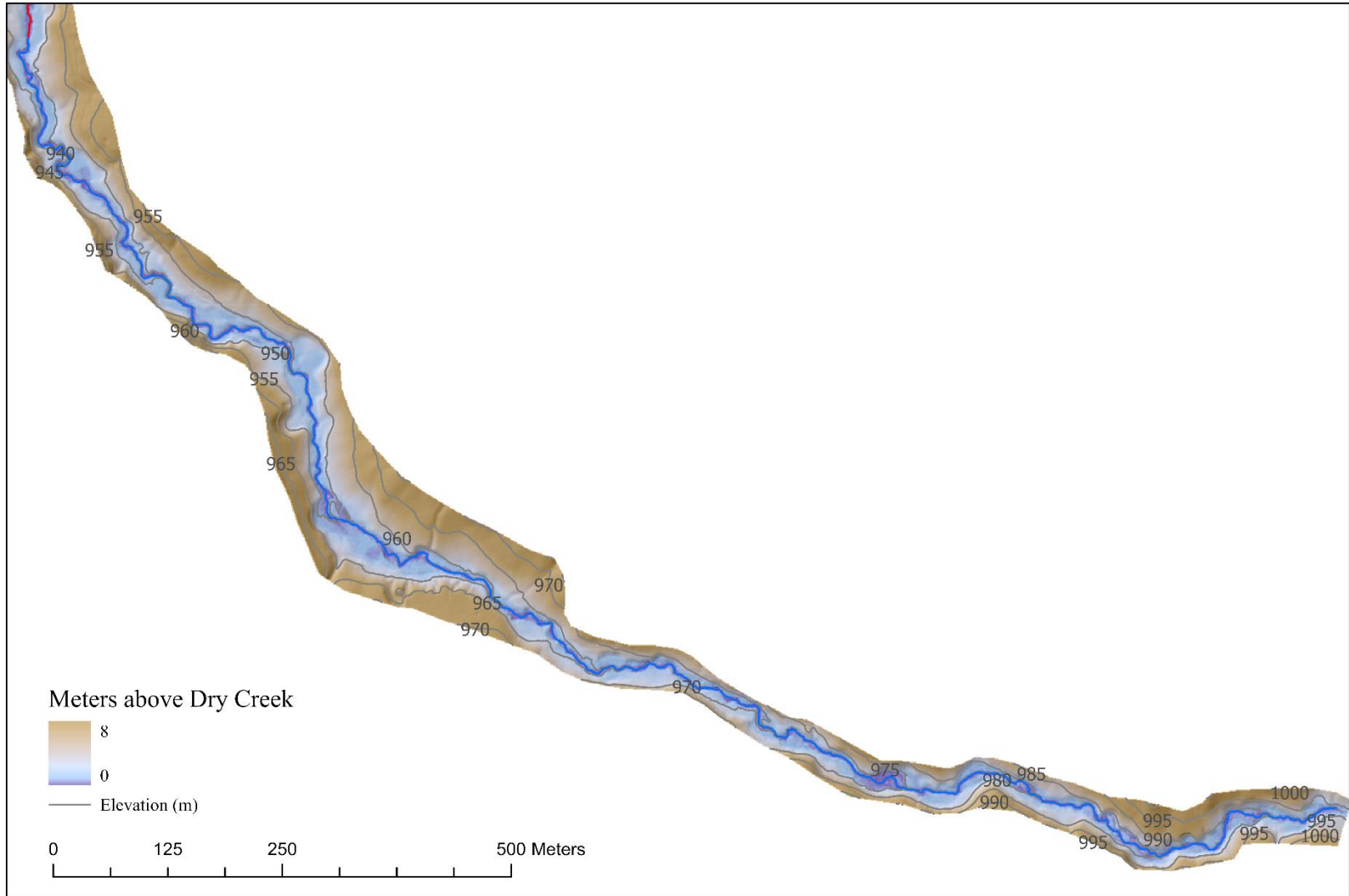
Figure D1   Relative elevation map of Reach 1.
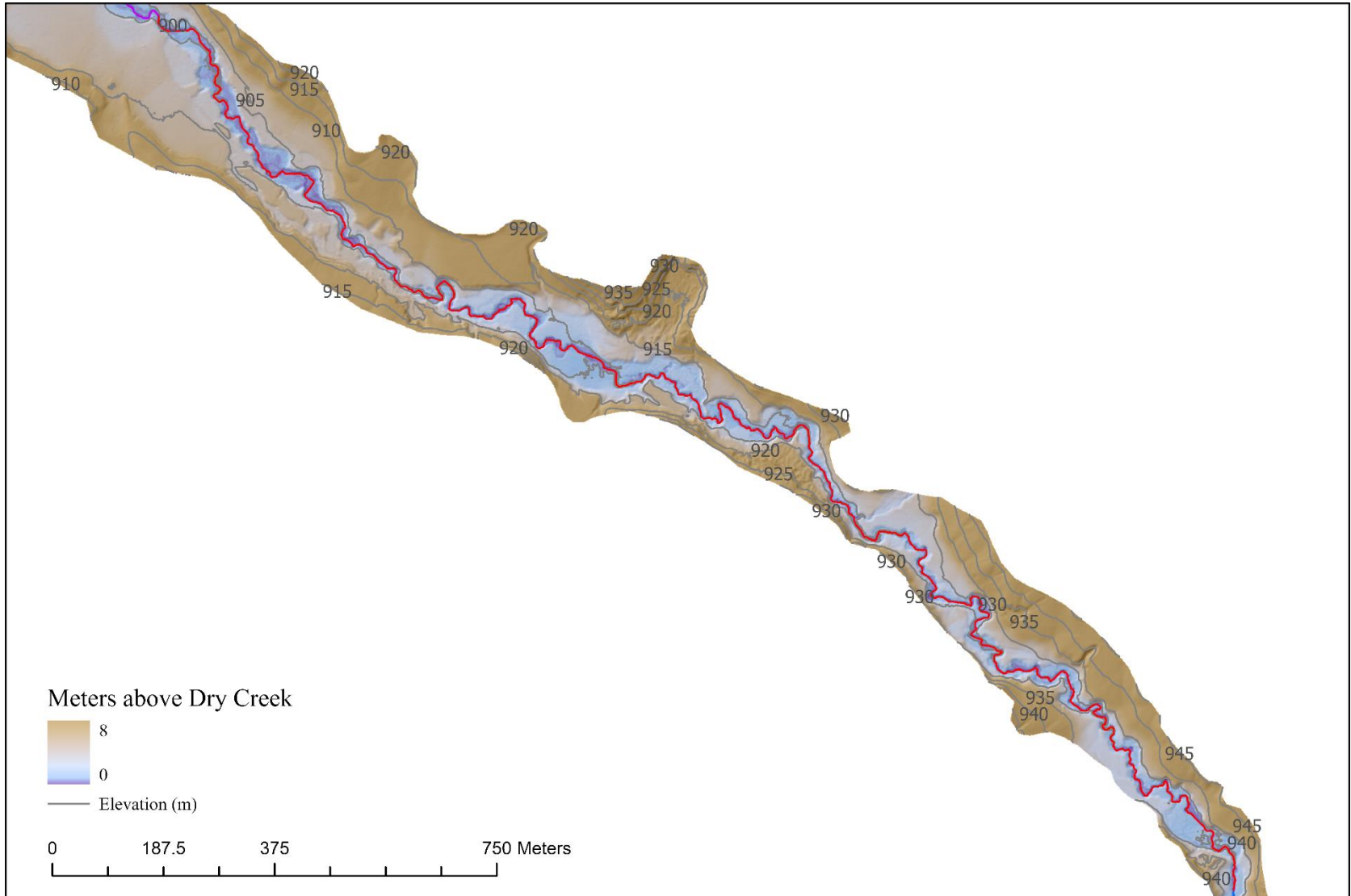
Figure D2   Relative elevation map of Reach 2.
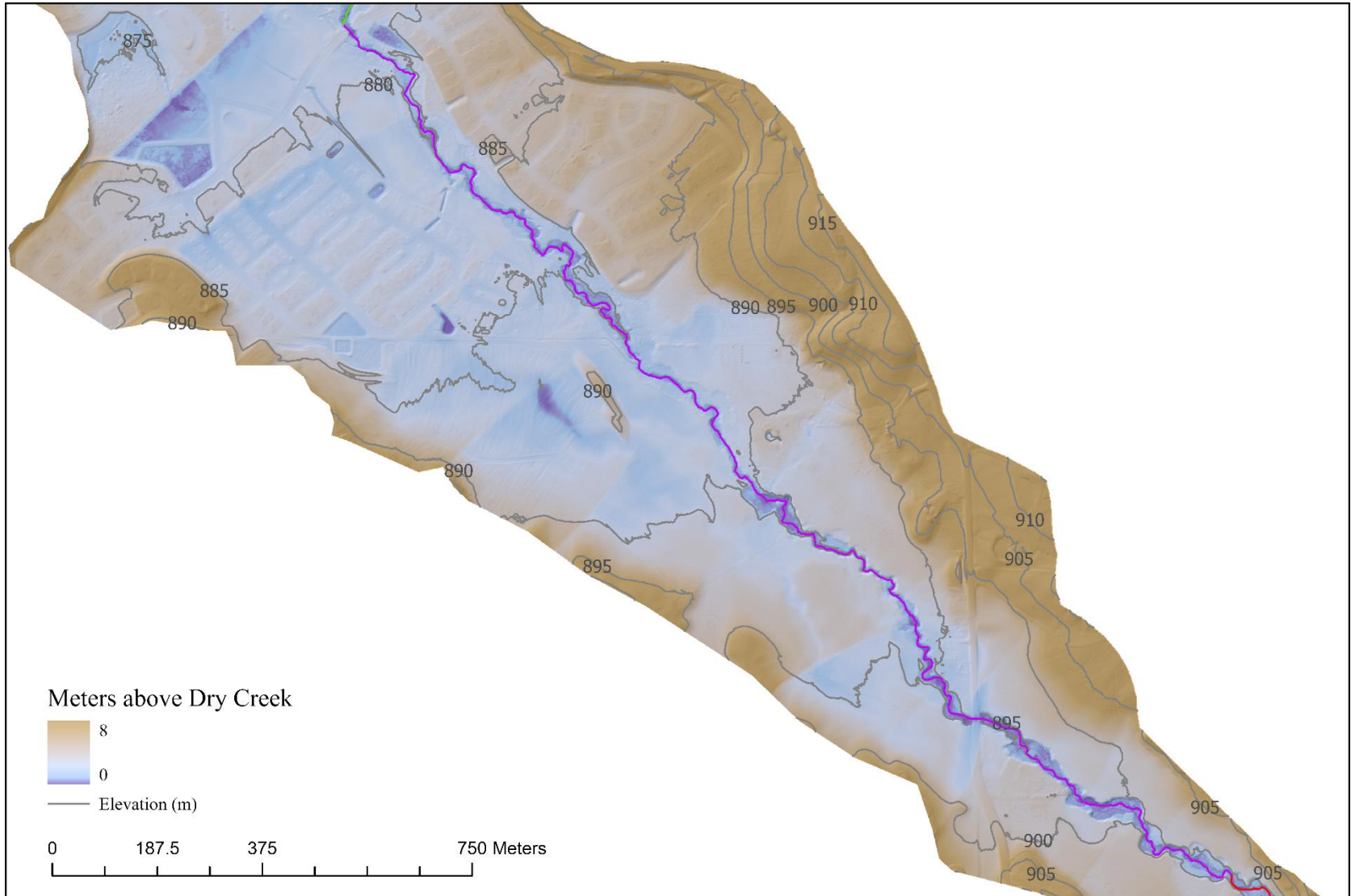
Figure D3 **Relative elevation map of Reach 3.**
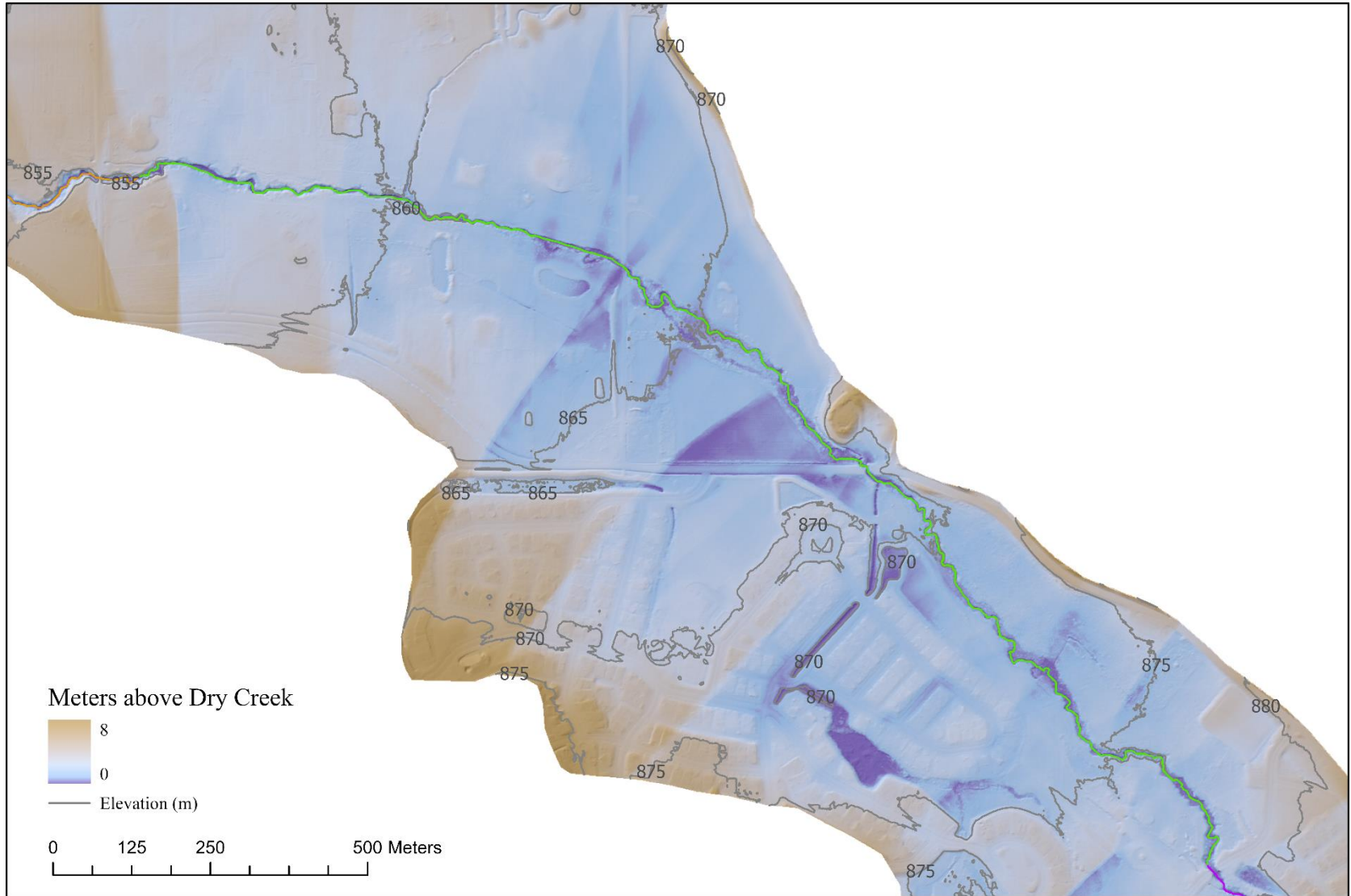
Figure D4   Relative elevation map of Reach 4.
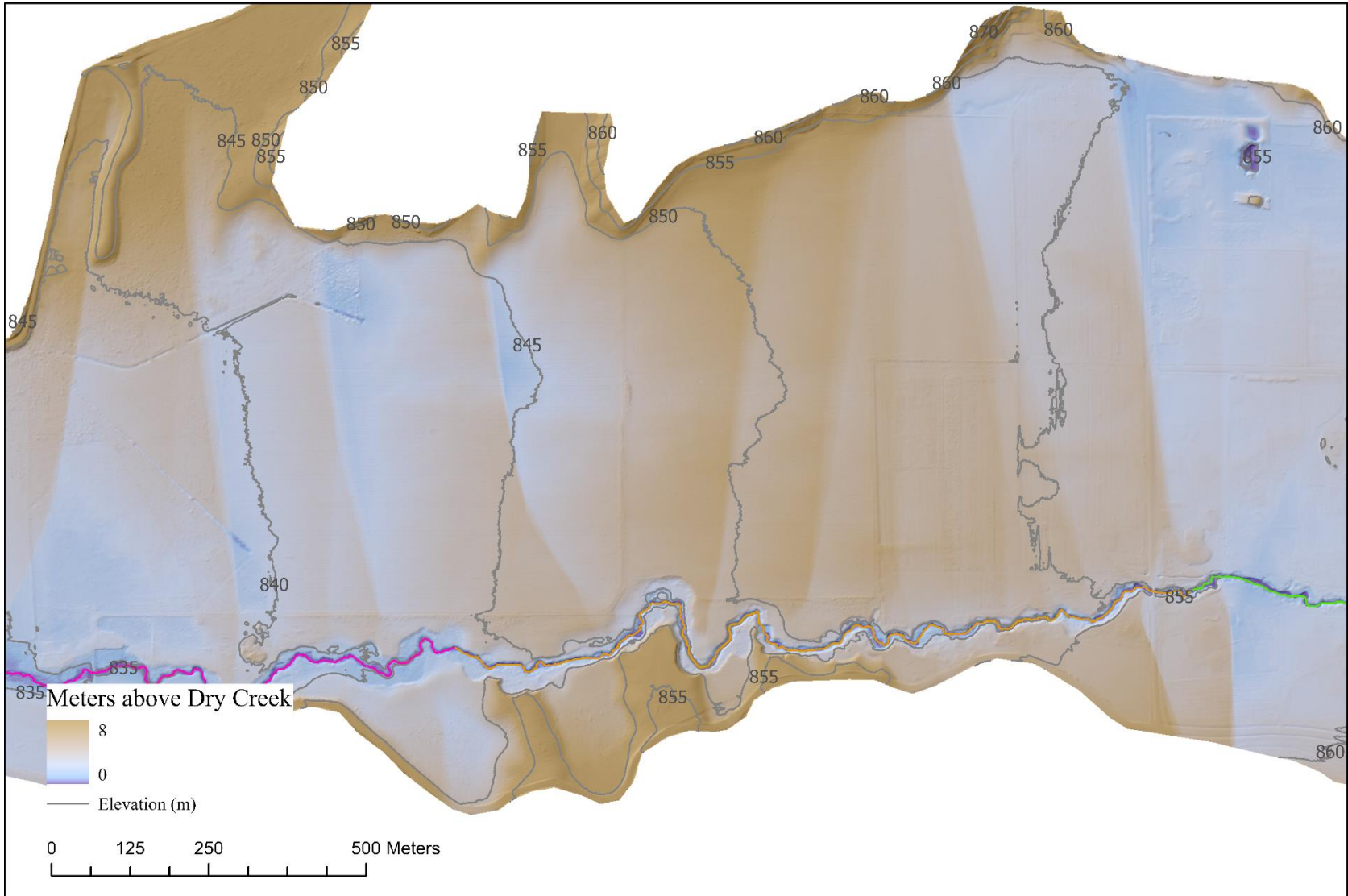
Figure D5   Relative elevation map of Reach 5.
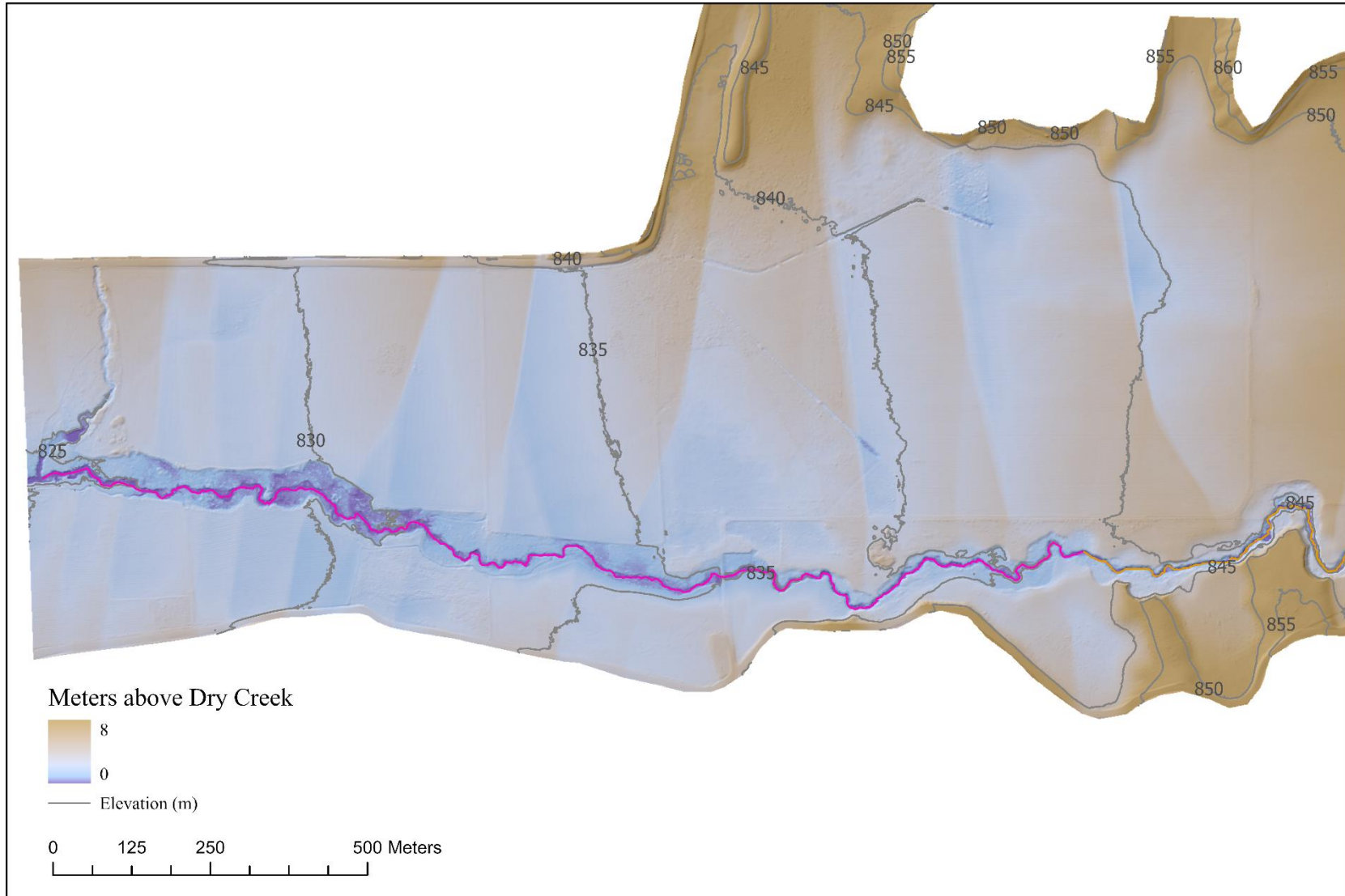
Figure D6   **Relative elevation map of Reach 6.**

APPENDIX E

Streambed Grain Size Distribution Sample Locations

Appendix E contains a map of the location of the streambed grain size samples collected from Lower Dry Creek. Also included are photos of the sample location and Universal Transverse Mercator coordinates.
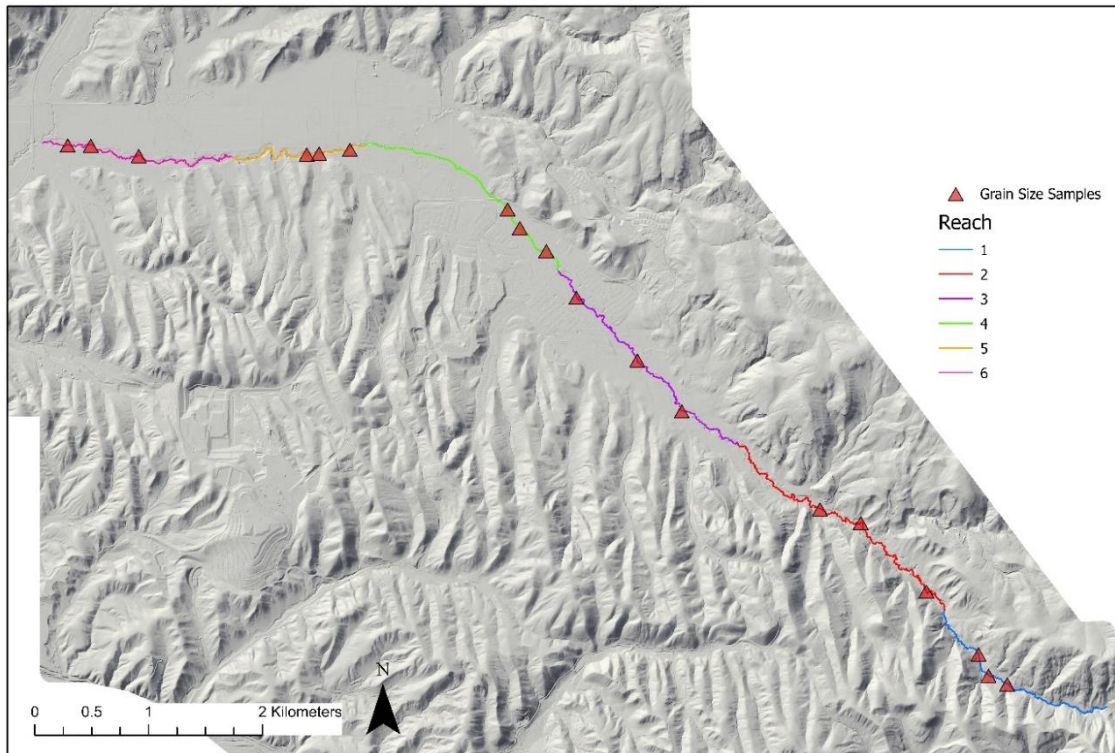
Figure E1   Map showing streambed grain size sample locations.

Figure E2   Photo of Reach 1-1 grain size sample location at 11T 564608N 4837647E.

Figure E3   Photo of Reach 1-2 grain size sample location at 11T 564444N 4837722E.

Figure E4   Photo of Reach 1-3 grain size sample location at 11T 564356N 4837910E.

Figure E5   Photo of Reach 2-1 grain size sample location at 11T 563897N 4838463E.

Figure E6   Photo of Reach 2-2 grain size sample location at 11T 563321N 4839063E.

Figure E7   Photo of Reach 2-3 grain size sample location at 11T 562962N 4839184E.

Figure E8 **Photo of Reach 3-1 grain size sample location at 11T 561747N 4840045E.**

Figure E9 **Photo of Reach 3-2 grain size sample location at 11T 561357N 4840493E.**

Figure E10   Photo of Reach 3-3 grain size sample location at 11T 560821N 4841043E.

Figure E11   Photo of Reach 4-1 grain size sample location at 11T 560556N 4841453E.

Figure E12   Photo of Reach 4-2 grain size sample location at 11T 560324N 4841656E.

Figure E13   Photo of Reach 4-3 grain size sample location at 11T 560216N 4841819E.

Figure E14   Photo of Reach 5-1 grain size sample location at 11T 558829N 4842342E.

Figure E15   Photo of Reach 5-2 grain size sample location at 11T 558558N 4842310E.

Figure E16   Photo of Reach 5-3 grain size sample location at 11T 558451N 4842303E.

Figure E17   Photo of Reach 6-1 grain size sample location at 11T 556973N 4842288E.

Figure E18   Photo of Reach 6-2 grain size sample location at 11T 556551N 4842379E.

Figure E19   Photo of Reach 6-3 grain size sample location at 11T 556349N 4842382E.

APPENDIX F

Automatic Level Survey and Lidar Derived Cross Section Comparison

Appendix F contains a map showing the location of the five cross sections of Lower Dry Creek surveyed for the study. Appendix F also includes plots comparing cross sections of Lower Dry Creek from automatic level surveying and LiDAR digital elevation model.
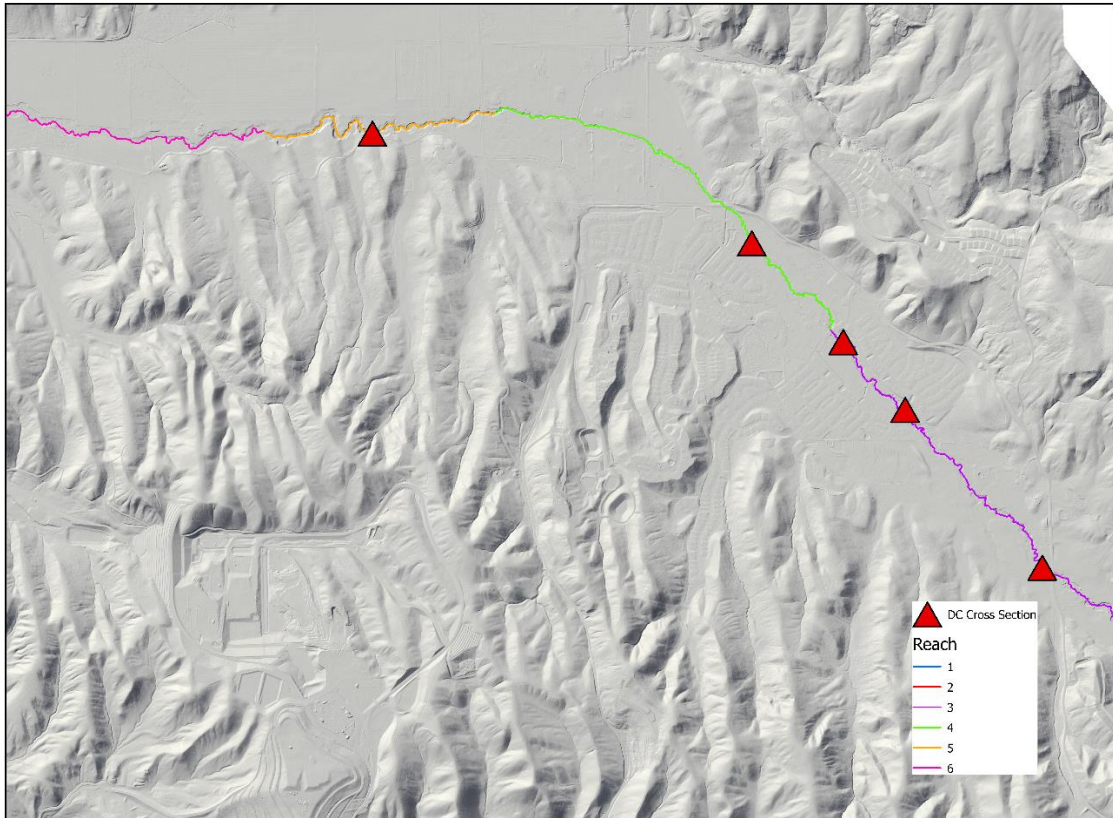
Figure F1   **Map of survey cross sections locations.**
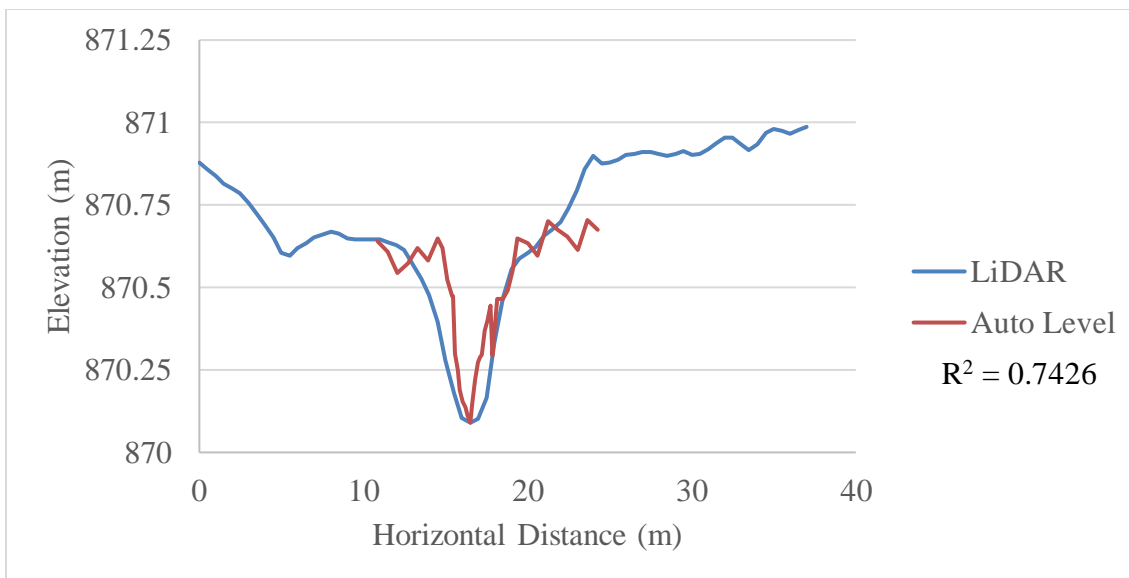
Figure F2   DC-Cross 1 cross section plot comparing survey data from the 2015 LiDAR DEM and using an automatic level. The cross section is located at 11T 560259N 4841720E.
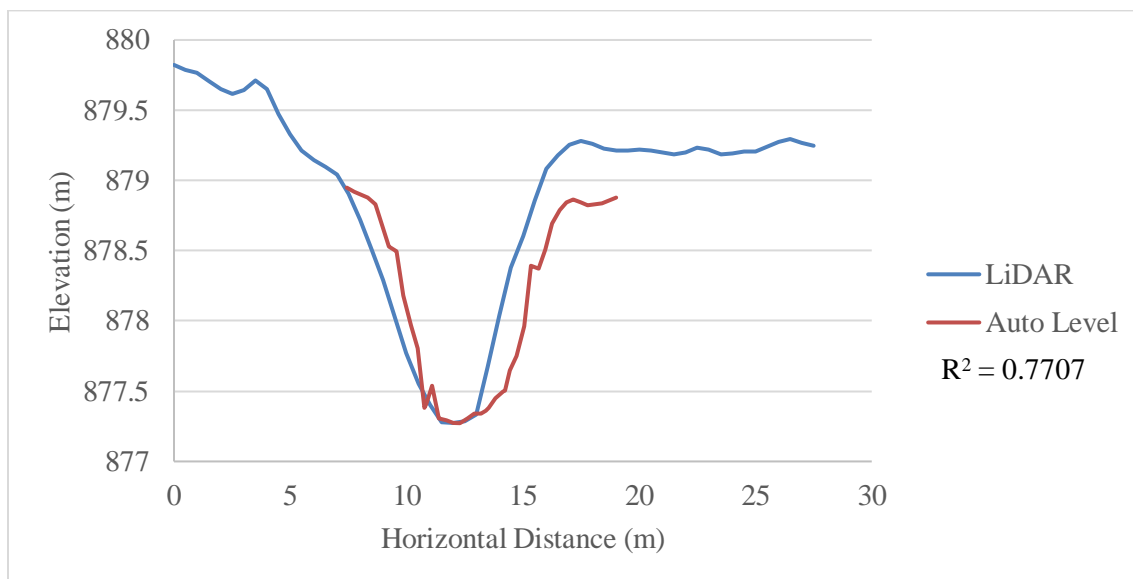
Figure F3   DC-Cross 2 cross section plot comparing survey data from the 2015 LiDAR DEM and using an automatic level. The cross section is located at 11T 560722N 4841221E.
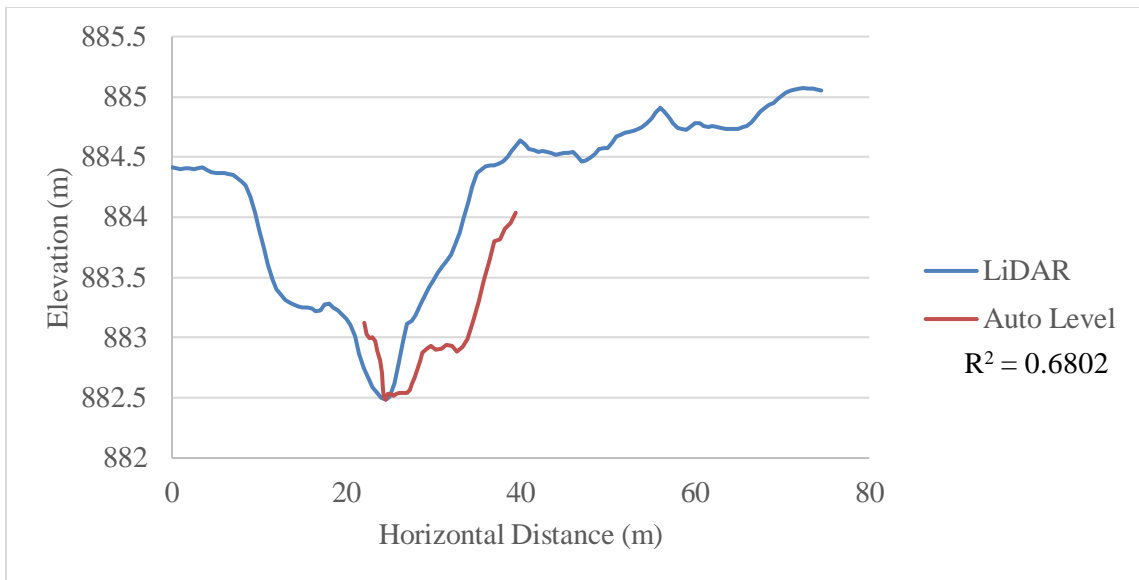
Figure F4   DC-Cross 3 cross section plot comparing survey data from the 2015 LiDAR DEM and using an automatic level. The cross section is located at 11T 561036N 4840878E.
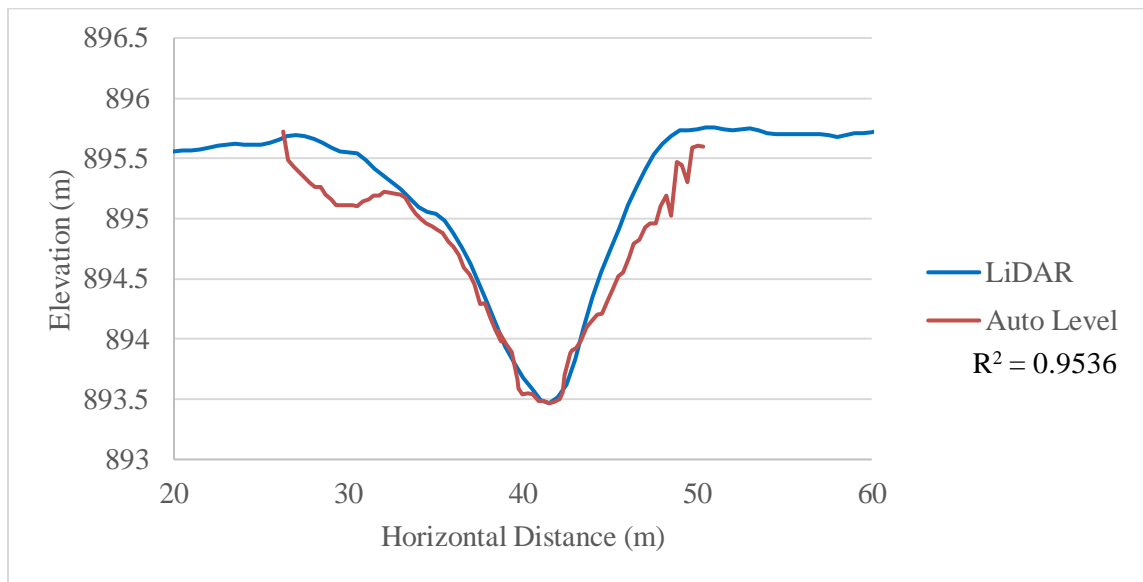
Figure F5   DC-Cross 4 cross section plot comparing survey data from the 2015 LiDAR DEM and using an automatic level. The cross section is located at 11T 561730N 4840080E.
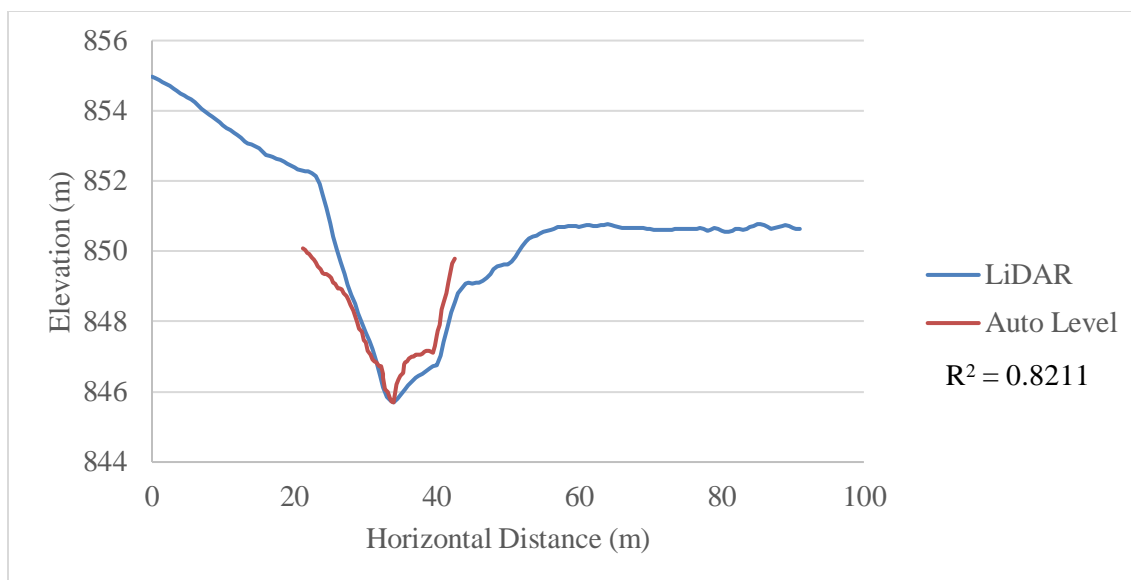
Figure F6   DC-Cross 5 cross section plot comparing survey data from the 2015 LiDAR DEM and using an automatic level. The cross section is located at 11T 558337N 4842275E.

APPENDIX G

HEC-RAS Model Results of Water Depth and Channel Velocity

Appendix G contains maps showing water depth and velocity from HEC-RAS modeling of Lower Dry Creek. The maps are divided by reach from upstream (Reach 1) to downstream (Reach 6). Discharge and Manning's n values used in the model are included in the figure caption.
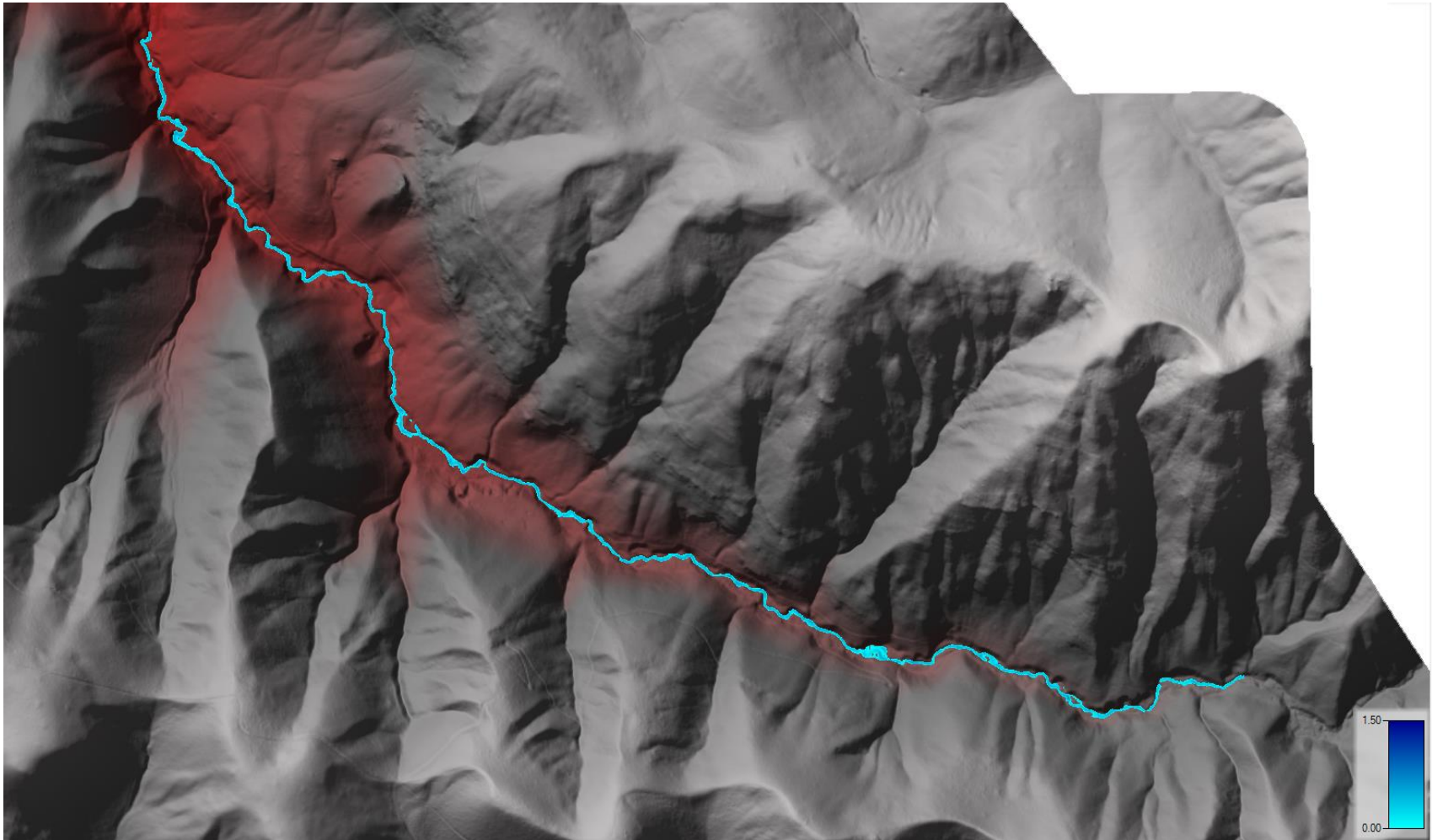
Figure G1   **Model results of Reach 1 water depth with a discharge of 1.13 m^3/s and a Manning n 0.065.**
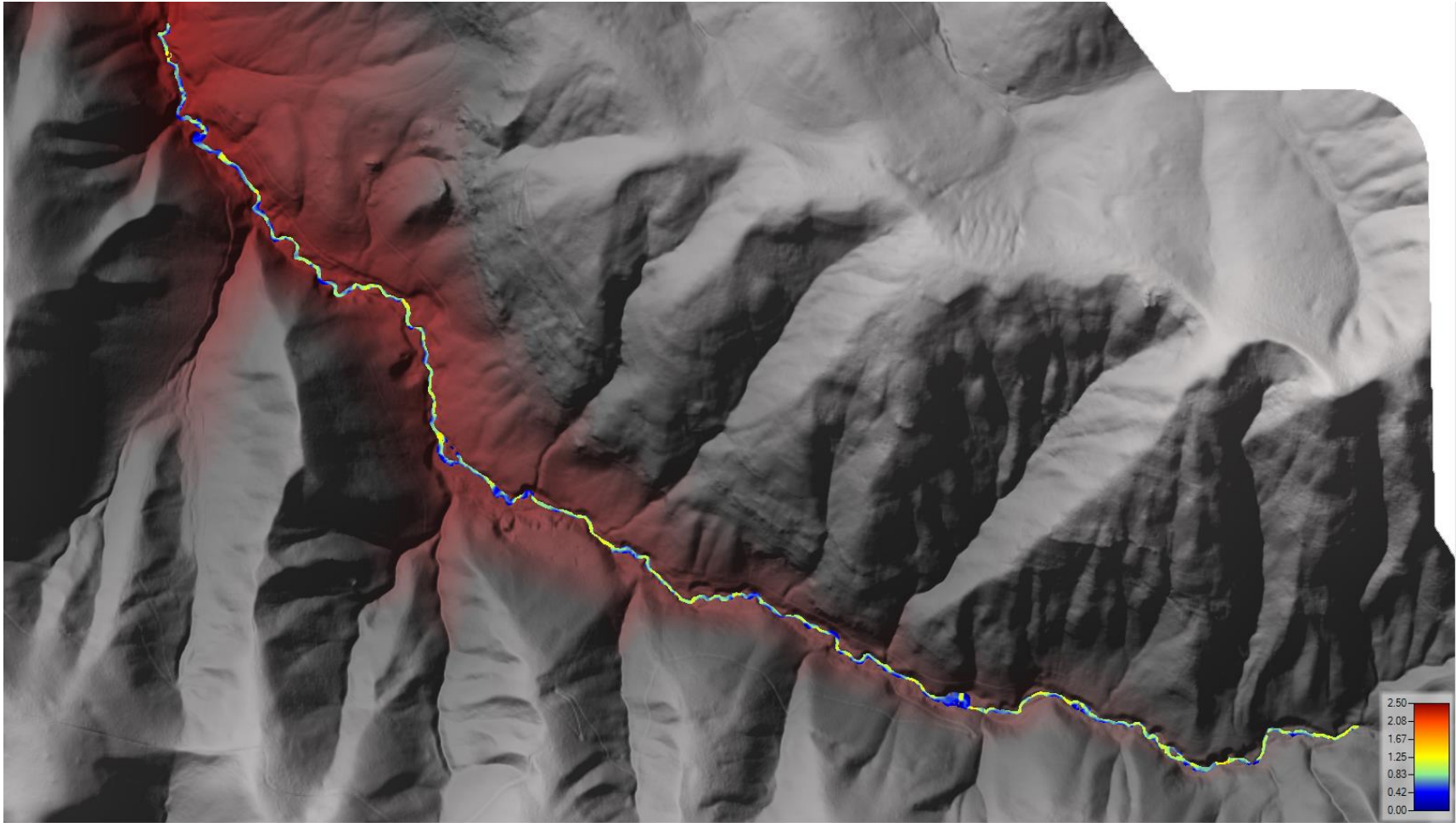
Figure G2   Model results of Reach 1 water velocity with a discharge of 1.13m³/s and a Manning n 0.065.
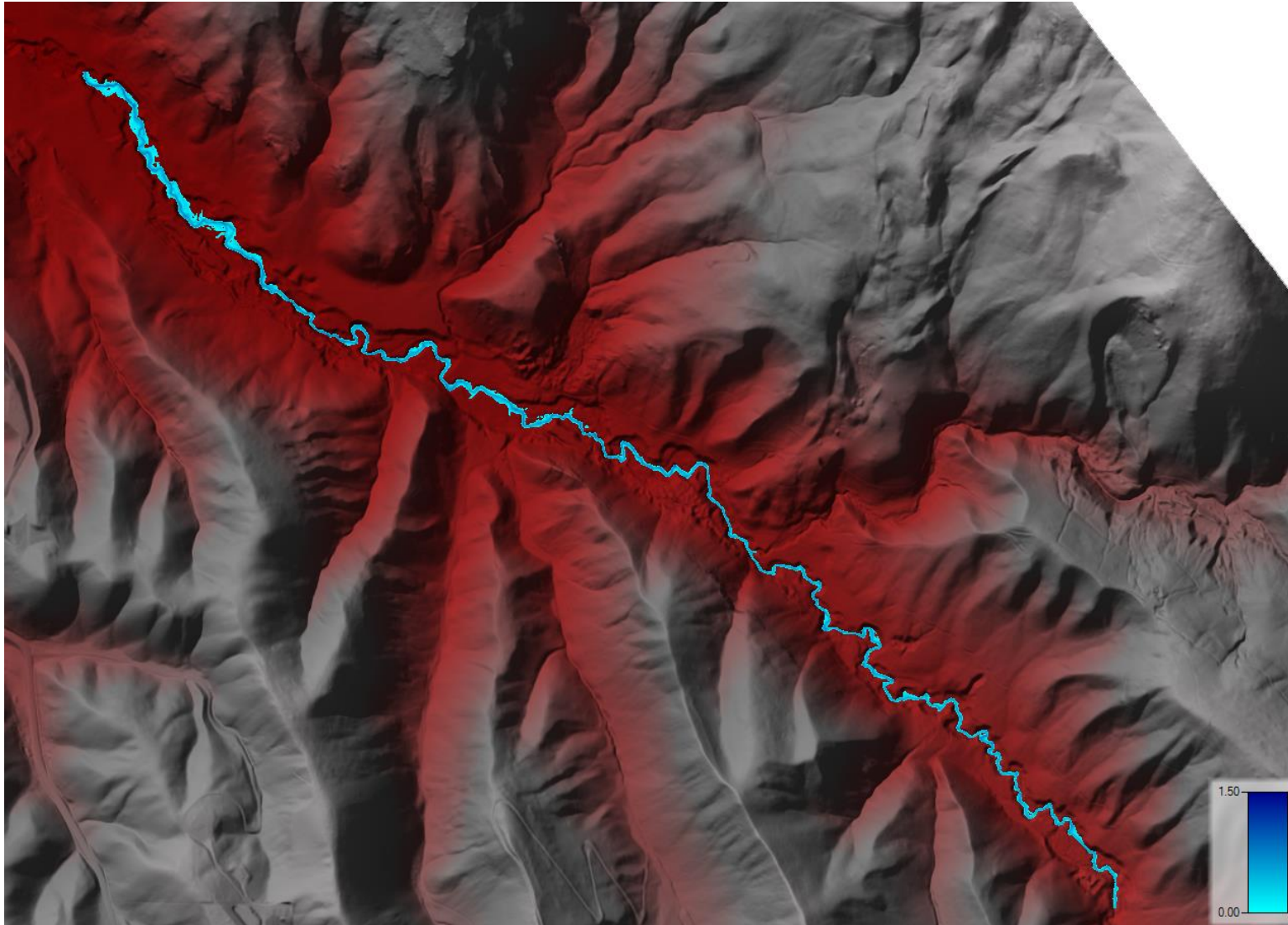
Figure G3   Model results of Reach 2 water depth with a discharge of 1.42m³/s and a Manning n 0.065.
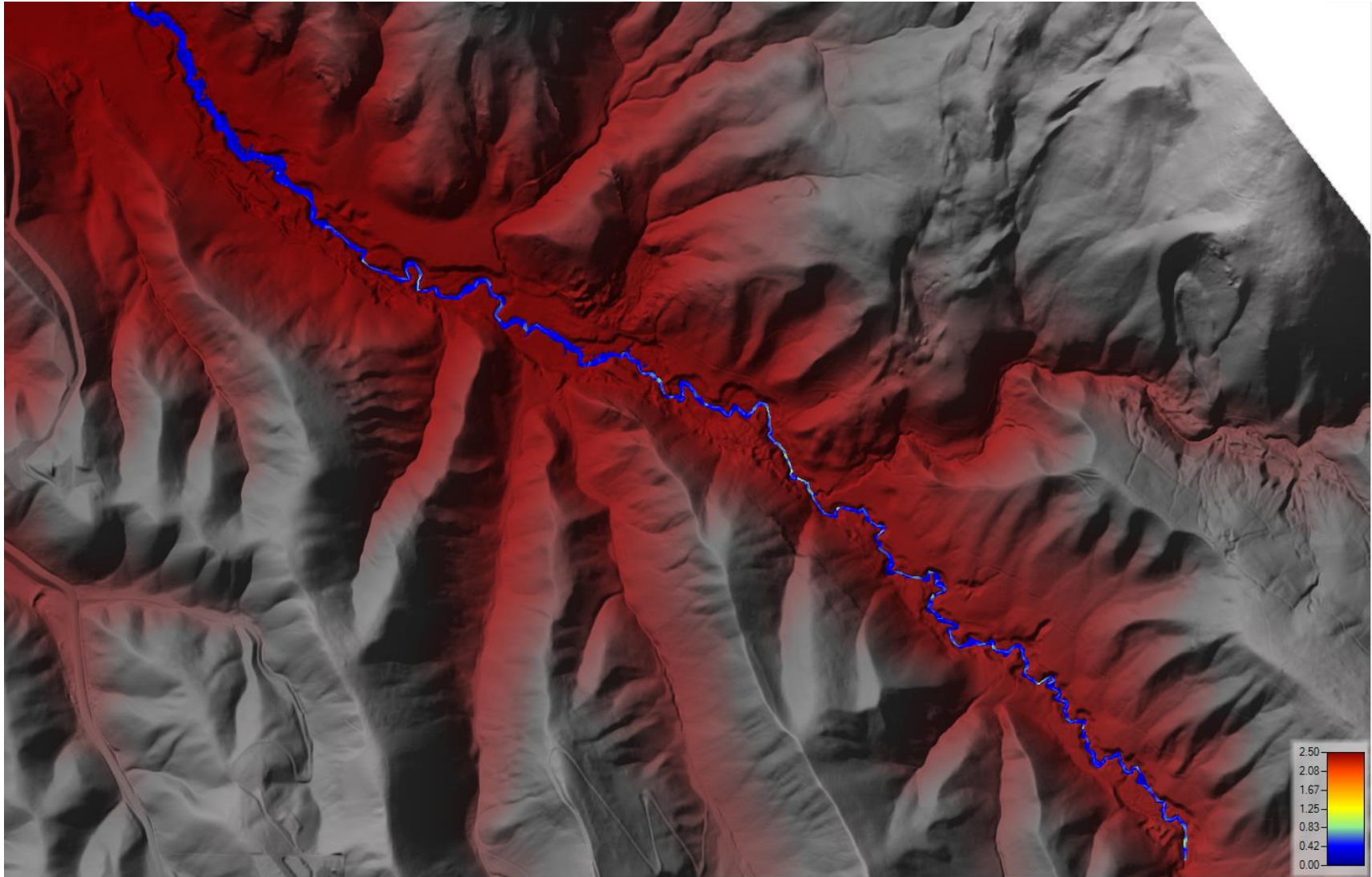
Figure G4 **Model results of Reach 2 water velocity with a discharge of 1.42m³/s and a Manning n 0.065.**
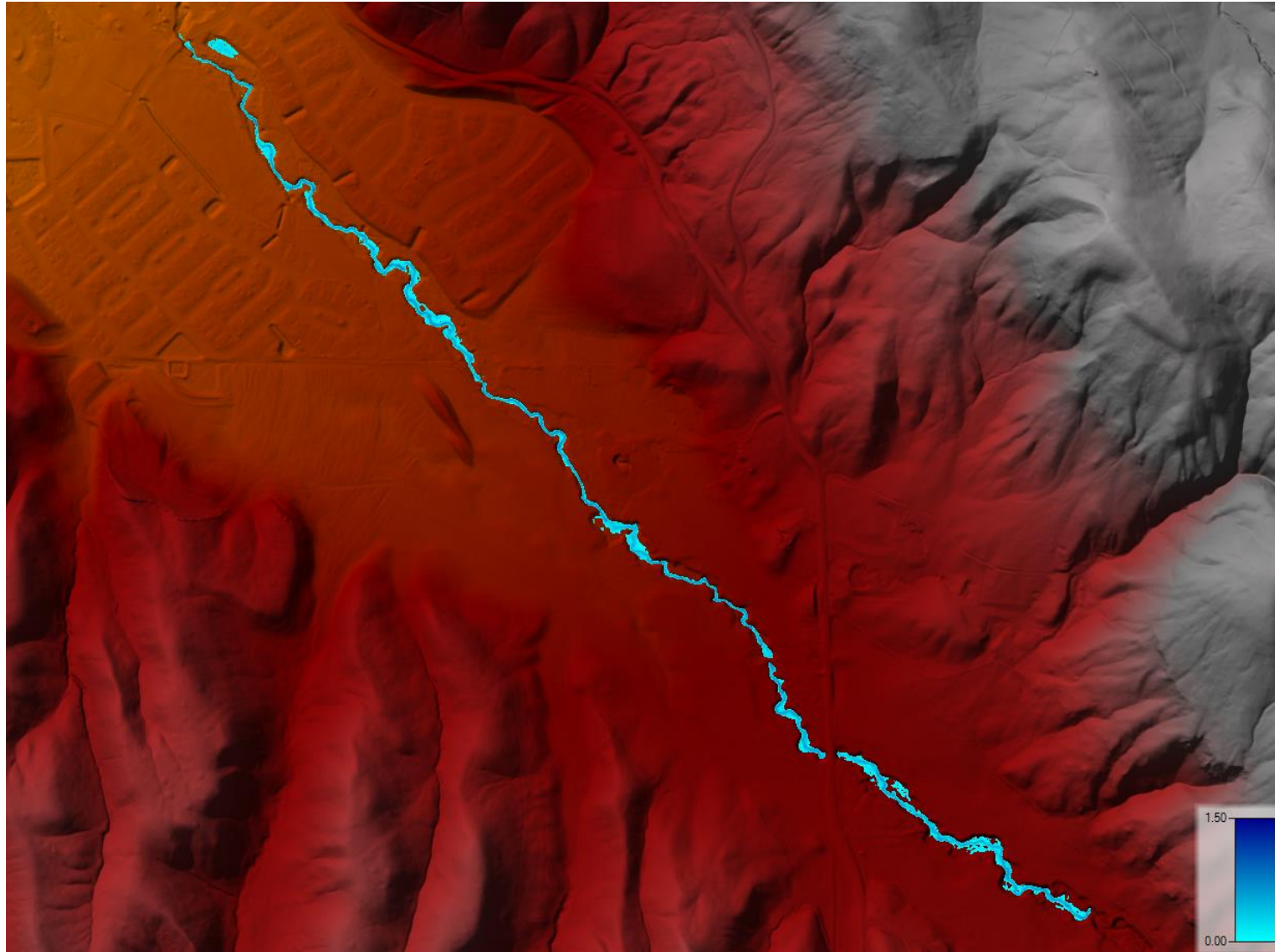
Figure G5   **Model results of Reach 3 water depth with a discharge of 1.42m^3/s and a Manning n 0.065.**
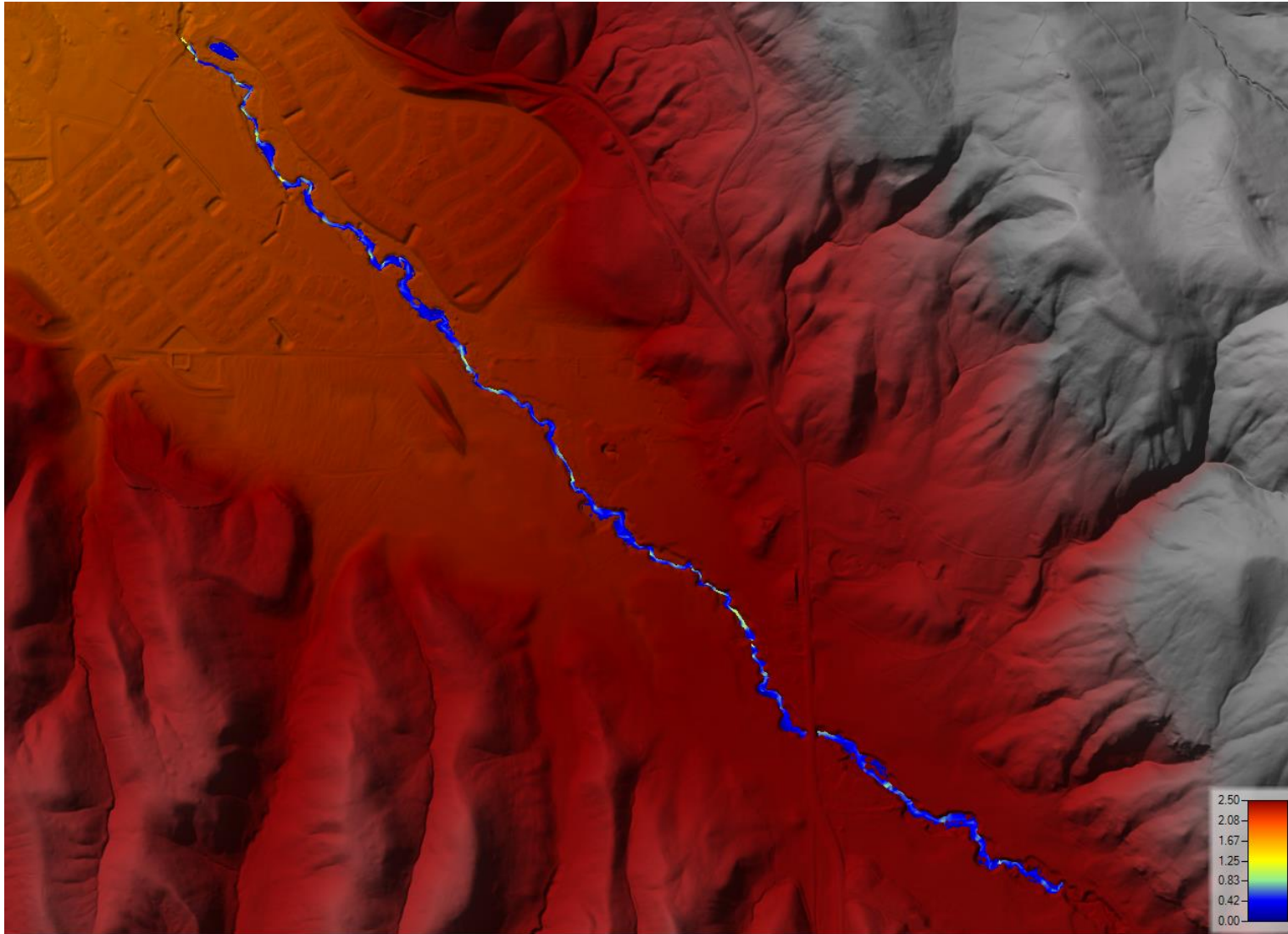
Figure G6   **Model results of Reach 3 water velocity with a discharge of 1.42m^3/s and a Manning n 0.065.**
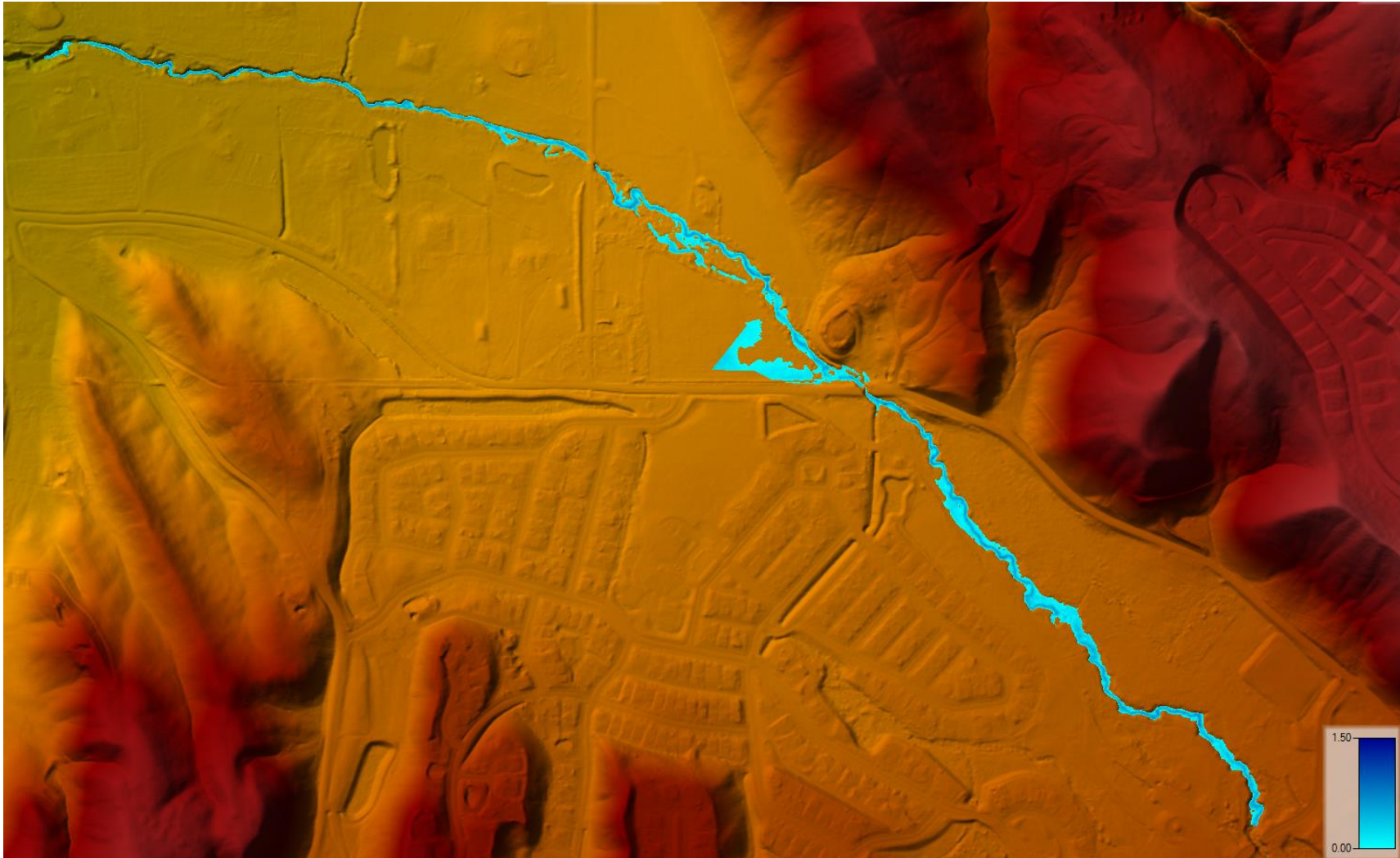
Figure G7   Model results of Reach 4 water depth with a discharge of 1.42m³/s and a Manning n 0.065.
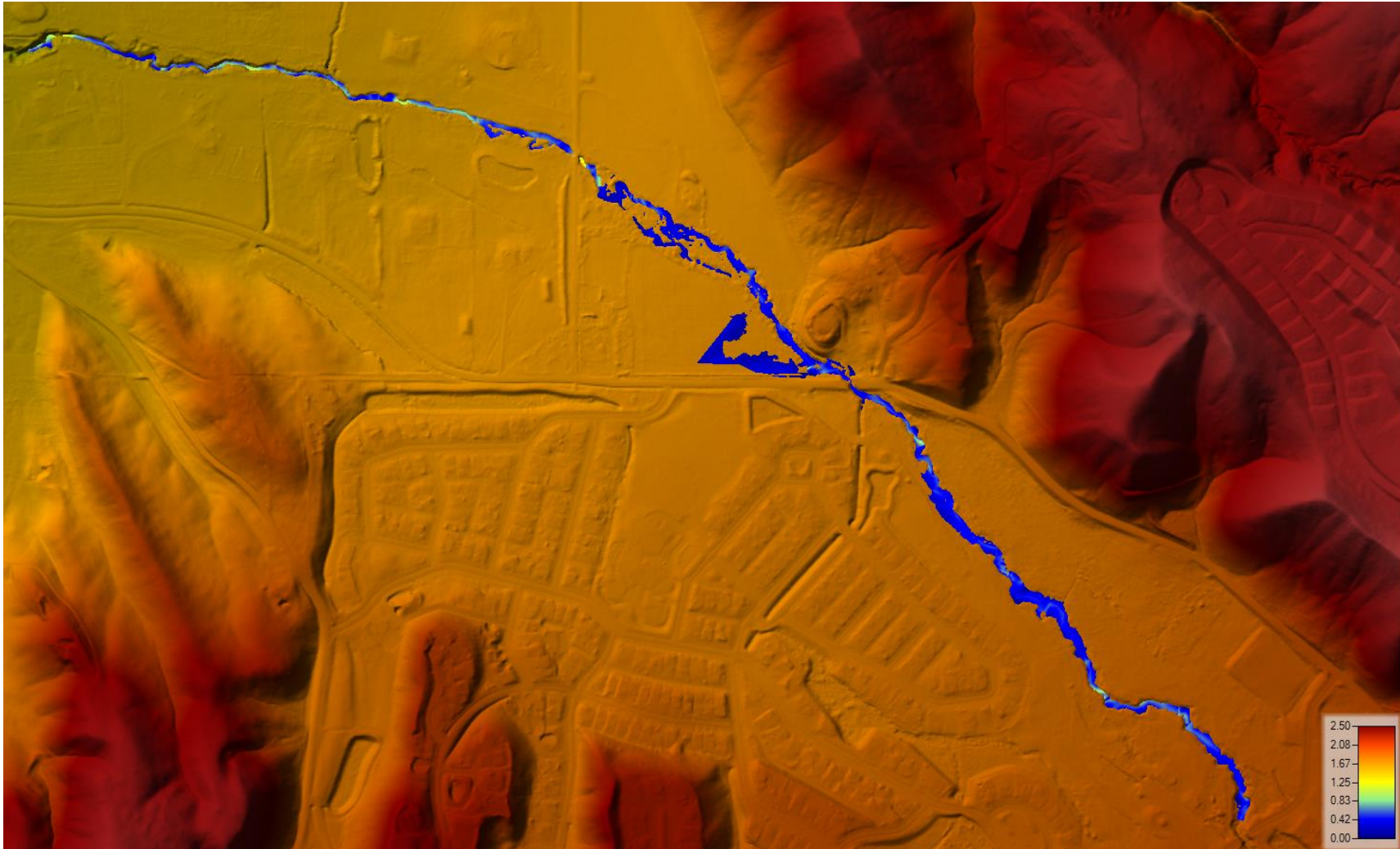
Figure G8 Model results of Reach 4 water velocity with a discharge of 1.42m^3/s and a Manning n 0.065.
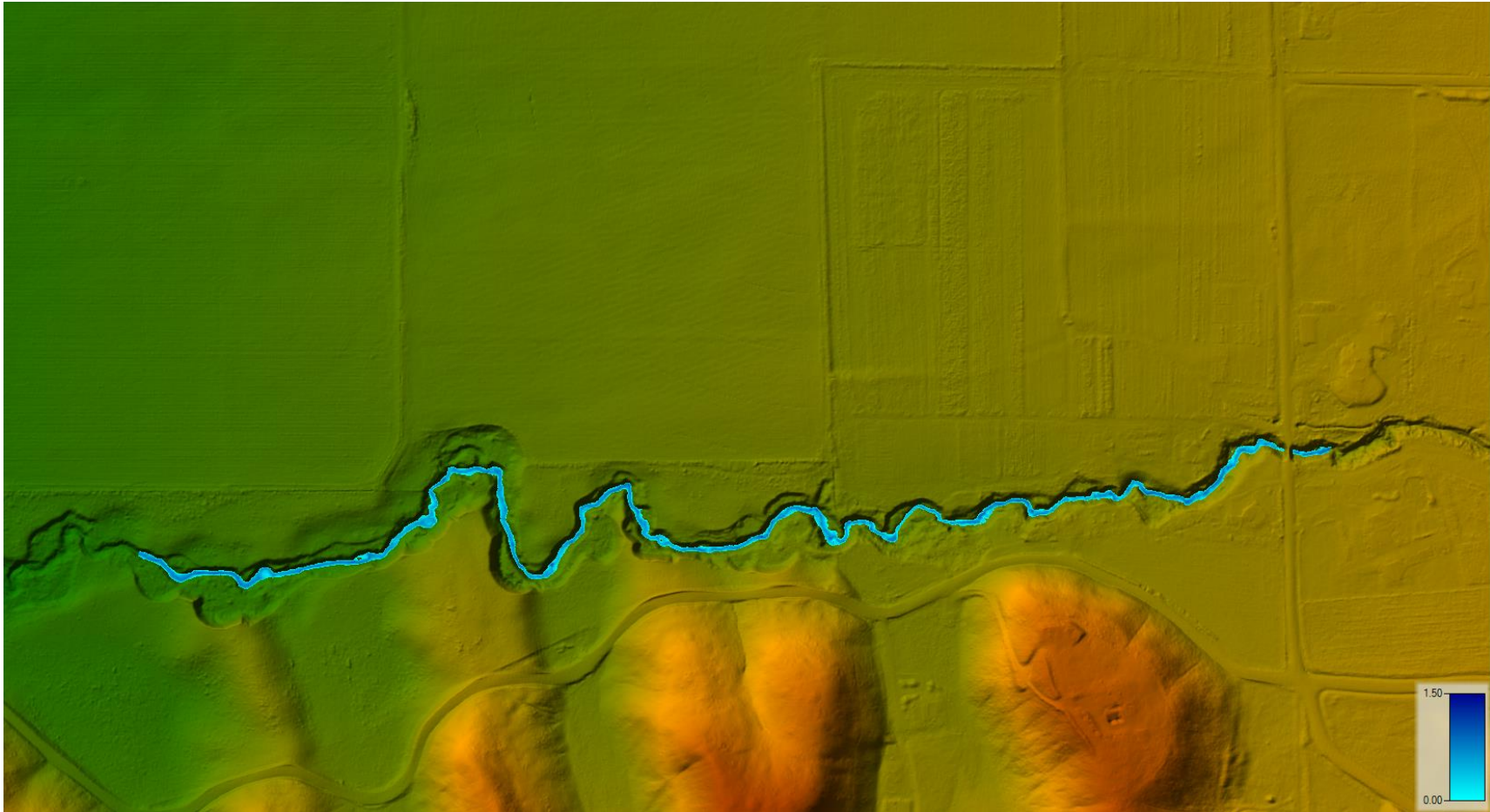
Figure G9 **Model results of Reach 5 water depth with a discharge of 1.42m^3/s and a Manning n 0.065.**
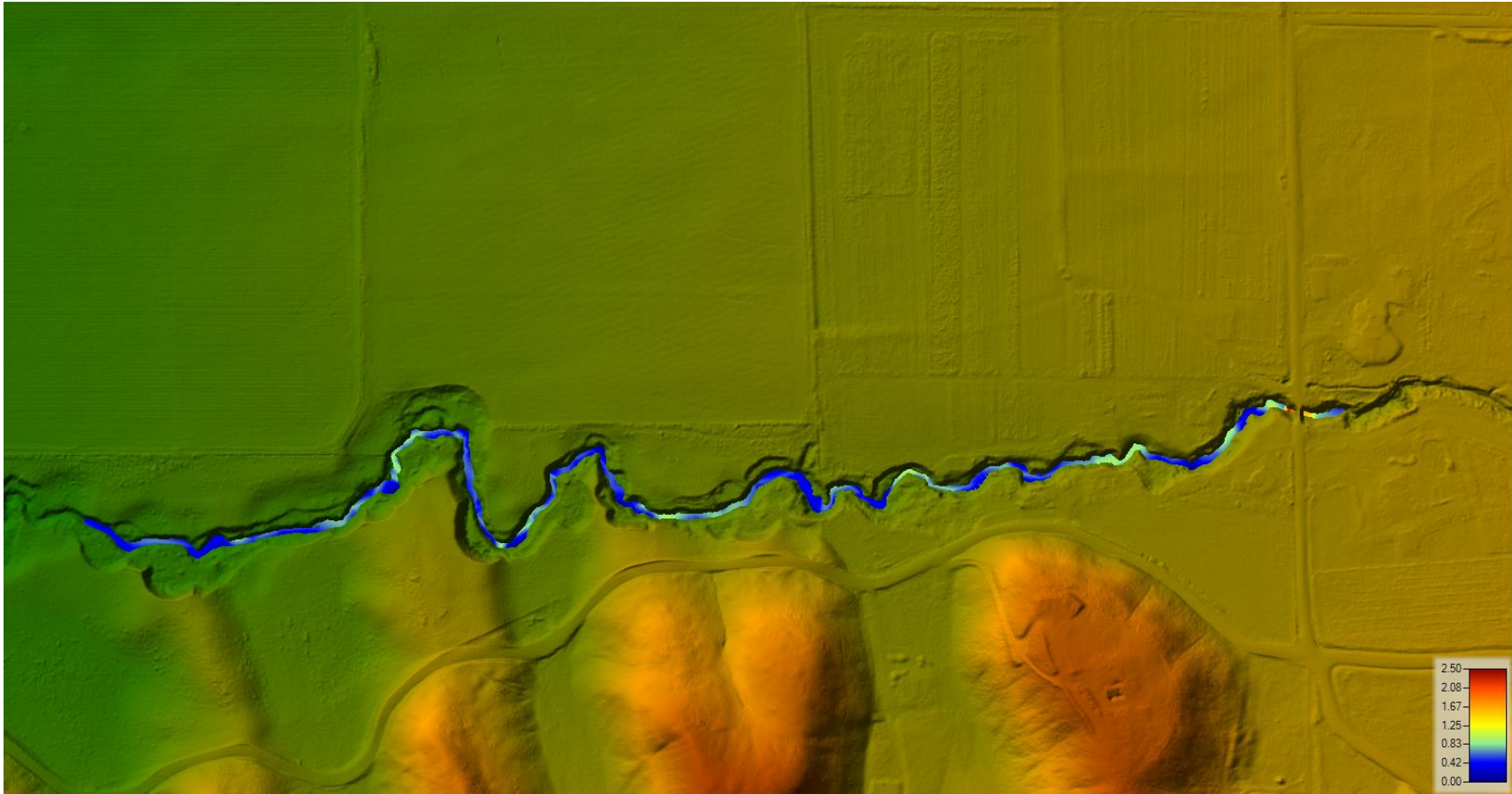
Figure G10   Model results of Reach 5 water velocity with a discharge of 1.42m³/s and a Manning n 0.065.
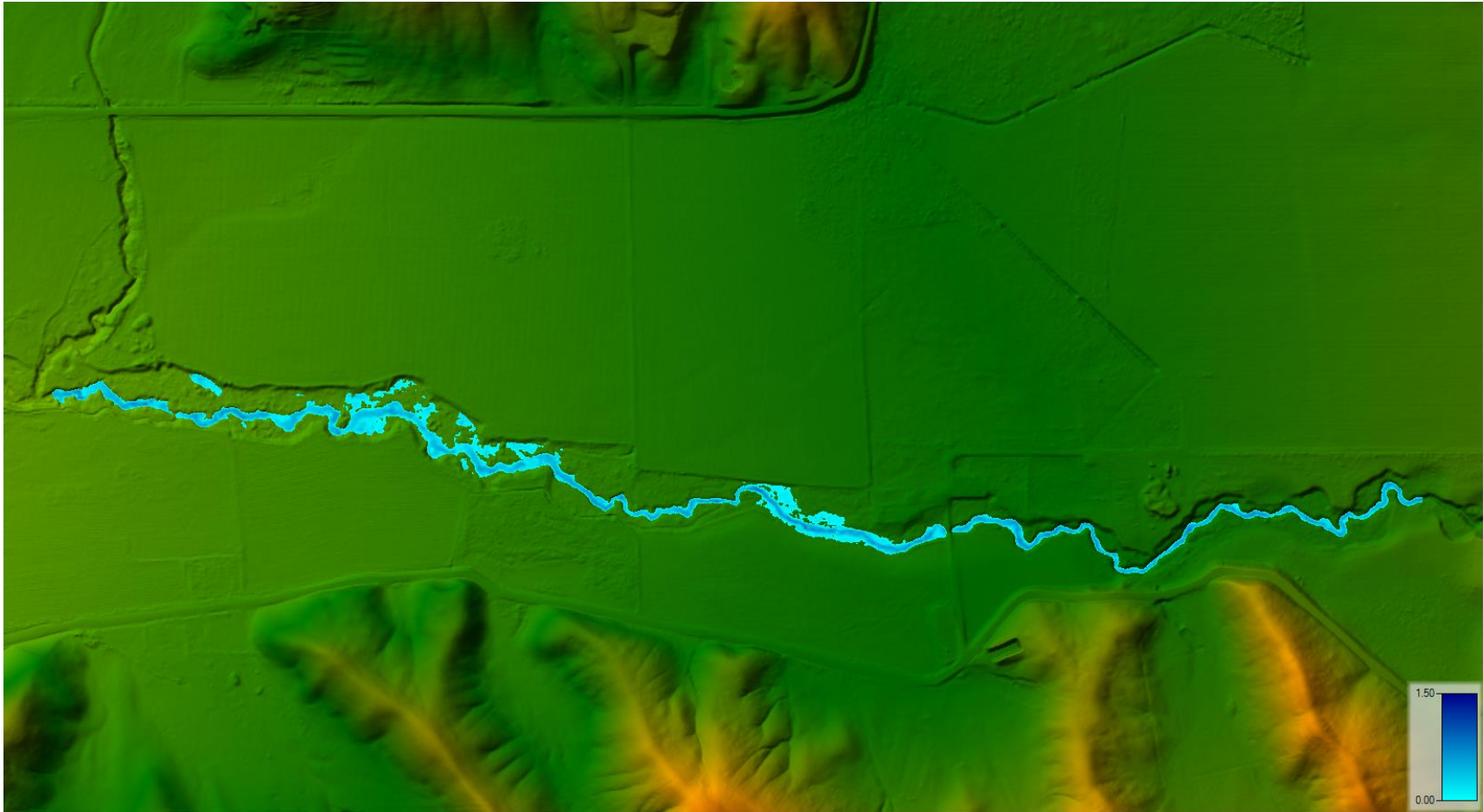
Figure G11   Model results of Reach 6 water depth with a discharge of 1.42m³/s and a Manning n 0.065.
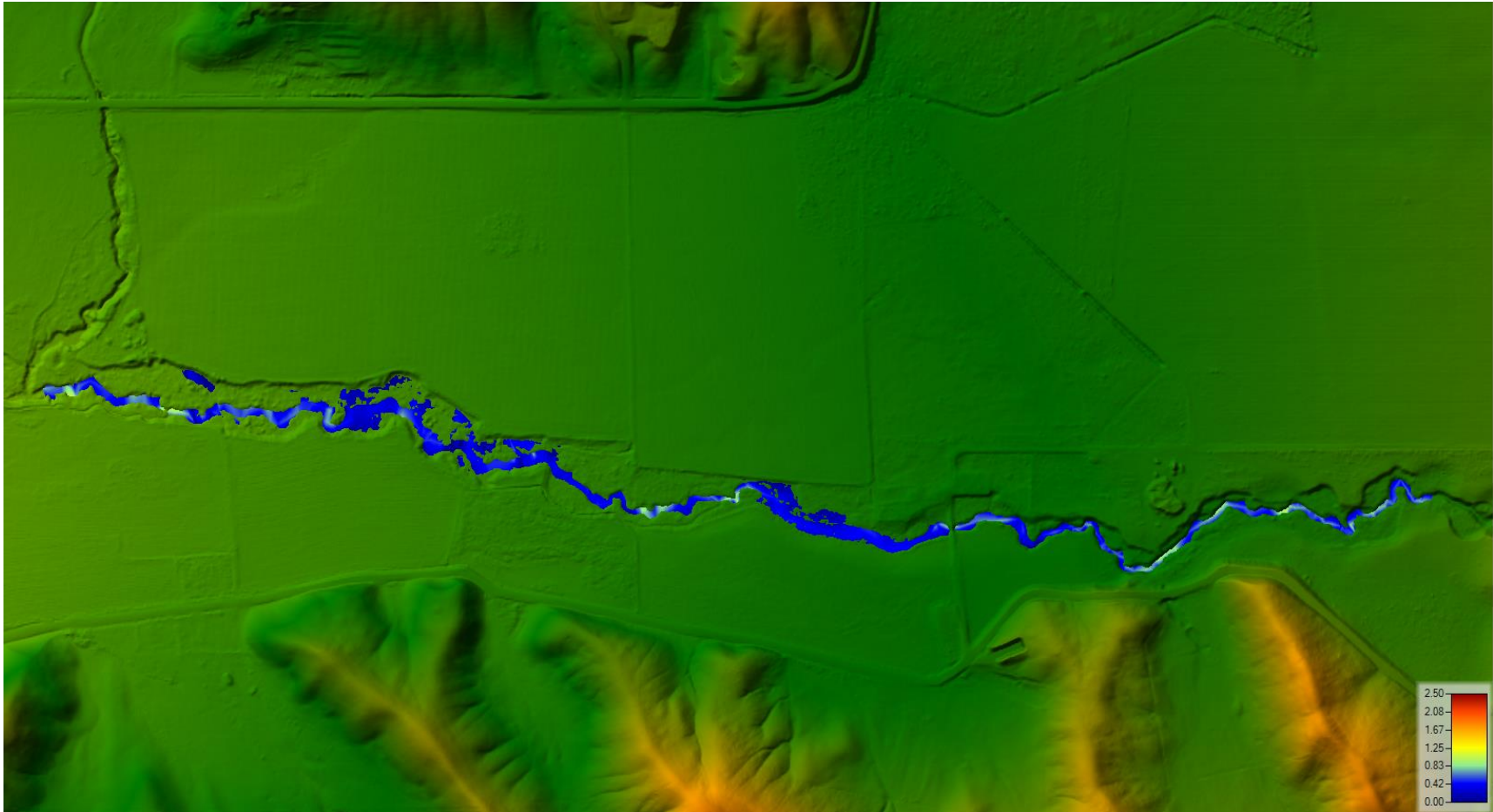
Figure G12   **Model results of Reach 6 water velocity with a discharge of 1.42m³/s and a Manning n 0.065.**